REPORT DOCUMENTATION PAGE

AFRL-SR-BL-TR-01-

0216

1. REPORT DATE (DD-MM-YYYY)	2. REPORT TYPE	3. DATES COVERED (From - To)
13-02-2001	Final Report	15Nov97 - 14Nov00

4. TITLE AND SUBTITLE
TOOLS FOR NONLINEAR CONTROL SYSTEMS ANALYSIS AND DESIGN FOR AEROENGINES

5a. CONTRACT NUMBER
F49620-98-C-0006

5b. GRANT NUMBER

5c. PROGRAM ELEMENT NUMBER

6. AUTHOR(S)
Andrzej Banaszuk
United Technologies Research Center
MS129-15
411 Silver Lane
East Hartford, CT 06108

5d. PROJECT NUMBER

5e. TASK NUMBER

5f. WORK UNIT NUMBER

7. PERFORMING ORGANIZATION NAME(S) AND ADDRESS(ES)

Dr. Marc Jacobs
801 N. Randolph St. Room 732
Arlington, VA 22203-1977

8. PERFORMING ORGANIZATION REPORT NUMBER

9. SPONSORING / MONITORING AGENCY NAME(S) AND ADDRESS(ES)

See Block 7

10. SPONSOR/MONITOR'S ACRONYM(S)
AFOSR/NM

11. SPONSOR/MONITOR'S REPORT NUMBER(S)

12. DISTRIBUTION / AVAILABILITY STATEMENT

Approved for public release;
distribution unlimited.

AIR FORCE OFFICE OF SCIENTIFIC RESEARCH (AFOSR)
NOTICE OF TRANSMITTAL DTIC. THIS TECHNICAL REPORT
HAS BEEN REVIEWED AND IS APPROVED FOR PUBLIC RELEASE
LAW AFR 190-12. DISTRIBUTION IS UNLIMITED.

13. SUPPLEMENTARY NOTES

14. ABSTRACT

The objective of this research was to develop tools for modeling, analysis, and control design for unsteady flow and combustion phenomena critical to operation of military aeroengines. We have made significant progress in control-oriented modeling, model validation and control design for processes affecting operation of aeroengines. The progress in modeling includes control-oriented reduced order models for turbomachinery flow including compressors, diffusers, recirculation zones, and jets in cross flow. Major breakthrough was achieved in the area of nonlinear model validation and parameter identification, with particular focus on models of combustion instability. In particular, method of nonlinear model validation and parameter identification for systems with non-equilibrium attractors and noise driv systems based on comparison of long-term statistics has been transitioned to internal UTRC projects. New results in control of limit-cyclin systems with bounded control were obtained. Significant progress was achieved in adaptive control of combustion instability, control of pressure recovery in diffusers, control of recirculation zone, and control of jets in cross flow. In particular, framework for control of mixin based on hierarchy of vorticity evolution models has been introduced. The framework has been used in control of mixing enhancement in jets in cross-flow and led to experimental validation of model-based analysis.

15. SUBJECT TERMS

16. SECURITY CLASSIFICATION OF: None			17. LIMITATION OF ABSTRACT	18. NUMBER OF PAGES	19a. NAME OF RESPONSIBLE PERSON
a. REPORT	b. ABSTRACT	c. THIS PAGE	SAR	75	Andrzej Banaszuk
					19b. TELEPHONE NUMBER (include area code) 860.610.7381

TOOLS FOR NONLINEAR CONTROL SYSTEMS ANALYSIS AND DESIGN FOR AEROENGINES

CONTRACT F49620-98-C-0006

FINAL REPORT

Andrzej Banaszuk
United Technologies Research Center,
MS129-15,
411 Silver Lane,
East Hartford, CT 06108,
tel. 860 610 7381, banasza@utrc.utc.com

0.1 Objectives

The objective of this research was to develop tools for modeling, analysis, and control design for unsteady flow and combustion phenomena critical to operation of military aeroengines.

0.2 Summary of accomplishments

We have made significant progress in control-oriented modeling, model validation, and control design for processes affecting operation of aeroengines. The progress in modeling includes control-oriented reduced order models for turbomachinery flow including compressors, diffusers, recirculation zones, and jets in cross flow. Major breakthrough was achieved in the area of nonlinear model validation and parameter identification, with particular focus on models of combustion instability. In particular, method of nonlinear model validation and parameter identification for systems with non-equilibrium attractors and noise drive systems based on comparison of long-term statistics has been transitioned to internal UTRC projects. New results in control of limit-cycling systems with bounded control were obtained. Significant progress was achieved in adaptive control of combustion instability, control of pressure recovery in diffusers, control of recirculation zone, and control of jets in cross flow. In particular, framework for control of mixing based on hierarchy of vorticity evolution models has been introduced. The framework has been used in control of mixing enhancement in jets in cross-flow and led to experimental validation of model-based analysis. Results of the research are in 13 conference papers (10 published, 3 submitted) and 7 journal papers (1 published, 4 submitted, 2 in preparation). 4 invited sessions were organized under this effort.

0.3 Organization of the report

We provide extended abstract for the results that are published and hence publily available. We provide more details for the results that are not available, like papers that are submitted or in the case of ungoing research. List of references is available in the last two chapters of the report. References to journal papers that were written under this contract are referenced with letter "j" in front ([j1], [j2], etc.). Conference papers written under this contract are referenced with letter "c" in front ([c1], [c2], etc.).

Contents

Chapter 1

Modeling and analysis of unsteady flows

1.1 Adaptive detection of instabilities and nonlinear analysis of a reduced-order model for flutter and rotating stall in turbomachinery

In paper [c1] by Copeland, Kevrekidis, and Ramiro Rico-Martínez system parameters were adaptively varied to identify bifurcations from equilibrium in simulations of a reduced-order model for turbomachinery aeromechanics. An element of the adaptive process is identification of a low-order locally nonlinear discrete-time map from the observables. The nonlinear behavior of the system in the neighborhood of the bifurcation is then estimated from the identified system.

Flutter and rotating stall are instabilities that can limit the design and operability of turbine engines. Rotating stall is primarily aerodynamic in nature. Flutter involves strong coupling between blade vibration and unsteady flow perturbations. Flutter also contributes to high-cycle fatigue and can be an important component of lifetime cost. In contrast to rotating stall, the current capability for flutter prediction is poor, hence problems are often found late in development cycle and remedial efforts are expensive. Nonlinear dynamics may be important because rotating stall typically occurs as a subcritical bifurcation. In the presence of subcritical instability, linear analysis alone is not sufficient to determine boundaries for safe operability.

A generic approach to mapping operability regions in an experiment is to successively *set* the operating parameters to fixed values and passively *observe* the system dynamics as the transients decay. When a qualitative change in the long-term behavior of the system is observed between two consecutive parameter settings it may be inferred that a bifurcation exists at some critical intermediate parameter value. This critical value may be bracketed to any acceptable accuracy through iterative bisection. This same procedure is applied generically to mathematical models when the only tool for investigation is *direct simulation*. This is often the case in computational fluid dynamics, for example.

The set-and-observe approach is straightforward but it has some obvious shortcomings. As one approaches a bifurcation point, the subcritical state of the system becomes less stable and the transients may take longer and longer to decay. In the detection of hard bifurcations such as the saddle-node bifurcation or the subcritical Hopf bifurcation there is the additional complication that overstepping the critical parameter value from subcritical to supercritical values drives the system far from the original neighborhood of phase space. Bringing the system back to the neighborhood of the bifurcation point may require excessive effort.

In this paper, detection of bifurcation points by adaptively varying the operating parameters is

demonstrated. A local low-order nonlinear model is identified from input/output data as the system evolves. This identified model is used to estimate critical parameter values for bifurcation. A controller then adjusts the parameters (using it essentially as an actuator) to bring the system progressively closer to the bifurcation point. The identified model may also be used to interpret the nonlinear dynamics in the neighborhood of the bifurcation.

For more details see [c1].

1.2 Analysis of low dimensional dynamics of flow separation

The increased interest in the modeling and active control of separation phenomena [21, 107] is motivated by their prevalence in several industrial situations where device performance is often hampered by large scale separation (e.g. flow within engine ducts and flow past high angle-of-attack airfoils). Until recently, separated flows have been studied and controlled using knowledge about the hydrodynamic instabilities that govern the dynamics near the separation location. These studies provide useful insights into the flow physics underlying separation, but do not produce models that can be used for prediction or control. The use of the dynamical systems approach in hydrodynamics [4] appears promising for the development of reduced-order models of flow separation dynamics. In particular, "parameter-dependent" models are desired that can be used to predict bifurcations of flow states and to design effective control methods.

Low-dimensional models for active control of flow separation are considered in the papers [c2] by S. Narayanan, A.I. Khibnik, C.A. Jacobson, Y. Kevrekedis , R. Rico-Martinez and[j1] by K. Lust and A.I. Khibnik, S. Narayanan, C.A. Jacobson, and K. Lust.

POD method was used to analyze the dynamics of flow separation in a planar diffuser. The parameter space of interest is associated with a variable diffuser geometry, given here by the expansion angle. Two-dimensional direct numerical simulations of the diffuser flow were performed at a Reynolds number of 5,200. For increasing diffuser angle, the flow transitions from a symmetric steady attached flow to an asymmetric separated unsteady flow (also termed transitory stall), followed by a steady separated (stalled) flow and leading to a fully separated jet-like flow. Numerical data corresponding to flow fields across the first transition (from attached flow to transitory stall) were combined to yield a set of POD modes that span the dynamics (both transients and attractors) for different expansion angles. The observed dynamics, inferred from the first few POD modes and their coefficients, included symmetry breaking, steady states, limit cycles, invariant tori and chaotic motion. Limit cycles involve low frequency oscillations associated with unsteady stall shedding, independently confirmed via laboratory experiments. A bifurcation scenario (see Figure 1.1) was hypothesized to provide insight into low dimensional dynamics underlying the first transition and to guide the development of a control strategy for separation. The POD modes were also used to construct reduced order models (Galerkin and neural network models). The paper briefly discusses these approaches and a proposed discretized Galerkin model.

We study the spatiotemporal dynamics of flow separation in a planar diffuser to extract reduced-order models that may be used to guide active separation control. Proper orthogonal decomposition of numerical simulation data revealed organized dynamics of the large-scale separated structures. This result, combined with the observation (in simulations as well as laboratory experiments) of limit cycle/quasiperiodic dynamics and spatial symmetry breaking, suggests an underlying low-dimensional dynamical system. Galerkin-based and neural network-based modeling of the POD modal coefficients lead to (parameter dependent) low-dimensional models of separation dynamics. The use of such models for active separation control appears promising.

Note that the application of the POD for the modeling of deparated diffuser flows has not been much explored. One of the obstacles that makes such an application to the diffuser non-trivial is the

Flow classification in the diffuser based on flow visualization and experimentally obtained diffuser pressure recovery.

The corresponding bifurcation diagram was obtained using POD modes from CFD computations.

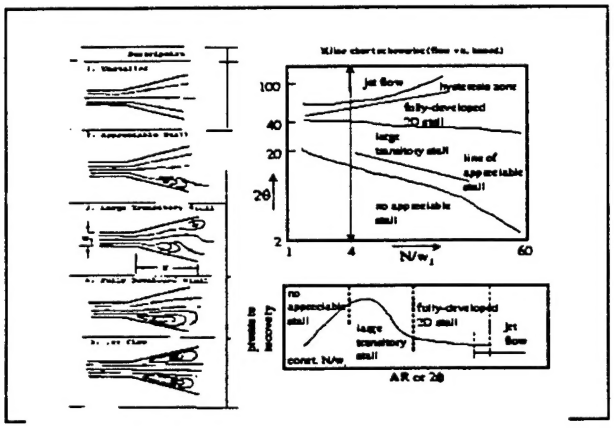

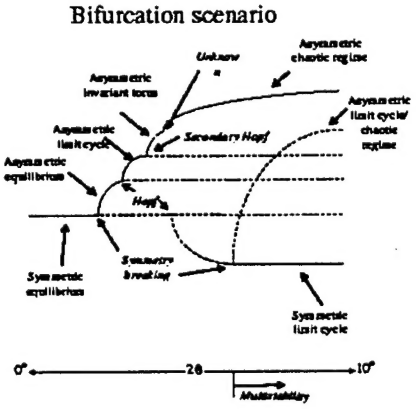

Figure 1.1:

variable geometry. In most known applications of POD to fluid flows, either the flow conditions or the parameters defining the boundary conditions are assumed to be fixed. Computed POD modes may still be used to span the flow fields for different flow conditions or parameters (e.g., varying Reynolds number). In our bifurcation studies, the parameters determine the geometry. This makes it difficult to compare flow fields at different angles and thus to compute a POD basis capable of approximating these flow fields. To address this issue, we transform the diffuser geometry to the "standard" geometry of a channel flow. Thus, the parameters enter the (transformed) governing equations while keeping the geometry and the boundary conditions fixed, enabling the analysis of a combined set of flow fields using a POD basis.

For more details, please refer to [c2,j1].

Chapter 2

Nonlinear model validation and parameter identification

2.1 Nonlinear model validation and parameter identification for systems with complex dynamics using long-term statistics of data

2.1.1 Introduction

In [j2,c8] we presented a formalism for comparing the asymptotic dynamics of dynamical systems with physical systems that they model. There is often no need for the detailed (trajectory-wise) comparison of a dynamical system and the physical system that it models, but only comparison in statistical sense. For that purpose, invariant measures are typically considered. But, invariant measures usually can not be observed directly in an experiment. Thus, we base our formalism on time-averages obtained from a single observable in the spirit of Takens embedding theorem. In particular, we constructively proved that, generically, a single observable is needed in order to recover an invariant ergodic measure. Pseudometrics on space of dynamical systems can be defined using this formalism in order to compare their statistical behavior. We also identified the need to go beyond comparing only invariant ergodic measures of systems and introduce an ergodic-theoretic treatment of a class of spectral functionals that allow for this. We discussed the extension of this theory to stochastic dynamical systems.

Both the concepts of invariant measure and the harmonic average formalism developed here are related to spectral properties (in particular, the point spectrum) of the so-called Koopman operator U, a linear operator that acts on functions on the phase-space . We stress that in this context questions of identification or validation of asymptotic properties of nonlinear finite-dimensional systems with complex dynamics is transferred to questions of identification or validation of a linear, albeit infinite-dimensional Koopman operator. Here we analyze only the point spectrum of that operator. Our hope is that some of the methods developed in control theory of linear systems can be used to study these issues further.

The ideas introduced in [j2,c8] can be used for parameter identification and model validation of stochastically driven nonlinear models with complicated behavior.

2.1.2 Example: Parameter identification of a reduced-order nonlinear combustion model with noise using data from a feedback control experiment

As an illustration we provided an example in which we compared the asymptotic behavior of a combustion system measured experimentally with the asymptotical behavior of the model that is a stochastic control dynamical system.

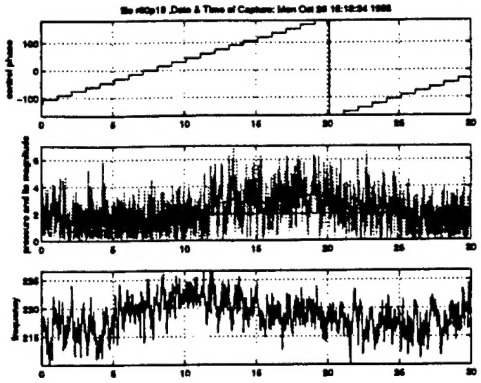

Figure 2.1: Control phase ramp experiment. Estimates of magnitude and frequency of pressure oscillations recorded. Uncontrolled mean magnitude level indicated.

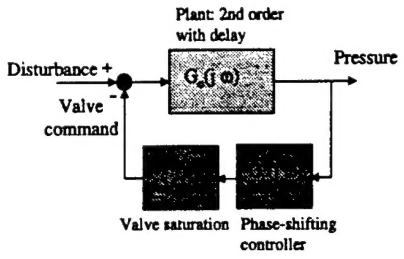

Figure 2.2: A model of a controlled combustion process

we present an example of using a finite number of functionals evaluated on trajectories to identification of parameters of a model describing a UTRC combustion rig operating close to an unstable condition associated with a low equivalence ratio condition. In an experiment a feedback loop has been closed around the combustor with a phase-shifting controller. The control phase has been varied and a time trace of pressure has been recorded. As the phase varies, both attenuation and excitation of the pressure oscillations have been observed. A simple model of the controlled combustion process consists of a linear plant, controller, a saturated actuator, and a driving broad-band stochastic disturbance. The linear model of the has been identified from an experimentally obtained frequency response. The model has a form of a lightly damped 2nd order system with delay. An analysis of the linearization of the system in the origin indicates that the linear eigenvalues of the closed-loop system can be moved away or towards the imaginary axis on the complex plane. In particular, it is possible to move the eigenvalues to the right-half plane. In this case, the oscillations would grow and settle on a limit-cycle, as the actuator saturation prevents an unbounded exponential growth. As one adds the strong driving disturbance in the model, an exact analytical study of the behavior of the system is no longer possible. One can still run a numerical simulation and compare the results with experiment. We assume that the disturbance driving the combustion model is a white Gaussian process with standard deviation σ. By adjusting the standard deviation of the disturbance and the value of delay one can qualitatively reproduce the results of the phase ramp experiment in a simulation. In what follows the delay of the plant τ and the standard deviation of the disturbance σ will be varied to match the results of experiment with closed loop control for several values of control phase. We will define a measure of a good fit by evaluating several long term statistics and combining them with some weights into a one number.

For each of the eight values of the control phase from the set (-165, -120, -75, -30, 15, 60, 105, 150)

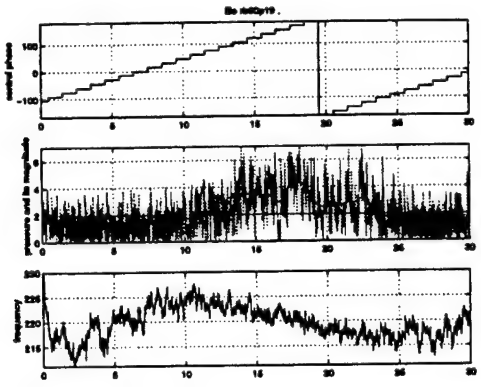

Figure 2.3: A control phase ramp obtained from a model simualtion.

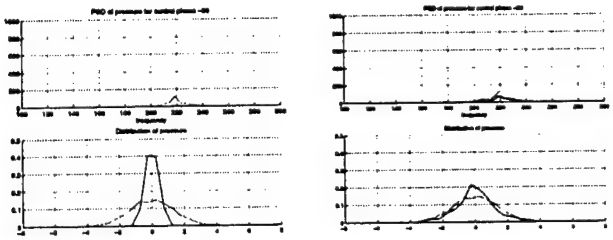

Figure 2.4: Comparison pf PSDs and distributions of pressure for control phase $\theta = -30$. Light lines: from experiment. Dark lines: from model simulation. Left: for $\tau = 0.006$ and $\sigma = 1$. Right: for $\tau = 0.006$ and $\sigma = 3$.

(in degrees) we chose a time interval containing about 0.5 seconds of pressure data (1024 samples of pressure sampled at 2000Hz) corresponding to a constant control phase.

Below we show the time traces, phase portraits, distributions, and PSDs of pressure for control phases $\theta = -30$ and $\theta = 150$ from experiment and from model simulations for delay $\tau = 0.006$ and for two diffrent values of the standard deviation of the disturbance: $\sigma = 1$ and $\sigma = 3$. The control phases $\theta = -30$ results in a supression of the pressure oscillations. The corresponding closed-loop model is a stable, disturbance driven system. On the other hand, the control phase $\theta = 150$ results in an enhancement of oscillations. The model analysis without disturbance predicts a limit cycling behavior.

To visualize the discrepancies between the data from the model simulations and from the experiment, we present the PSDs and distributions of pressure from both models (darker line) on the same plot with the experimental PSDs and distributions (lighter lines). We can see that the lower value

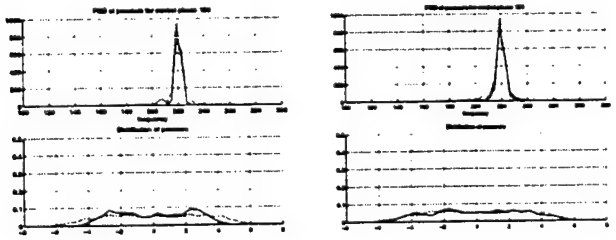

Figure 2.5: Comparison pf PSDs and distributions of pressure for control phase $\theta = 150$. Light lines: from experiment. Dark lines: from model simulation. Left: for $\tau = 0.006$ and $\sigma = 1$. Right: for $\tau = 0.006$ and $\sigma = 3$.

of the standard deviation of the disturbance σ in the model leads to an underestimation of the pressure oscillation level in experiment for both control phases. We also observe that the distribution of pressure in the data from the model simulation for high value of standard deviation resembles the one from experiment better than the data from the low disturbance model simulation.

To quantify the discrepancies of the data from experiment and model simulations we would like to choose some quantities that describe the average frequency of the oscillations, the average size of the oscillations, and somehow distinguish a disturbance-driven limit cycle from a disturbance-driven stable system. With this goal in mind, for each time interval corresponding to a given control phase θ we calculated the following measures of the long term statistics:

1. The mean frequency of the pressure oscillations.
2. The standard deviation of the frequency pressure oscillations.
3. The standard s deviation of the pressure signal.
4. The ratio of pressure measurements in the interval $[-s/2\ s/2]$ to the number of all pressure measurement in a given time interval.

(In the sequel we will refer to these measures as the *long term statistics*).

The mean frequency and the standard deviation of the frequency of pressure oscillations has been calculated from the Power Spectral Density of the pressure signal. The mean frequency of the pressure oscillations and the standard deviation of the pressure signal are of obvious interest. For a stable linear system the standard deviation of the frequency is a measure of the damping of the system. The ratio of pressure measurements in the interval $[-s/2\ s/2]$ to the number of all pressure measurement in a given time interval was chosen to distinguish between a disturbance-driven stable system from a disturbance-driven linearly unstable, limit-cycling system. As we will see, on the stable side this value is typically around .35-.4, while on the unstable side it drops below .3.

A measure of a discrepancy of the statistics from experimental data and model simulation was obtained by taking the absolute value of the difference of the statistics and dividing it by the value of the statistic for the experimental data. A mean value of this relative measure for all eight control phases is called in the sequel a *relative error* for a given statistic.

From the four relative errors we construct a total error measure by adding the four relative errors with the following weights:

1. The weight for the mean frequency of the pressure oscillations. 0.3
2. The weight for the standard deviation of the frequency pressure oscillations. 0.1
3. The weight for the standard s deviation of the pressure signal. 0.4
4. The weight for the ratio of pressure measurements in the interval $[-s/2\ s/2]$ to the number of all pressure measurement in a given time interval. .2

The values corresponding to the lowest total relative error of 0.09321 are $\tau = 0.006$ and $\sigma = 3$. The comparison of the long term statistics from experiment and model simulation for this case is shown in Figure 2.6. Note that the long term statistics introduced in this section to select a combustion model that best matches data were chosen in an arbitrary manner, to measure various features that were considered of merit. The results of this paper were not a necessary for being able to pick certain statistics in this particular example. What we would like to stress here is that all these different and somewhow unrelated statistics are constructed as certain functionals defined on recorded trajectories from an experiment and from a model simuation. The results of this paper provide a new insight into what is the precise mathematical meaning of often ad hoc chosen measures of a distance between two dynamical systems.

A single peak in PDF of pressure indicates a stable driven system. Double peak indicates a noisy limit cycle. An alternative method of distinguishing whether a model that is a noise-driven stable system or a noise-driven limit cycling system better mathces experimental data is presented in [36].

The method proposed in [j2,c8] became a standard method for validation of reduced order models

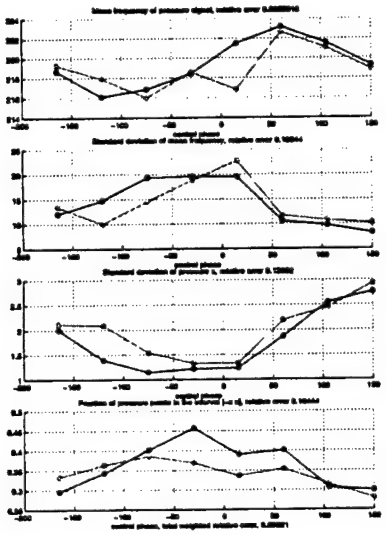

Figure 2.6: Long term statistics from experiment and model simulation for $\tau = 0.006$, $\sigma = 3$.

of combustion instability used at UTRC. In particular, the method was used in an internally funded combustion programs for model validation and parameter identification a single-nozzle rig model. Figure 2.7 shows comparison of Power Spectral Density and Probability Density Function of the pressure data from experiment and model simulation. Moreover, the method has been applied to identification of a reduced order model of combustion instability in an advanced military engine and to distinguish regions of validity of stable driven and limit cycling models of military aeroengines and industrial gas turbines. The method can be also used for validation of reduced order models of shear flows.

2.2 Nonlinear model validation using frequency reponse data

In [c4] we presented a model validation problem using a frequency response data, motivated by the modeling of a combustion process at UTRC. The system excitation was well modeled by a stochastic source and this dominated the response. The number of data points that must be recorded to capture the system behavior precluded the use of time-domain model validation techniques. A critical analysis of the results of the linear model validation indicated the limitations of the linear model validation techniques in the context of nonlinear feedback systems. The need for new model validation techniques that take into account nonlinear model perturbations and the effect of the driving broad band disturbance was indicated.

Frequency response measurements of UTRC single nozzle rig combustor were taken in both open-loop and closed-loop configurations using swept-sine experiments. The results of these experiments are shown in Figure 2.8. In both cases a very good fit to the response was obtained with a stable linear transfer function consisting of a 2nd order system with delay.

The nonlinearity assumed in the model did not manifest itself by distorting the experimental frequency response estimates. As a consequence, it is natural to quantitatively investigate the extent to which a linear model—with a norm bounded perturbation—can describe the system behaviors. Such a model structure is illustrated in Figure 2.9.

Both linear and nonlinear models contain bounded perturbations, which allow each to describe a set of behaviors. This structure is commonly used in robust control and provides a degree of robustness with respect to the designer's uncertainty about the true range of system behaviors. Given

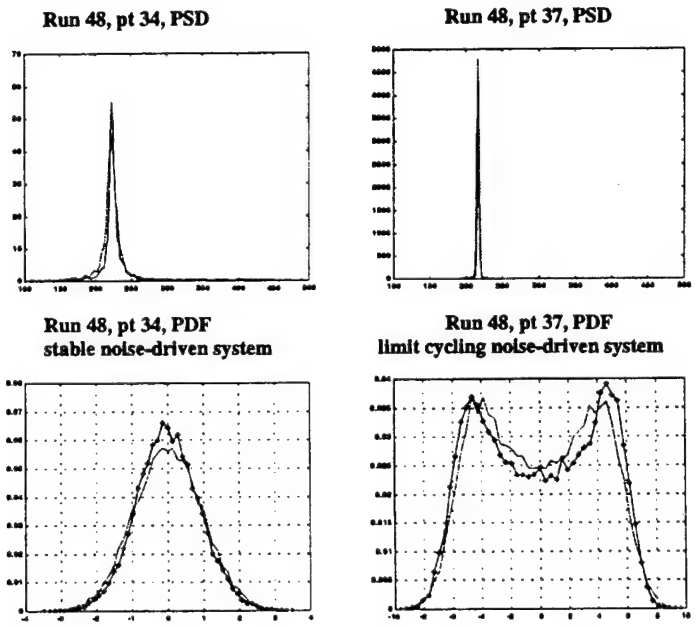

Figure 2.7: Results of model parameters fitting using statistics of data from experiment and model simulation.

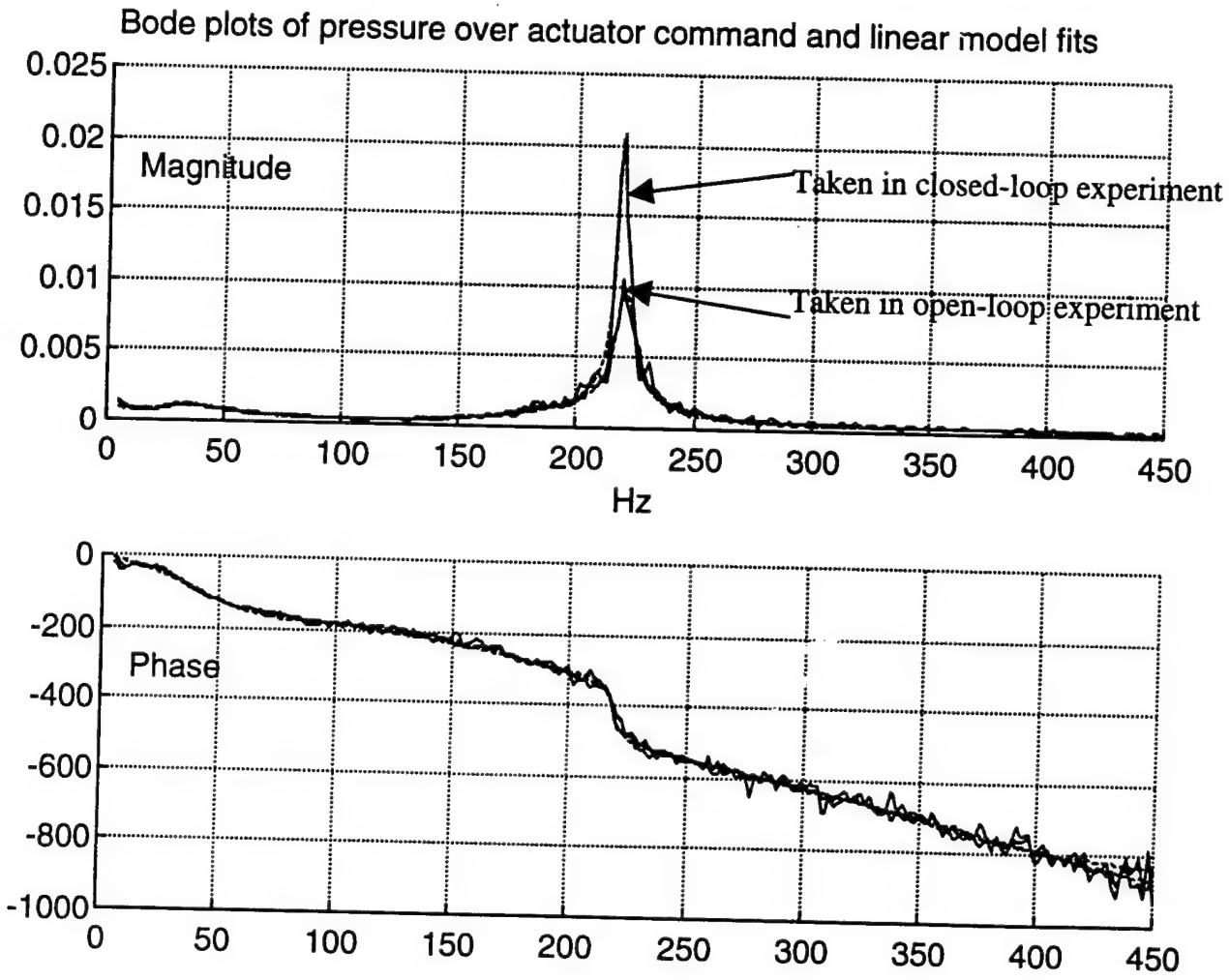

Figure 2.8: Experimental frequency responses of valve command to pressure taken under open-loop and closed-loop control.

experimental input-output data, model validation techniques provide a means of comparing the ability of each model to account for the observed experimental data.

While the observed closed-loop response appeared linear, it was significantly different from that which could be predicted from the open-loop model. In the closed-loop response the resonant peak was twice that of the open-loop case, and the damping was half that of the open-loop case (refer to Figure 2.8). This was true even though the pressure oscillations in the closed-loop case were half those of the open-loop situation. A linear analysis of the control design indicates that we would expect the damping to increase under closed-loop control.

An interpretation of this unexpected behavior can be made based on the nonlinear model as follows. A strong driving noise adds to the sinusoidal driving signal at the input of the nonlinear function and a large portion of the saturated part of the function is visited. In a closed-loop experiment the controller reduces the size of the disturbance and less of the saturated portion of the nonlinear function is visited. Effectively, the nonlinearity provides a higher gain to the sinusoidal signal and hence the positive feedback in the internal loop is stronger. This manifests itself as a higher resonant peak and lower damping in the linear model fit to the combustor frequency response in the closed-loop experiment.

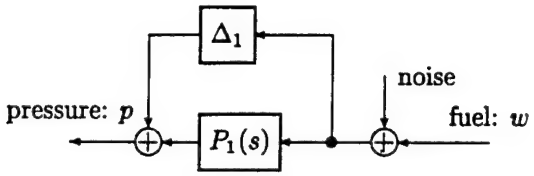

Figure 2.9: Linear perturbation model of the combustion process

Figure 2.10 illustrates a model structure capable of reproducing the observed behavior.

The closed-loop system, illustrated in Figure 2.10, has been simulated and used to obtain the simulated frequency response measurements shown in Figure 2.11. The simulation is a very good qualitative match to the observed experimental behavior: the damping ratio of the oscillatory mode is reduced in both the closed-loop model simulation and experiments.

2.3 Nonlinear model identification using frequency reponse data

2.3.1 Introduction and problem formulation

In papers [j7,c13], we propose a describing function based procedure for identifying the shape of the nonlinearity in the thermoacoustic feedback loop. We describe the procedure in two cases:

1. where no driving noise is present and the system is either stable or in self-sustained limit cycling oscillations and

2. where Gaussian driving noise alone is present and limit cycle is absent.

In the case where no driving noise is present, we show that the nonlinearity shape may be recovered by using experiments with feedback control where the control is used to vary the amplitude of the limit cycle from zero to the maximum value. At each fixed amplitude, standard linear identification is used for identifying the harmonic balance gain. These gains are then used to determine the shape of the nonlinearity function.

In the case where Gaussian driving noise is present, a procedure is proposed whereby an external controller is used to manipulate the variance of the Gaussian noise seen by the nonlinearity. At each controller setting, small amplitude sinusoidal forcing is used to determine the harmonic balance gain (in this case, for the Gaussian noise). The shape of the underlying nonlinearity is recovered from these harmonic balance gains.

A simplified version of UTRC combustion model of a premixed combustion process is an interconnection of a linear lightly damped oscillator, delay, and a saturating nonlinearity in a feedback loop. Figure 2.12 gives the block diagram schematic of the combustion model. The oscillator represents the acoustic waves in the combustion chamber. The delay represents the time it takes the fuel and air to mix in a premixing nozzle, transport to the flame front, and react. The saturating nonlinearity represents the dependence of a heat release rate on the fuel to air ratio at the flame front. The feedback loop represents the effect of oscillations of air mass flow in the nozzle on the fuel to air ratio and hence on the heat release rate. The delay is such that the internal feedback loop provides a positive feedback around the oscillator. Only the output of the oscillator (pressure) is accessible for measurement. Depending upon the experimental conditions, a strong broad band disturbance (representing turbulent velocity fluctuations) may be driving the system at the input of the linear oscillator. The control input (representing fuel modulation) adds to the disturbance input.

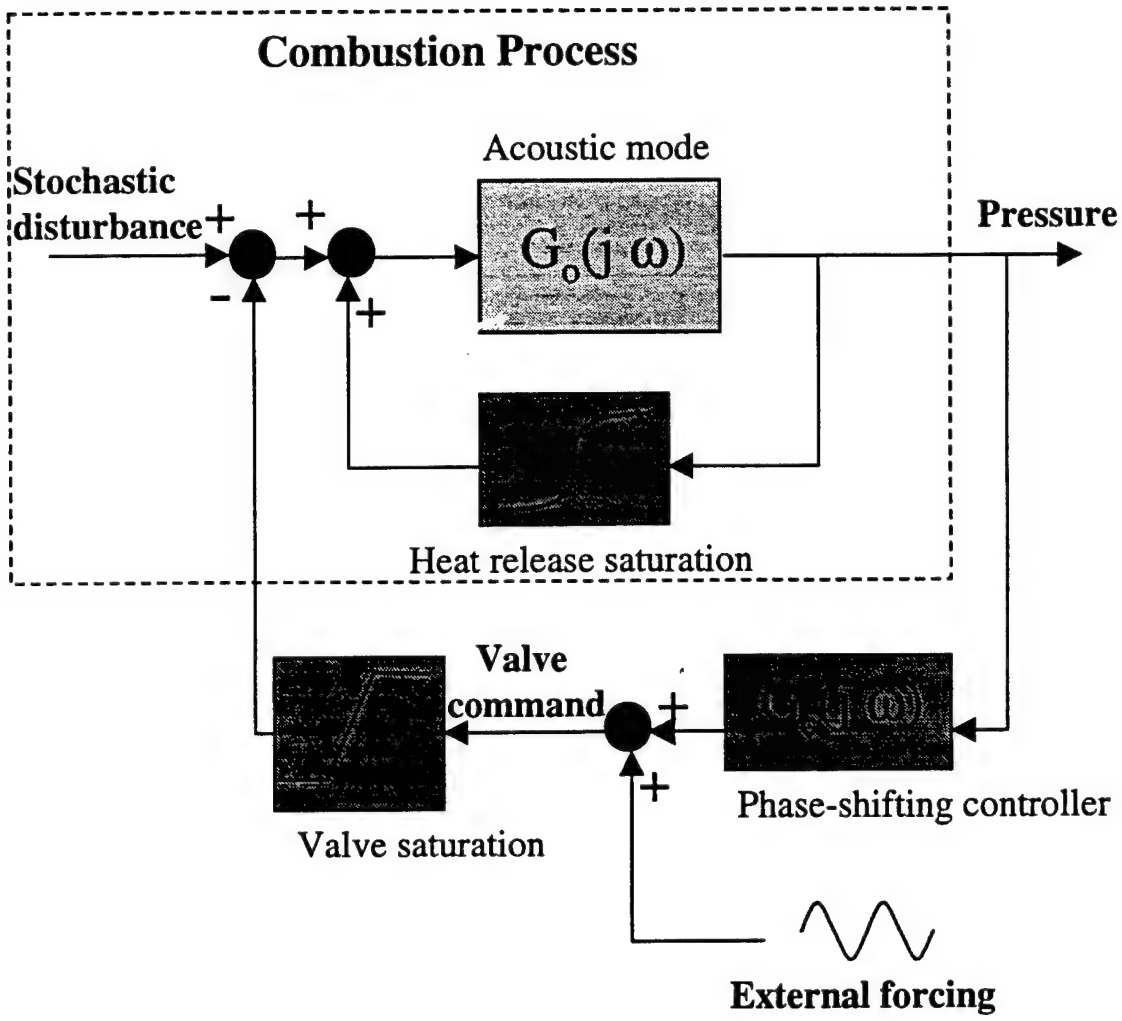

Figure 2.10: Nonlinear model structure matching the observed closed-loop experimental frequency responses.

Bode plots of pressure over actuator command from a model simulation

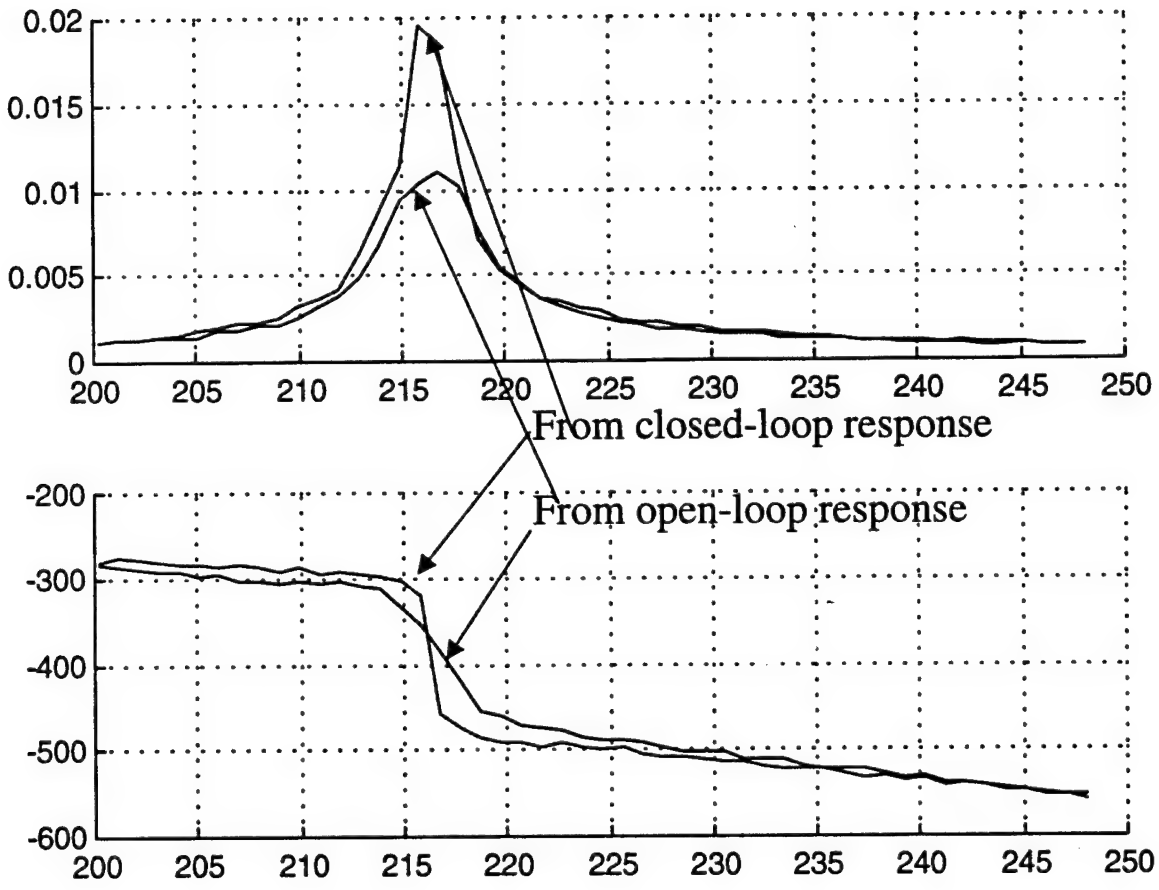

Figure 2.11: Open- and closed-loop frequency responses generated by the nonlinear model simulation.

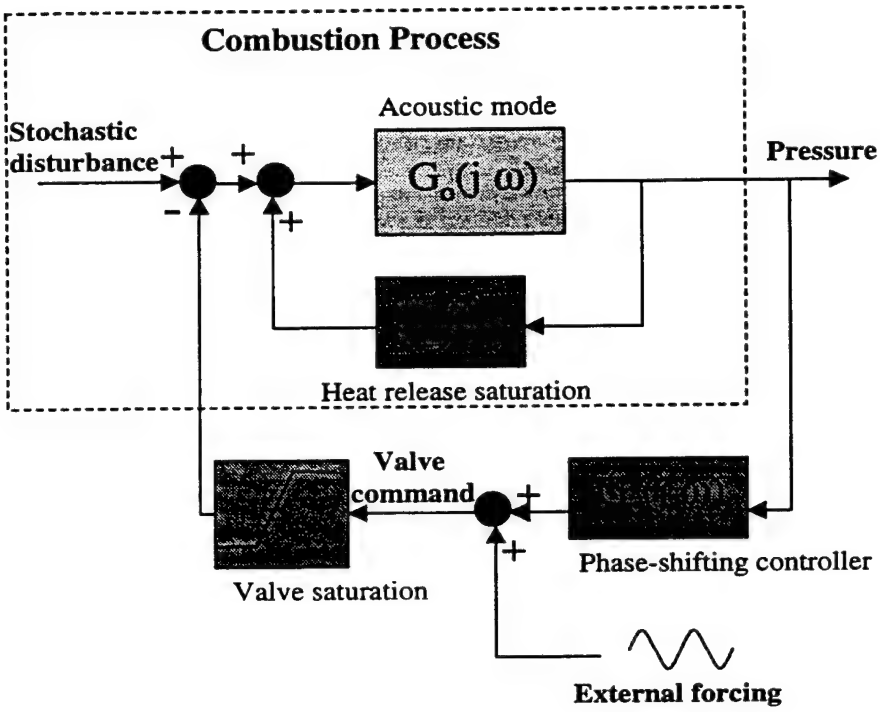

Figure 2.12: Nonlinear model's block diagram

The nonlinear identification objective is to obtain the shape of the heat release nonlinearity by using the control and/or the external forcing (see Figure 2.12). For the purpose of this note, it is assumed that the linear dynamics (acoustics and delay) have already been obtained using a frequency response test and are known. Additionally, we impose a special structure on the heat release nonlinearity as described by the following definition.

Definition. The heat release nonlinearity $h(u)$ is a static function of its input u such that the following three requirements are satisfied

1. $h(0) = 0$,
2. h is a non-decreasing odd function ($h(-u) = -h(u)$) and
3. For $u > 0$, $h(u)$ is a concave function, i.e.

$$h(\lambda u + (1-\lambda)v) \geq \lambda h(u) + (1-\lambda)h(v). \tag{2.1}$$

For such a non-linearity and for $u > 0$, we have

$$h(\lambda u) \geq \lambda h(u), \quad 0 \leq \lambda \leq 1 \tag{2.2}$$

$$\lambda h(u) \geq h(\lambda u), \quad \lambda \geq 1. \tag{2.3}$$

We will have the need to use these inequalities in certain proofs to follow. A relay nonlinearity is an example of heat release nonlinearity.

Remark. If additionally, h is assumed to be a C^1 function then the requirement (3) in the definition of the heat release nonlinearity can be shown to be equivalent to the derivative h' being a non-increasing function of its argument.

2.3.2 Identification without noise

In the absence of noise, harmonic balance for the limit cycling system yields the sinusoidal describing function gain

$$N_A = \frac{1}{\pi A}\int_0^{2\pi} h(Asin(\theta))sin(\theta)d\theta \tag{2.4}$$

for the static nonlinearity h where A represents the amplitude of the sinusoid at the input of the heat release nonlinearity. This sinusoid may arise either due to the external forcing or due to the limit cycling oscillations. In the limit cycling case, the loop equation

$$1 + N_A G_0(i\omega)e^{-(i\omega\tau)} = 0 \tag{2.5}$$

needs to be additionally satisfied. In this section, we do not consider the case where both the forcing and limit cycle oscillations are present.

If the thermoacoustic system is non limit cycling and the presence of the sinusoidal forcing does not cause the system to exhibit limit cycling behavior then harmonic balance may be used together with the sinusoidal forcing to estimate the feedback gain due to the nonlinearity (at a fixed forcing amplitude). By estimating this gain for many forcing amplitudes, the harmonic balance gain is computed for different amplitudes at the nonlinearities input.

If the thermoacoustic system is limit cycling then the same procedure is applied but this time with an external controller. The controller is gain and phase adjusted to tune the amplitude of the limit cycle. The harmonic balance gain is now evaluated at the different limit cycle amplitudes.

To compute the nonlinearity shape from these gains identified using linear techniques, we arrive at the operator equation

$$g(A) = Lh(A) \equiv \frac{1}{\pi}\int_0^{2\pi} h(Asin(\theta))sin(\theta)d\theta \tag{2.6}$$

which needs to be solved to determine the shape of the nonlinearity. For the heat release nonlinearity (see definition in section 2.3.1), this equation is invertible and the inverse is given by

$$h(A) = \sum_{n=0}^{\infty} M^n g(A) \tag{2.7}$$

where the operator

$$M \equiv I - L. \tag{2.8}$$

The proof that the series actually converges for the heat release nonlinearity requires $\|M\|$ to be less than 1. This follows because

$$\begin{aligned} Mh(A) &\equiv (I-L)h(A) \\ &= h(A) - Lh(A) \\ &= \frac{1}{\pi}\int_0^{2\pi} h(A)sin^2(\theta)d\theta - \frac{1}{\pi}\int_0^{2\pi} h(Asin(\theta))sin(\theta)d\theta \\ &= \frac{2}{\pi}\int_0^{2\pi} \left[h(A)sin(\theta) - h(Asin(\theta))\right] sin(\theta)d\theta \end{aligned} \tag{2.9}$$

because h is assumed to be an odd function. Finally, because h is concave, we use the inequality (2.2) to estimate a bound for the operator as

$$\begin{aligned} |Mh(A)| &\leq \frac{2}{\pi}\int_0^{2\pi} \left[1 - sin(\theta)\right] h(A)sin(\theta)d\theta \\ &= (\frac{4}{\pi} - 1)h(A). \end{aligned} \tag{2.10}$$

We thus have a bound on the operator norm of M as

$$\|M\| \leq (\frac{4}{\pi} - 1) < 1. \tag{2.11}$$

A Matlab code has been written to compute the terms in the series iteratively (see Appendix). The series representation of the inverse also allows one to obtain bounds on the error. For example, a relay type nonlinearity

$$\begin{aligned} h(A) &= b, \quad A > 0 \\ &= -b, \quad A < 0 \end{aligned} \tag{2.12}$$

yields through a harmonic gain analysis $N_A = \frac{4b}{\pi A}$ or equivalently

$$g(A) = \frac{1}{\pi}\int_0^{2\pi} bsin(\theta)d\theta = \frac{4b}{\pi}. \tag{2.13}$$

The computations are then easily performed to recover the shape of the nonlinearity. The $O(0)$ computation yields

$$h^0(A) = g(A) = \frac{4b}{\pi} = 1.2723b \tag{2.14}$$

with relative error bounded by

$$\frac{|e(A)|}{\|h\|} \leq \|M\| \leq (\frac{4}{\pi} - 1). \tag{2.15}$$

The $O(1)$ computations yield

$$\begin{aligned} h^1(A) &= g(A) + Mg(A) \\ &= \frac{4b}{\pi} + \frac{2}{\pi}\int_0^{\pi}\left[\frac{4b}{\pi}sin(\theta) - \frac{4b}{\pi}\right]sin(\theta)d\theta \\ &= 0.9253b \end{aligned} \tag{2.16}$$

with relative error bounded by

$$\frac{|e(A)|}{\|h\|} \leq \|M\|^2 \leq (\frac{4}{\pi} - 1)^2 = 0.0747. \tag{2.17}$$

Similarly relative error for $O(2)$ compuations is bounded by 0.0204 and so on.

2.3.3 Identification with noise

In the presence of Gaussian noise, the random input describing function framework is used to do harmonic balance. Throughout this section, we assume that limit cycle is not present and the harmonic balance due to the noise alone accounts for the signals in the loop. If the variance of the signals at the input and the output of the nonlinearity is known, the operator equation

$$g(\sigma) = Lh(\sigma) \equiv \frac{1}{\sqrt{2\pi}}\int_{-\infty}^{\infty} h(\sigma s)se^{-s^2/2}ds \tag{2.18}$$

needs to be solved to obtain the nonlinearity shape h. For the heat release nonlinearity, the solution may again be obtained in a series form

$$h(\sigma) = \sum_{n=0}^{\infty} M^n g(\sigma) \tag{2.19}$$

where the operator

$$M \equiv I - L. \tag{2.20}$$

For the heat release nonlinearity (see Definition in section 2.3.1)), the inequalities (2.2) and (2.3) may be used to carry out an analysis similar to the one described in previous section to show that

$$\begin{aligned} |Mh(\sigma)| &= |\sqrt{\frac{2}{\pi}} \int_0^\infty [h(\sigma)s - h(\sigma s)]\, se^{-s^2/2} ds| \qquad (2.21) \\ &\leq |\sqrt{\frac{2}{\pi}} \int_0^1 [h(\sigma)s - h(\sigma s)]\, se^{-s^2/2} ds| + |\sqrt{\frac{2}{\pi}} \int_1^\infty [h(\sigma)s - h(\sigma s)]\, se^{-s^2/2} ds| \\ &\leq \|h\| \sqrt{\frac{2}{\pi}} \left(\int_0^1 (1-s) se^{-s^2/2} ds + \int_1^\infty (s-1) se^{-s^2/2} ds \right) \\ &= 0.435 \|h\| \\ &< 1 \|h\|. \qquad (2.22) \end{aligned}$$

For the relay type nonlinearity, the harmonic balance gain $N_R = \sqrt{\frac{2}{\pi}} \frac{b}{\sigma}$ and equivalently

$$g(\sigma) = \frac{1}{\sqrt{2\pi}} \int_{-\infty}^{\infty} bse^{-s^2/2} ds = \frac{\sqrt{2}}{\pi} b. \tag{2.23}$$

The series evaluation for the inverse then gives

$$\begin{aligned} h^0(\sigma) &= g(\sigma) = \frac{\sqrt{2}}{\pi} b \approx 0.8b, \qquad (2.24) \\ h^1(\sigma) &= g(\sigma) + Mg(\sigma) \approx 0.96b. \qquad (2.25) \end{aligned}$$

with corresponding relative errors bounded by 0.435 and 0.189 respectively.

In combustion applications the variance of the signals both at the input and the output of the nonlinearity is not known (as heat release rates can not typically be directly measured). As a result, the procedure described above may not be directly applied. In the following paragraphs, we describe a procedure for estimating the heat release nonlinearities random input describing function gain by using small magnitude sinusoidal forcing. Before describing the procedure, we state a key result which makes the estimate feasible.

Result For a heat release nonlinearity, the random input describing function gain

$$N_R(\sigma) = \lim_{A \to 0} N_A(\sigma). \tag{2.26}$$

If the function h is additionally C^1, this gain is given by

$$N_R(\sigma) = \frac{1}{\sqrt{2\pi}} \int_{-\infty}^{\infty} h'(\sigma s) e^{-(s^2/2)} ds. \tag{2.27}$$

Proof. We first assume the function h to be C^1. The random input describing function gain (in the absence of any limit cycle oscillations) is given by

$$N_R(\sigma, A = 0) = \frac{1}{\sqrt{2\pi}} \int_{-\infty}^{\infty} \frac{h(\sigma s)}{\sigma} se^{-s^2/2} ds. \tag{2.28}$$

Using integration by parts, we may express the right hand side as

$$\begin{aligned} N_R &= \frac{1}{\sqrt{2\pi}} \frac{h(\sigma s)}{\sigma} e^{-s^2/2} \Big|_{-\infty}^{\infty} + \frac{1}{\sqrt{2\pi}} \int_{-\infty}^{\infty} h'(\sigma s) e^{-s^2/2} ds \\ &= \frac{1}{\sqrt{2\pi}} \int_{-\infty}^{\infty} h'(\sigma s) e^{-s^2/2} ds. \qquad (2.29) \end{aligned}$$

This gain needs to be estimated using sinsuoidal forcing. The sinsusoidal describing function gain (in the presence of noise of variance σ)

$$N_A(\sigma, A) = \frac{2}{(2\pi)^{3/2}A}\int_0^{2\pi} d\theta \int_{-\infty}^{\infty} ds\; h(Asin(\theta) + \sigma s)sin(\theta)e^{-s^2/2}. \tag{2.30}$$

Since $\int_0^{2\pi} sin(\theta)d\theta = 0$, we may write this gain as

$$N_A(\sigma, A) = \frac{2}{(2\pi)^{3/2}}\int_0^{2\pi} d\theta \int_{-\infty}^{\infty} ds \frac{[h(\sigma s + Asin(\theta)) - h(\sigma s)]}{A} sin(\theta)e^{-s^2/2}. \tag{2.31}$$

Now applying Dominated Convergence Theorem we have

$$\begin{aligned} \lim_{A\to 0} N_A(\sigma, A) &= \frac{2}{(2\pi)^{3/2}}\int_0^{2\pi} d\theta \int_{-\infty}^{\infty} ds\; h'(\sigma s)sin^2(\theta)e^{-s^2/2} \\ &= \frac{1}{\sqrt{2\pi}}\int_{-\infty}^{\infty} h'(\sigma s)e^{-s^2/2}ds, \end{aligned} \tag{2.32}$$

The equations (2.29) and (2.32) together give the result for a C^1 nonlinearity. For arbitrary bounded nonlinearity function h, we simply approximate the nonlinearity by a sequence of C^1 functions which converge (in a pointwise sense) to the function h and apply DCT to obtain the result.

The significance of the result is that the random input describing function gain may be estimated by carrying out a frequency response test with vanishing sinusoidal signal amplitude. Of course, for a system forced with very large bandwidth noise, one would get in to problems related to SNR so any estimate of the noise gain N_R would necessarily be biased.

Remark. The exact expression for N_R, the random input describing function gain also shows that as the variance σ of the Gaussian noise at the input of the heat release nonlinearity decreases, the gain $N_R(\sigma)$ increases.

The random input describing function gain is estimated by using a frequency response test. A feedback controller is used to manipulate the variance of the Gaussian noise seen at the input of the heat release nonlinearity. For each setting of the controller, a sinusoidal input is used to estimate the random input describing function gain N_R and this together with the variance computed from the time series is used for estimating the variance of the signals at the input and the output of the nonlinearity. By procuring these variances at different control settings, sufficient data is obtained to apply the procedure to compute the nonlinearity shape.

2.3.4 Simulations

A simulink model was used to build a mathematical model for the combustion block diagram described in Figure 2.12. We describe two simulations which were carried out to demonstrate the procedure described in sections 2.3.2 and 2.3.3.

First, we consider the no noise case. In the absence of noise, the combustion is unstable and a limit cycling system. The controller is used to vary the linear dynamics of the loop and the resulting amplitude of the pressure time series oscillations and the control input time series oscillations observed. These two amplitudes together with their phase differences and information on the linear dynamics present in the loop are used to estimate the amplitude information at the input and the output of the nonlinearity. These estimates are then used to estimate the nonlinearity shape. Figure 2.13 compares the actual nonlinearity with the one obtained from the experiment.

Next, we consider the case where a strong Gaussian noise component is present. In the absence of control, Gaussian noise balance accounts for the signals in the thermoacoustic loop (actually, a small limit cycle is present - see Figure 2.15). The control is used to manipulate the variance of the

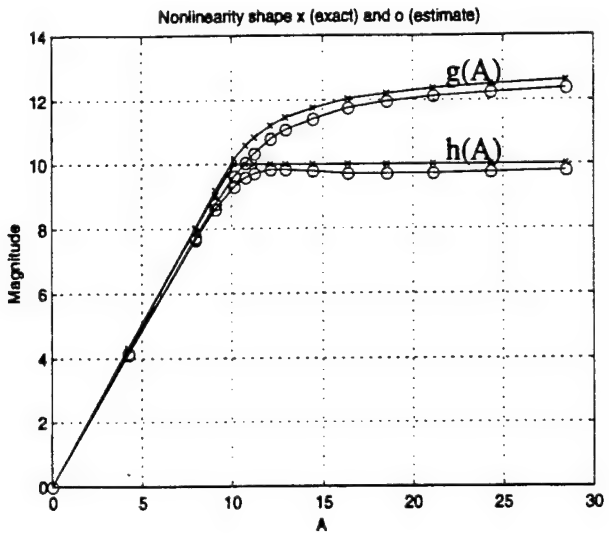

Figure 2.13: Estimate of the nonlinearity from the harmonic gains - limit cycling case

signal as seen at the input to the nonlinearity. A small amplitude forcing may be used to estimate the nonlinearity gain at each control setting as described before. The objective of this forcing test is to estimate the random input describing function gain. However, we have not been able to succesfully carry out this portion of the simulation yet.

Instead, we use the signals at the input and the output of the nonlinearity directly to estimate the harmonic balance gains. Figure 2.14 compares the nonlinearity shape estimated with this procedure versus the actual nonlinearity. The error between the two is due to the fact that the input and the output signals are not pure Gaussian signals rather are a combination of Gaussian and a sinusoidal limit cycle. Figure 2.15 plots the PDF (histograms) for the pressure time series. A single peak in PDF of pressure indicates a stable driven system. Double peak indicates a noisy limit cycle. For stabilizing control action (positive control gains), the signals are Gaussian and the PDF does not display any limit cycle component while for destabilizing gains(negative control gains), the limit cycle becomes prominent.

If one were to blindly treat the signals as Gaussian (as we have done here), the variance estimate is biased and the harmonic balance gains thus derived are incorrect. By the nature of the procedure, the error is larger for large σ where the control is most destabilizing (and hence the limit cycle component is the largest). A partial fix to this problem is to use Prabhir's algorithm to isolate the σ for the input and the output signals and use these instead. This will provide an improved estimate of the nonlinearity shape if the limit cycle amplitude is not significant.

However, a complete solution of the problem where both the limit cycle and the Gaussian noise components are together present requires an identification algorithm which incorporates the multiple input describing function. Though, this will be subject of future work, next section discusses some of the issues.

2.3.5 Limitations of the identification procedure

The available control authority fundamentally limits the identification of the nonlinearity. In the simulations provided here, unlimited control authority was assumed. However, the effect of limited control authority for the Gaussian noise and the limit cycling cases are fundamentally different.

For the limit cycling case, if one has information on harmonic balance gains for limit cycle ampli-

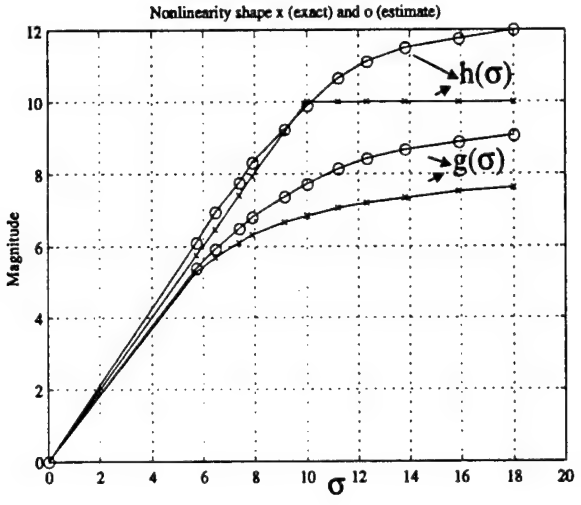

Figure 2.14: Estimate of the nonlinearity from the harmonic gains - Gaussian noise case

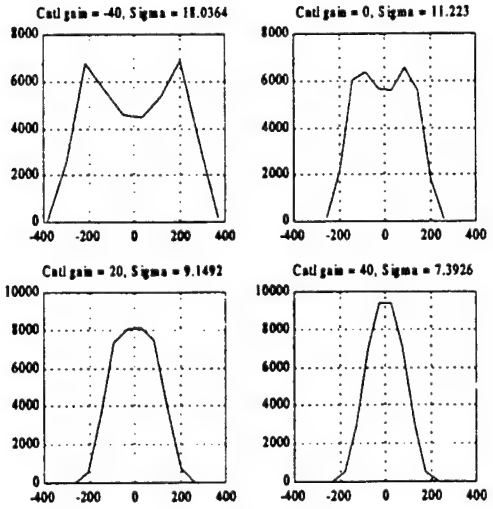

Figure 2.15: PDF of the pressure time series (input to nonlinearity) for different control gains - positive control gains are stabilizing and negative destabilizing

tudes from 0 to A then one can (in theory) identify the nonlinearity shape for *all* values of input from 0 to A with out any error. This is because of the nature of the operator M in the case of limit cycling (or sinusoidally forced) systems.

For the noise driven system however, in order to identify the nonlinearity precisely at any input level, information on harmonic balance gains from 0 to ∞ is required. This information is impossible to obtain from any realistic experiment. In any practical implementation of the procedure, the data points outside the range available are interpolated to recover the shape of the nonlinearity. As a result, any identification with Gaussian noise is necessarily prone to errors.

Finally, we discuss the problem where both the limit cycles and the Gaussian noise are together present. The problem there is to back out the nonlinearity shape from informations on N_R and N_A (the harmonic balance gains for the noise and limit cycles respectively) together with associated σ and A.

Chapter 3

Control of non-equilibrium behavior in aeroengines

3.1 Control of planar limit cycles

This section is an extended abstract of results presented in paper [c3].

There are numerous examples of systems where oscillations are attributed to stable limit cycles. Reduced order models of combustion instability [93] and compression system dynamics [37] are in this category. The control goal is to reduce the size or elimination of the limit cycle. One group of methods for control design are linear methods for damping augmentation of the unstable origin. The methods are essentially the same as the ones for damping augmentation of the stable linear systems. With large control authority the origin can be stabilized globally and the limit cycle will be eliminated. With small control authority the region of attraction of the origin will be extended, but the limit cycle will persist, possibly modified. In general, one cannot claim that the locally stable limit cycle will be reduced in size, even though this it typically expected. In fact, one can construct examples where the control action that extends the domain of attraction of the origin actually increases the size of the locally stable limit cycle.

In the case of limited control authority, when the elimination of the limit cycles is impossible, a control design aimed at reducing the size of limit cycles usually involves approximate methods based on harmonic balance (cf. describing function methods) where the controller is designed using the harmonic balance equation.

In paper [55] we investigated alternative methods of reducing the size of large limit cycles using control in the case of limited authority. We consider a planar nonlinear oscillatory system with bounded control. It is shown that under weak assumptions one can identify the controller that shrinks the existing limit cycles and maximizes the domain of attraction of the origin. Away from a small neighborhood of the origin, the optimal control action results in switching between the positive and negative saturation values. The switching happens on the curve where transverse linear controllability is lost and a collection of vector fields defining the local control properties of the system change orientation.We briefly compared the optimal approach to controllers suggested by a number of well known approximate techniques.

The control concepts are illustrated using the Greitzer compressor surge model. In the situation when the throttle is set so that the uncontrolled system exhibits a surge cycle, a control via small throttle variation can reduce or eliminate the surge cycle. It is also shown that in the case of the surge model the controller that locally minimizes the rate of divergence from the origin (in the given metric) is not optimal in the sense of convergence to a smallest possible periodic orbit.

We illustrated the results on Greitzer compressor surge model. Figure 3.1 shows the uncontrolled

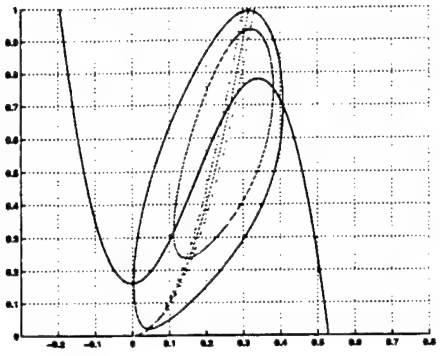

Figure 3.1: Uncontrolled and controlled surge cycle

and controlled surge limit cycles when the optimal control is used.

3.2 Adaptive control of combustion instability

Adaptation of control algorithm parameters to optimize the performance was demostrated at UTRC in combustion instability and in diffuser flow separation control. AFOSR-sponsored research played an important role in this development. Details are presented in papers [c10,c5,c7,j4].

Experiments and model-based analysis of combustion instability determined that pressure measurement and a simple phase-shifting algorithm with an appropriately chosen control phase is sufficient for suppression of oscillations, given enough control authority ([81, 82, 69, 94, 88, 96, 63, 70, 53, 54]).

The goal of using active combustion instability control on a gas turbine engine is to keep pressure oscillations at an acceptable level over a large range of operating conditions, without a perfect model of the process dynamics. Model based analysis determined that minimum information needed to calculate the best control phase for the combustion instability control requires estimation of parameters, including transport delay (or at least the corresponding phase shift), that are hard to obtain from pressure measurements alone [70, 53, 54]. Even if this difficulty could be circumvented, the sensitivity to modeling errors was likely to be high.

Need for developing an algorithm that would allow finding the best phase with minimum amount of a priori information that would work over large range of operating conditions and with minimum model assumptions seemed apparent. The operating conditions include fast engine acceleration and deceleration transients.

The algorithms developed at UTRC and presented in [56, 59, 60, 109] allow fast automatic tuning of control parameters and (under reasonable assumptions) can be guaranteed not to amplify the oscillations. Two extremum-seeking algorithms [98, 99, 78] have been selected for the tuning of the control phase. Model analysis indicated that the combustion process can include a simple pressure magnitude dynamics and fast stable dynamics describing other elements of combustion process and actuator dynamics. When an extremum-seeking algorithm is applied to such a model, it is possible to guarantee both convergence of the control parameter to the optimal value and the stability of the overall system. The analysis uses only the fact that the variable to be minimized (in our case the pressure magnitude) has an almost static dependence on the control parameter. The stability proof is possible if one exploits the time scale separation between the slow dynamics of the control parameter update law and the fast dynamics of pressure magnitude. There was a technical challenge in finding a phase shifting mechanism that works for pressure oscillations varying over large frequency range and in developing a reliable pressure magnitude detection mechanism. This challenge has been overcome with a frequency tracking observer algorithm (based on Extended Kalman Filter described in [83])

that allows for fast and reliable estimation of the in-phase and quadrature components of the bulk pressure mode over large range of frequencies.

Performance specifications for extremum-seeking algorithms have been defined for algorithm initialization transients and engine acceleration transients. When initialized with a phase corresponding to amplification of oscillations, the algorithms should quickly produce and maintain phases corresponding to suppression of the oscillations. In the engine acceleration transients the algorithms should be able to suppress oscillations relative to uncontrolled levels.

Experiments with an extremum-seeking adaptive scheme were conducted on a 4MW single nozzle rig at United Technologies in August 1998. The control gain was fixed and only the control phase has been updated. One of the algorithms relied on estimation of the derivative of the pressure magnitude with respect to control phase by introducing a small sinusoidal variation in the control phase and measuring the response of the pressure magnitude at the corresponding frequency. The mean control phase was incremented by an amount proportional to the estimated derivative.

Initialization transients were introduced where the initial control phase varied significantly from the optimal one. The algorithms behaved very well at high power condition (small pressure oscillations and medium level of broad-band disturbance) and reasonably well at low power conditions (large pressure oscillations and large level of broad-band disturbance). Once reaching a neighborhood of the optimal value, the control phase usually stayed in a reasonably small neighborhood of that value, rarely produced control phases corresponding to level higher than uncontrolled levels, and always provided better average pressure oscillations levels than uncontrolled levels. Figure 3.2 shows typical performance of the algorithms. Some control experiments were conducted with the sole purpose to

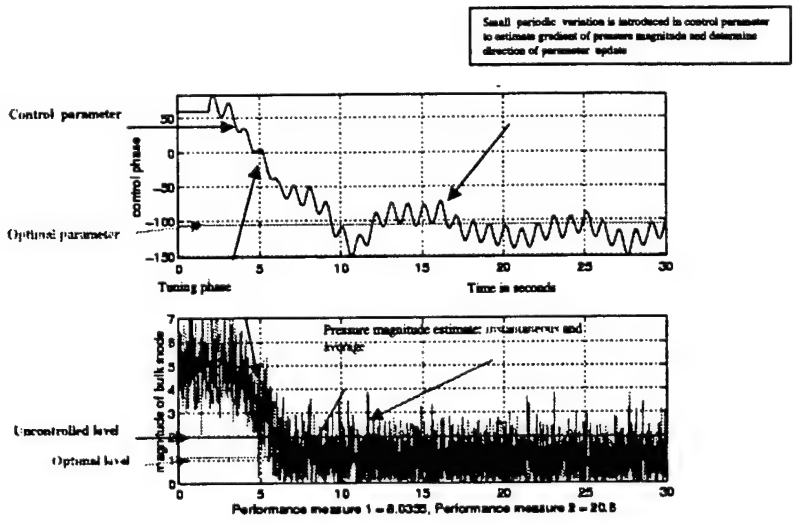

Figure 3.2: Extremum-seeking experiments: initialization transients. The initial control phase is strongly destabilizing. An optimal stabilizing phase is reached within three seconds.

identify the pressure magnitude dynamics and the noise to obtain a simple model of the slow part of the combustion process. This research was supported by the AFOSR grant. The model obtained at UTRC by Kartik Ariyur working under direction of Andrzej Banaszuk was used to study the adaptive algorithms off-line [60] and simulate fast engine transients that could not be introduced in the rig [56, 59].

A detailed model-based analysis of the adaptive algorithm based on averaging was conducted by Miroslav Krstic from UCSD and his student, Kartik Ariyur. This analysis provides two linear models, one for tracking reference changes and the other for sensitivity to noise, which offer insight into how

different parameters influence the performance [79, 60]. Details are presented in papers [c10,c5,c7,j4].

3.3 Control of vortex motion and chaotic advection

3.3.1 Introduction

This section is an extended abstract of the work described in detail in [c9,j3].

In the last two decades, much progress has been made in employing dynamical systems theory to laminar mixing [1, 2, 46, 48]. In much of this work the emphasis has been on *understanding the mechanisms* of mixing in laminar flows. For example Melnikov theory and associated lobe dynamics have been used to study transport and mixing in and out of the recirculation bubble of the vortex Batchelor couple in a pioneering study of Rom Kedar et al [47]. Those mechanisms are now well-understood in two-dimensional flows and partially in three-dimensional flows. In AFOSR-sponsored paper [44] we pursued a related question of *optimizing and controlling* transport and mixing in two-dimensional flows. Akin to first chaotic advection studies we chose a simple vortex model - a single vortex in a corner subject to a potential field. The motivation for the present study comes from studying flows in a combustor. (Vortex models have been used before for this purpose [31], but without forcing.)

In the absence of time-dependent forcing (introduced by modulating the potential field) the vortex wass either at a stable equilibrium position or was moving on a periodic trajectory in the plane. The first question that we asked was: if we allow for the arbitrary time-modulation of the potential field, can we move the vortex from an arbitrary initial position to an arbitrary final position in the plane? The answer to this question is shown to be positive using the transformation to the so-called *flat coordinates* [43, 18]. Having this result, we could proceed to search over all the trajectories of the vortex in a bounded domain of the plane and determine the optimal one with respect to a suitable measure. We chose this measure to be the flux through the heteroclinic orbit connecting two stagnation points of the partivcle dynamics (called separatrix), thus linking control theory and chaotic advection theory. Once the optimal trajectory was found, we stabilized it using a feedback law. The search for the optimal trajectory was pursued here using the numerical simplex method. Finally we showed that the problem presented here could be put in the context of Pontryagin maximum principle which provides a necessary condition for an optimal trajectory without utilizing the transformation to flat coordinates.

The results apply to the case of single vortex motion in an arbitrary domain driven by a potential velocity field with streamfunction Ψ_c.

For more details see [c9,j3].

3.3.2 Flattness-based control of vortex motion in a combustor recirculation region

The equations of motion for the vortex are given by

$$\begin{aligned} \dot{x}_v &= \frac{\partial \Psi}{\partial y_v} + \epsilon(t)\frac{\partial \Psi_c}{\partial y_v}, \\ \dot{y}_v &= -\frac{\partial \Psi}{\partial x_v} - \epsilon(t)\frac{\partial \Psi_c}{\partial x_v}, \end{aligned}$$

where $\epsilon(t)$ is the control input. The streamfunction of the control field can again be chosen as a flat coordinate, $z_1 = \Psi_c$. The other coordinate, z_2 is chosen such that $\dot{z}_1 = z_2$. Thus,

$$z_2 = \{\Psi_c, \Psi\} = \frac{\partial \Psi_c}{\partial x_v}\frac{\partial \Psi}{\partial y_v} - \frac{\partial \Psi_c}{\partial y_v}\frac{\partial \Psi}{\partial x_v},$$

where $\{\Psi_c, \Psi\}$ is the usual notation for a Poisson bracket of functions Ψ_c, Ψ. It is easy to see that

$$\dot{z}_2 = \{\{\Psi_c, \Psi\}, \Psi\} + \epsilon(t)\{\{\Psi_c, \Psi\}, \Psi_c\}.$$

Thus, the motion of a single vortex in a container of arbitrary shape under the influence of a potential field with a streamfunction Ψ_c is locally controllable if

$$\{\{\Psi_c, \Psi\}, \Psi_c\} \neq 0 \tag{3.1}$$

on the domain. (Another generalization holds for the case of n vortices under the influence of n potential fields. See [44] for details.)

In the corner problem the instantaneous flow is determined by the vortex position. Under periodic conditions, i.e. at natural or controlled periodic vortex motion, the fluid motion may be characterized by the Poincaré map $x^\star = \Phi_T(x)$, where x represents the initial position of the fluid particle and $x^\star$ the position one period T_{per} later. At small amplitudes, the Poincaré map has (at least) three fixed points, one at the origin, one x_s on the x-axes and one x_u on the y-axis (see Fig. 3.3). The fixed point x_s (x_u) has a stable (unstable) manifold $W_s(x_s)$ ($W_u(x_u)$) extending into the domain. The manifolds intersect each other infinitely many times near the fixed points [23]. Fixed points and invariant manifolds can be shown to be symmetric with respect to the $x = y$ bisector, if the vortex motion has the same symmetry and if the initial position of the vortex is on the $x = y$ line. We define a curve C which consists of the sections of the invariant manifolds from the fixed points to the first intersection point (Fig. 3.3). For the considered parameters, the curve is nearly circular. The recirculation region R shall be defined by the region bounded by the x- and y-axis and C. In the limit of small amplitudes R, the curve C converges to the steady state separatrix, except in an arbitrary small neighborhood around the fixed point. In the sequel, vortex motion is assumed to be periodic.

Mixing is associated with the behaviour of an ensemble of fluid particles over a finite period of time. A necessary condition for mixing between the free stream and the recirculation region is the fluid exchange across C, realizing that the net flux vanishes for incompressible flow. The instantaneous rate of fluid exchange is quantified by

$$\Phi_{inst} = \int_C ds\, |u_n|$$

where ds represents an arc element of C and u_n the normal component of the velocity. A suitable mixing measure Φ may be defined by the flux averaged over one period and normalized with the area $|R|$,

$$\Phi = \frac{1}{T_{\text{per}}\,|\mathcal{R}|} \int_0^{T_{\text{per}}} dt \int_C ds\, |u_n|. \tag{3.2}$$

Numerous measures for mixing can be considered depending on the application. Examples are (1) the flux according to Eqn. (3.2), (2) the fluid discharge during one period, (3) the size of the mixing region, (4) the average residence time of the transient fluid particles in the mixing region, (5) the average strain rate, since the strain is related to stretching of material lines and surfaces, (6) the growth rate of material lines and surfaces, (7) the average divergence rate of neighboring fluid particles (Kolmogorov-Sinai entropy), (9) any measure for the degree of finite-time homogenization of an ensemble of fluids particles. In [44] we restricted to a few of these quantities which can be expected to be of importance in the combustor. In particular case of the corner flow the lobe of the stable manifold W_s contains the fluid which leaves the recirculation region R during the period described by the Poincaré map (Figure 3.3). This fluid is bounded by the first intersection point, the W_s-lobe and the initial W_u section. The lobe of the unstable manifold W_u contains the fluid which enters R during the same interval. This fluid is bounded by the first intersection point, the W_u-lobe and the initial W_s section.

Hence, the intersection of both areas identifies the fluid which enters and leaves during the considered time interval, i.e. the area between invariant manifolds connecting intersection points 2 and 3. Thus, the total fluid exchange $T_{\text{per}}|R|\Phi$ during one period is represented by the areas bounded by C and both lobes, W_s, W_u, counting the overlap area twice. The region around the vortex which is embraced by both lobes neither leaves nor enters the recirculation zones during the considered period. The embraced region can roughly be identified as the trapped region neglecting convection effects due to the thin higher-order lobes near the axes (not resolved by present computations). Thus, the Poincaré map allows to draw many quantitative and qualitative conclusions about the mixing measures discussed in [44].

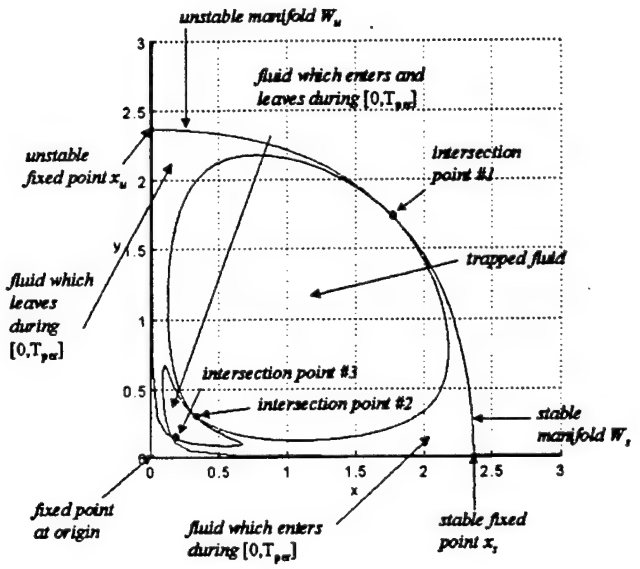

Figure 3.3: Invariant manifolds for the Poincare map of the controlled particles motion

Figure 3.4 illustrates the concept of using vortex model and methods from control theory and dynamical systems theory for control of mixing in the corner flow example.

For more details see [c9,j3].

3.3.3 Observer based control of vortex motion in a combustor recirculation region

The tracking control developed above postulates the availability of vortex coordinates for feedback. To become part of a plausible implementation framework it therefore needs to be complemented by a dynamic observer that translates some feasible sensor readings to state estimates. This section briefly summarizes aspects of an observer based design. More details are provided in [c11,j5].

The assumed measurements are of the x-direction fluid velocity, denoted u, at the normalized wall point[1] $(1,0)$. The following is an explicit expression for u

$$u = \partial_y(\Psi_{av} + (1+\epsilon)\Psi_c)|_{x=1,y=0} = 0.5(1+\epsilon) - \frac{8x_v y_v}{(x_v^2 + y_v^2 + 1)^2 - 4x_v^2} \tag{3.3}$$

The component $0.5(1+\epsilon)\alpha$ adds no information and will be ignored.

[1]Since our model does not account for viscosity, the idealization of velocity measurement at the wall is admissible.

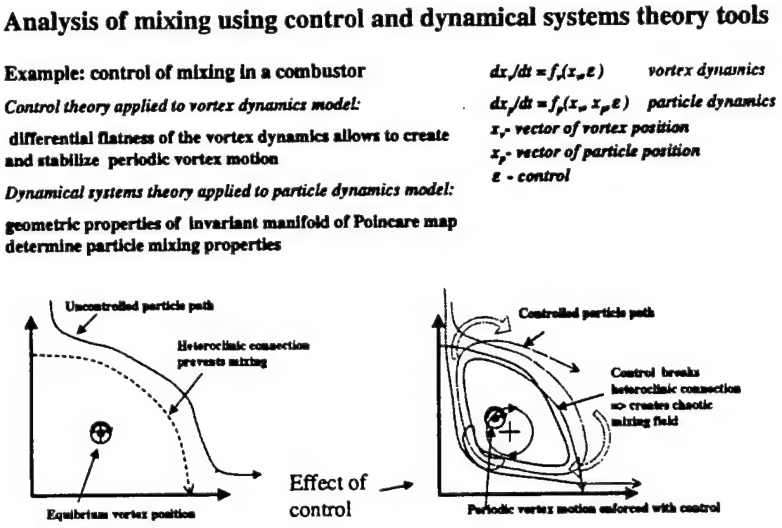

Figure 3.4: Illustration of control of mixing in the corner flow.

Straightforward analysis (left out) verifies that local linearizations of our system are observable almost everywhere, relative to the output u, and that the set (curve) formed by points of lost observability are not invariant. Nonetheless, we chose not to attempt to design a global observer. This was motivated by the level of nonlinearity of our system (including the vortex model and (3.3) and the fact that a global observer would require sensitive, state-estimate dependent gain scheduling. For example, an observer based on the canonical local coordinates $(u, \dot{u})$ [76, 58], would require back-and-forth coordinate change $(x_v, y_v) \leftrightarrow (u, \dot{u})$. Instead we opted for a local but more robust, fixed structure observer that will cover a neighborhood about the fixed point to which designated tracking orbits will be restricted. This observer will be used in conjunction with the state feedback policy proposed in previous section. It will be complemented by a dissipative feedback control, used to drive the vortex into the designated neighborhood. The latter does not require a detailed state estimate, and makes do with direct feedback of the measurement signal.

3.3.4 A Dissipative Constant Structure Observer for Small Deviations

To match the tracking feedback, the suggested observer is written in the flat coordinate system, and is thus form

$$\begin{aligned} \dot{\hat{z}}_1 &= \hat{z}_2 + \zeta_1(\hat{u} - u) \\ \dot{\hat{z}}_2 &= \hat{p} + \epsilon\hat{q} + \zeta_2(\hat{u} - u) \end{aligned} \tag{3.4}$$

where a hat indicates an estimated variable and where ζ_i are correction terms. The simplest option is that of using a constant linear gain -

$$\begin{bmatrix} \zeta_1 \\ \zeta_2 \end{bmatrix} = -\begin{bmatrix} L_1 \\ L_2 \end{bmatrix} \delta u \approx -\begin{bmatrix} L_1 \\ L_2 \end{bmatrix} [\partial_{z_1} u \;\; \partial_{z_2} u] \begin{bmatrix} \delta z_1 \\ \delta z_2 \end{bmatrix} \tag{3.5}$$

where δ indicates an estimation error. Using linear, small deviations approximations, the dynamics of state estimation errors are then governed by -

$$\frac{d}{dt}\begin{bmatrix}\delta z_1\\ \delta z_2\end{bmatrix}=\begin{bmatrix}-L_1\partial_{z_1}u & 1-L_1\partial_{z_2}u\\ -\frac{1}{z_1^2}(1-z_2^2)-L_2\partial_{z_1}u & 2z_2\left(1+\epsilon-\frac{1}{z_1}\right)-L_2\partial_{z_2}u\end{bmatrix}\begin{bmatrix}\delta z_1\\ \delta z_2\end{bmatrix} \tag{3.6}$$

and the selection of gains L_i should stabilize this system.

An intuitive guidance for such selection is based on assuring stability of the frozen time systems: it is an obvious fact that systems of the form

$$\frac{d}{dt}\begin{bmatrix}\delta z_1\\ \delta z_2\end{bmatrix}=\begin{bmatrix}-a & b\\ -c & -d\end{bmatrix}\begin{bmatrix}\delta z_1\\ \delta z_2\end{bmatrix} \tag{3.7}$$

with (constant) b, $c>0$, $a\geq 0$ and $d>0$, generates stable dynamics. Direct evaluation reveals that the signs of both partial derivatives $\partial_{z_i}u$ are both positive in a neighborhood of the rest point $(1,1)$. Following the frozen time intuition, this suggests using $L_1=0$ and $L_2>0$.

Since stability of frozen time system neither implies, nor is it implied by stability of the actual, time varying system, the latter has to be analyzed. To the very least, such an analysis needs to be applied to a periodic linearization, in a neighborhood of the designated reference trajectory. A useful tool here is to replace that periodic system by a linear time invariant model for *approximate dynamic phasors* of the error signal . The term dynamic phasors is used in reference to the time varying Fourier coefficients of a trajectory that is dominated by a known period T -

$$<x>_k(t)=\frac{1}{T}\int_T^0 x(t+r)e^{-j\frac{2\pi}{T}(t+r)}dr \tag{3.8}$$

Differential equations governing the evolution of dynamic phasors can be formally derived from the differential equation for the original time trajectory, using the equality -

$$\frac{d}{dt}<x>_k(t)=-j\omega<x>_k(t)+<\dot{x}>_k(t) \tag{3.9}$$

where $\omega=2\pi/T$. Approximate models are based on truncated Fourier series expansions. Dynamic phasors of a T-periodic trajectory are constant, and a desired periodic trajectory is thus represented by a desired set point in phasor representation. The linearized dynamic phasor model, about a desired set point is thus time invariant. Local stability analysis and guidance for parameter selections thus reduces to eigenvalue analysis in the respective model. In the present case, such analysis (left out here) reveals that stability is attainable for reference trajectories with a period of $\omega=1$, dominated by their first harmonic (in the flat coordinates), centered at the rest point and with a radius of ≈ 0.5.

3.3.5 A Simple Dissipative Measurement Feedback

The dynamic observer suggested above is restricted to periodic orbits in a neighborhood of the rest point. An additional control mechanism is therefore needed to drive the vortex into such a neighborhood. In the absence of an observer, such a mechanism cannot require detailed state information. The tool of choice here is the equation -

$$\frac{d}{dt}(\Psi_{mv}+(1+\epsilon)\Psi_c)=\dot{\epsilon}\Psi_c \tag{3.10}$$

By (3.10), any control selection that forces $\dot{\epsilon}\Psi_c<0$, is dissipative, and will drive the vortex towards the rest point. Moreover, since Ψ_c is close to periodic under low gain actuation, the same holds if $\dot{\epsilon}$

is selected to be (close to) zero mean, with $\dot{\epsilon}(\Psi_c - \overline{\Psi}_c) < 0$, where $\overline{\Psi}_c$ is the average over a period. The advantage of a zero-mean $\dot{\epsilon}$ is that it prevents a drift in ϵ, and results with a practically feasible bounded actuation signal.

Figure 3.5 shows plots of $\Psi_c - \overline{\Psi}_c$ and of a low-pass version of $u - \overline{u}$; both trajectories are associated with a vortex trajectory that slowly spirals towards the rest point. The phase match is obvious and a path to a stabilizing control is set. Figure 3.6 depicts the stabilizing effect of a low gain negative integral feedback $\dot{\epsilon} = -\delta(u - \overline{u}) - \rho\epsilon$, where $\delta > 0$ is a small gain and $\rho > 0$ is a small "forgetting factor" that is used to eliminate long term effects of deviations from the ideal zero-mean condition.

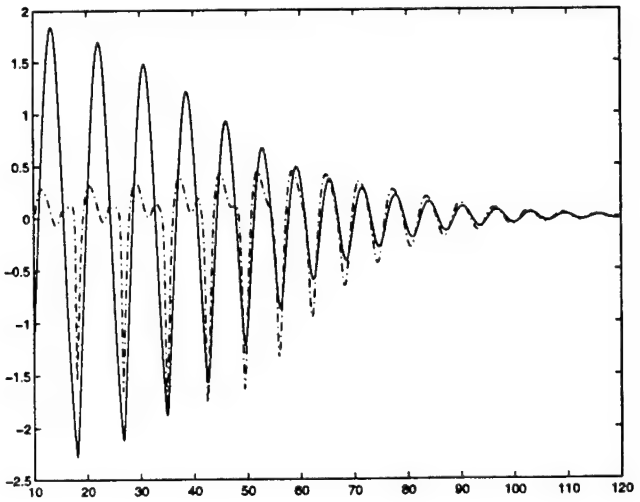

Figure 3.5: Plots of $z_1 - \overline{z}_1$ (solid) and a (low pass filtered) $u - \overline{u}$ (dashed) under low gain actuation.

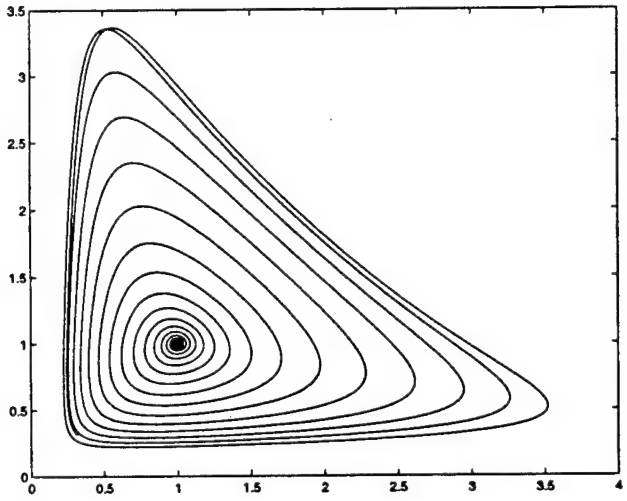

Figure 3.6: Phase portrait of vortex motion under the simple dissipative feedback

One practical aspect that needs to be resolved in implementing the dissipative control suggested above is a means of estimating the period of motion during weakly actuated, "large deviations". Such estimates are needed in order to extract $\overline{u}$ from velocity measurements. Additionally, an estimate of the total energy stored (based on the combined Hamiltonian $\Psi_{mv} + \epsilon\Psi_c$) is needed, in order to be able to determine whether the vortex entered (or left) the domain of the dynamic observer. Direct inspection reveals that (in the weakly actuated system), there is a monotonous, easily tabulated

relationship between both these quantities and the minimum over a period of the measured velocity u as depicted in Figure 3.7. Since period variations (in the normalized coordinates) are roughly bounded between $[2\pi, 3\pi]$, the estimation of both quantities - without a priori information - requires less then two periods.

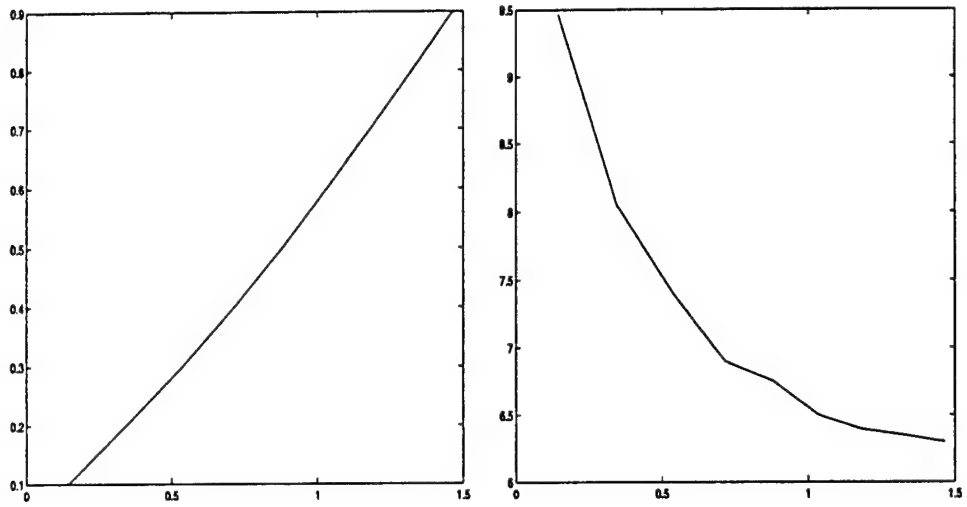

Figure 3.7: Plots of the approximate value of z_1 - when crossing the level $z_2 = 0$ (left) - and of the approximate period (right) in unactuated dynamics, as functions of the minimal absolute value over a period of the measured fluid velocity

3.3.6 A Global Observer Based Tracking Controller

A global controller is formed by patching the large deviations dissipative controller, as described right above, with a controller that combines the state-feedback tracking controller and the dynamic state observer, in a neighborhood of the prescribed vortex trajectory. As is usually the case, safe switching between different controllers is a delicate job. Critical issues include stability under the switching procedure and using hysteretic bands in the switching region, to avoid chatter. Details of these mechanisms are not specific to the focal points of this article and are left out. A demonstration of a response of the bi-modal closed loop system is depicted in Figure 3.8, where the controller - in dissipative mode - drives the vortex from the far field to the desired neighborhood, and then switches to steady state tracking of the designated trajectory.

3.3.7 Remarks On Generic Aspects

As some details of the developments described in this section may appear to be peculiar to the specific system at hand, it is worth highlighting those aspects that are likely to be generic to similar control problems involving low order vortex models.

• The first comment concerns the emphasis on a simple structure / constant gain observer. The systems under consideration are characterized by the facts that detailed models are both distributed and highly nonlinear, and that nonlinearity is a dominating aspect of even the simplest, lumped, low order models, used in control design. Absent reliable modeling error bounds, avoiding the use of a continuum (or a very large number) of local linearizations and elaborate, state estimate dependent coordinate change mappings, seems to be a matter of common sense prudence. Our example illustrates the fact that the domain of validity of a fixed structure observer may be large enough to cover the desired region of operation. In other systems, switching between a small number of fixed observers may

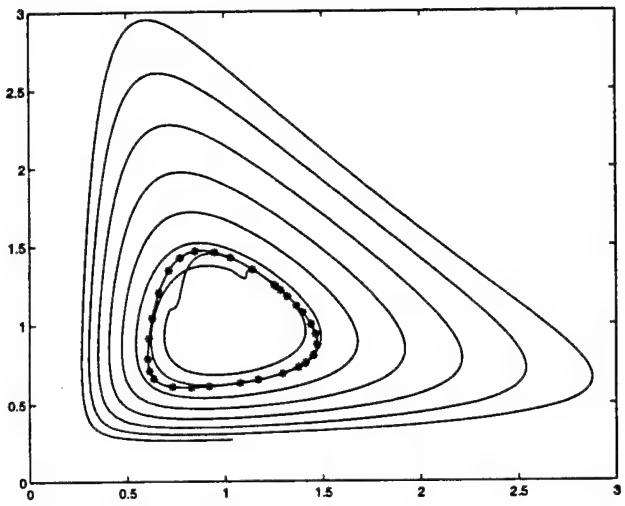

Figure 3.8: Closed loop tracking of a vortex orbit reference. asterisks: tracking reference orbit; bold: actual vortex trajectory

be necessary to cover the area of interest, but the objective of avoiding a continuous gain scheduling may still be attainable.

• When both free and controlled dynamics are periodic, direct readings of "over a period" properties of the sensed signal may provide valuable information. In particular, it may provide the triggers needed to switch between different modes of a multi modal controller, or even for direct feedback stabilization, as demonstrated by the present example.

• Continuing the focus on periodicity, linearized dynamic phasor models provide a useful tool for stability analysis and design parameter assignments.

• Its simplicity notwithstanding, a very interesting observation concerns the dissipative mode of the suggested controller. While standard dissipative controllers are based on adding or increasing some natural form of damping (e.g., current resistance or mechanical friction), our vortex model is inherently lossless in steady operation and control is not used to add damping in the above sense! Here we use an altogether different mechanism, based on the fact that the total stored energy is the sum of two distinct Hamiltonians (Ψ_{mv} and Ψ_c) and that control actuation is used to vary the relative weight of each of the two Hamiltonians in the combined energy term. In words, dissipation is achieved by varying the relative weight of Ψ_c in opposite phase to the variations in Ψ_c.

3.4 Diffuser pressure recovery control

UTRC has range of flow control programs, including DARPA Micro Adaptive Flow Control program aimed at helicopter retreating blade stall control. Recently, dynamical systems and control theory methods were applied to control of flow separation in diffusers within the Dynamic Separation Control project. This effort was partially sponsored by AFOSR. Details are decribed in paper [c6].

Aggressively open diffusers are subject to flow separation and hence loss of performance measured by the pressure recovery coefficient. This coefficient is defined by $C_p = \frac{\Delta p}{\frac{1}{2}\rho U_1^2}$, where $\Delta p = p_2 - p_1$ represents the static pressure difference between inlet and exit, ρ the density and U_1 the mass- and time-averaged inlet velocity. The subsonic diffuser performance measured by pressure recovery coefficient can be improved by increasing mixing of the high momentum free stream and low momentum fluid at the wall. Separation control in a diffuser at large angles of expansion was acchieved at UTRC experiments described in [38, 42, 12] via periodic forcing using a synthetic jet actuator located usptream

of the separation point. (Previously such concepts were used to control of airfoil separation [49]). Figure 3.9 shows the experimental setup. In particular, in [12] UTRC team and Brianno Coller

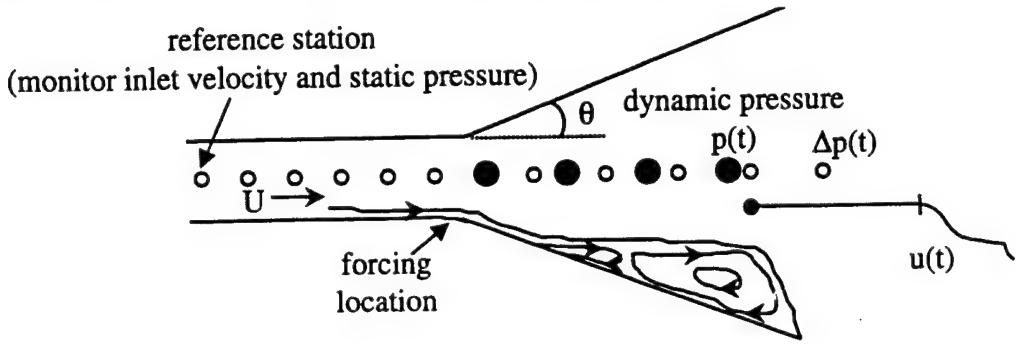

Figure 3.9: *Flow facility schematic*

has studied diffuser pressure recovery control using models and experiments. The new concepts in this study was to use control to excite beneficial non-equilibrium dynamics in the separating shear layer. Acoustic forcing at the beginning of the expanding section of the diffuser resulted significant performance enhancements for certain actuation frequencies as shown in Figure 3.10. Brianno Coller

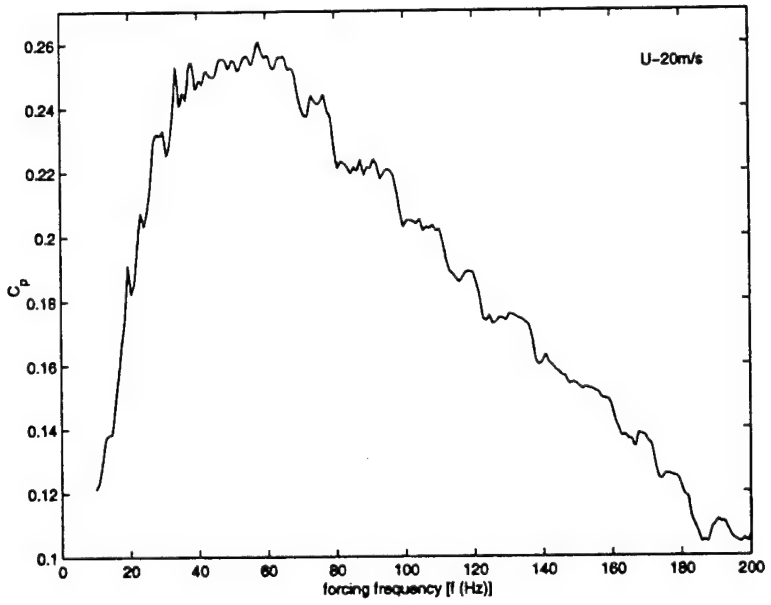

Figure 3.10: *Pressure recovery coefficient in terms of the frequency at the diffuser exit plane for the forced separated flow, showing sensitivity of performance to frequency.*

(in collaboration with UTRC reseachers) has developed a Lagrangian point vortex simulation [33, 35] to predict pressure recovery enhancement in a planar diffuser as a result of actuation [12]. Numerical results compared well with experiment. Qualitative evolution and interaction of the controlled vortices near the wall are visualized using smoke and are also found to match the model simulation results well.

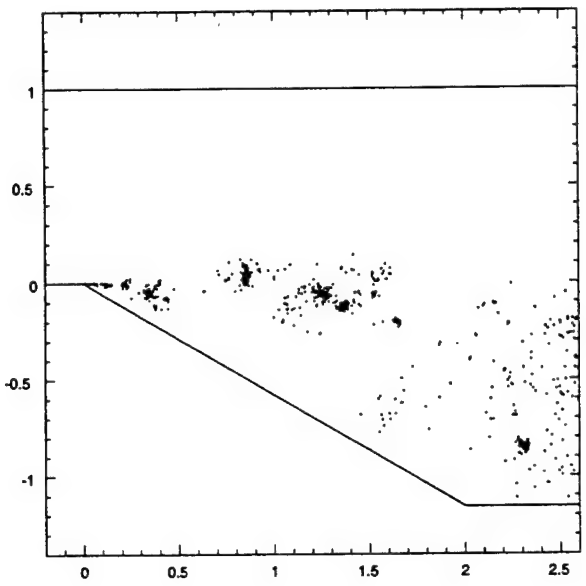

Figure 3.11: *Vortex formation of a diffuser flow forced with a Strouhal frequency of* $St = 0.3$.

For more information, please refer to paper [c6].

3.5 Control of mixing in jets in cross-flow

3.5.1 Introduction

Mixing in various places in combustor is the key to aeroengine performance and durability of its parts. The temperature *pattern factor* is a measure of nonuniformity of the temperature profile of the air approaching the aeroengine turbine. Nonuniformity creates excess oxidation and large thermal stresses in the turbine guide vanes that lead to destruction of the metal and hence to reduced turbine durability. On the other hand, because of high engine thrust requirements in military aeroengines, one needs to operate at high turbine inlet mean temperature conditions. This leads to high maintainance costs, as the vanes must be replaced often. The temperature profile is controlled by the mixing rate of the air jets injected into the combustion chamber along the combustor. Improved mixing of the air jets with the cross-flow carrying hot combustion products would allow a more uniform temperature profile of the air at the turbine exit, with reduced peak temperature and gradients, while maintaining the same mean temperature, and hence thrust. In this way an increase of mixing rates of jets in cross-flow using control would improve aeroengine affordability.

3.5.2 Description of Dynamic Combustion Enhancement project

The AFOSR sponsored research at UTRC in 2000 was focused on control-oriented modeling and model-based control of jets in cross flow. This work was an integral part of larger effort in Dynamic Combustion Enhancement (DCE), mostly sponsored by corporate sources. The goal of DCE project in 2000 was to demonstrate in experiment a significant mixing enhancement in jet in cross-flow using flow control, or prove using a model that this is impossible using low actuation level. The AFOSR project

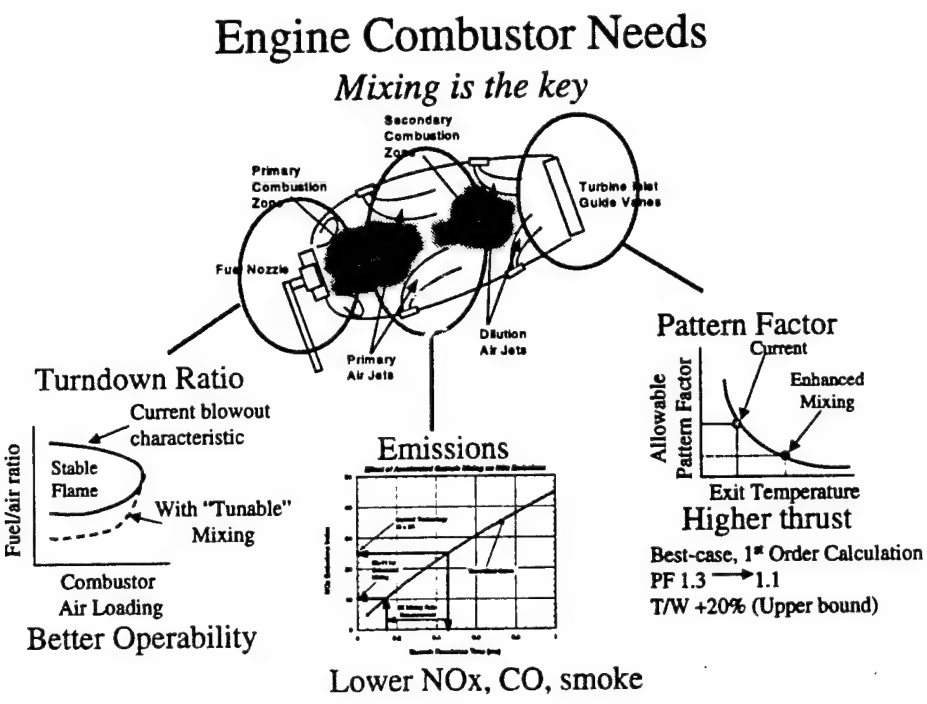

Figure 3.12:

was focused on development of tools for determining actuator placement and control laws based on reduced-order models. DCE project used the tools designed within AFOSR project and demonstrated mixing enhancement with control in experiments.

3.5.3 Physical phenomena observed in jets in cross-flow

It was determined from the literature studies done in January and February 2000 and from results of UTRC experiments and Large Eddy Simulations (LES) that the dynamics of the jet in cross-flow is dominated by two types of coherent structures (see Figure 3.13). The shear layer Kelvin-Helmoltz type structures occur where the jet bends in the direction of the cross-flow. Downstream of the bend the dynamics is dominated by streamwise counter-rotating vortices. This *counter-rotating vortex pair* (CVP) seems to be the main mixing mechanism of the uncontrolled jet. It is aggreed in the literature that CVP is the major mixing structure in the jets in cross-flow. The dominance of the coherent structures is a strong indication that reduced-order modeling is a viable modeling path. We would like to mention that even though the jets in cross-flow have been subject of extensive studies, the mechanism of creation of CVP is still a matter of controversy and active research.

Any study of mixing requires investigation of particle motion. In experiments this is done using Planar Laser Induced Fluorescence (PLIF) or MIE-scattering. For instance, in PLIF technique fluorescent particles are introduced to the jet flow and fast speed camera takes pictures of a planar sheet where a pulsed laser excites the fluorescence of the acetone. Figure 3.14 shows a typical experimental setting. In this way instantaneous measurements of the concentration of passive scalar introduced in the jet can be obtained with spatial resolution of 30 microns and temporal resolution of 30Hz. Averages of many snapshots allow to obtain spatial probability distribution of the passive scalar in the *measurement plane*. The probability distribution allows to calculate one of the commonly accept-

Jet in cross-flow: unsteady fluid structures determine mixing

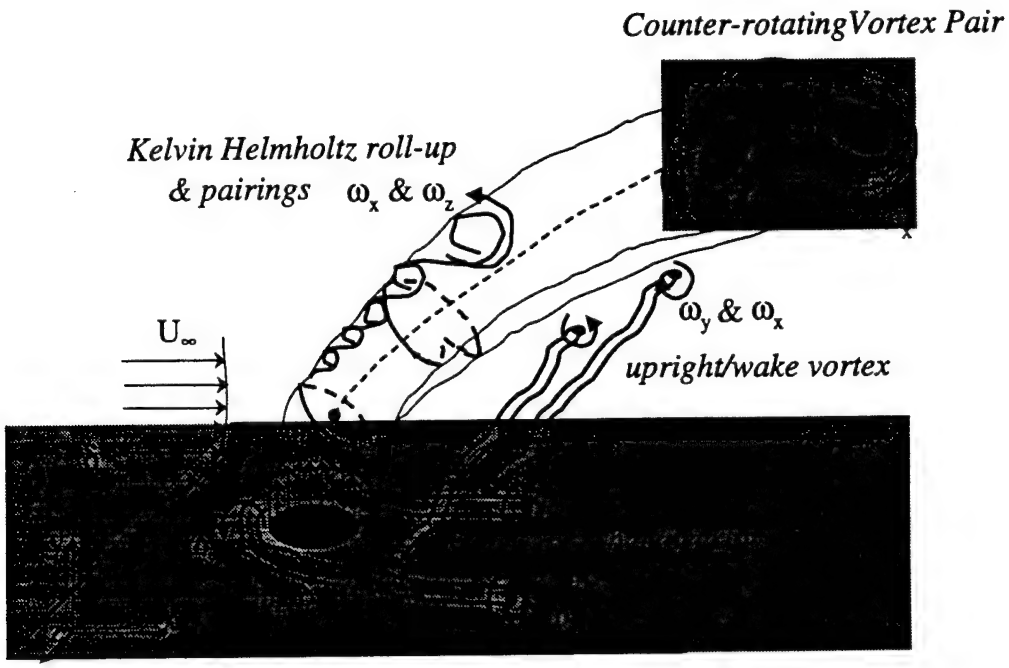

Figure 3.13: Coherent structures dominating in jets in cross-flow

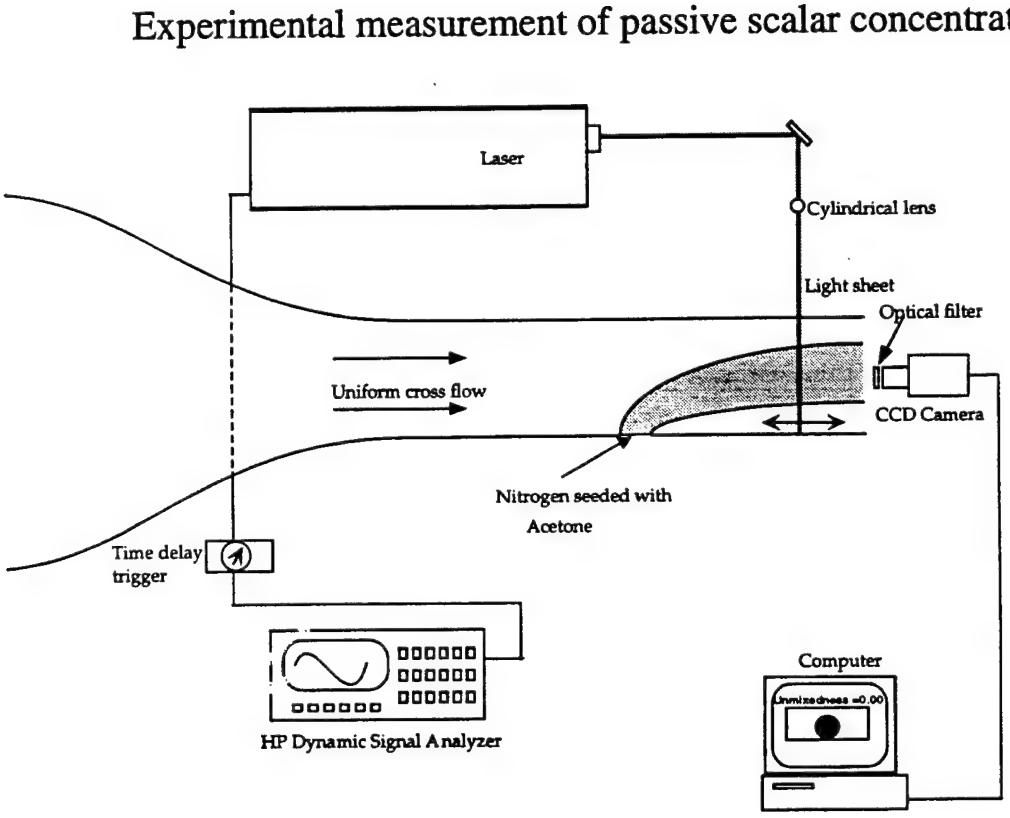

Figure 3.14: Measurement of passive scalar concentration in PLIF experiment

ed measures of mixing called *unmixedness*, defined as the ratio of the standard deviation of passive acalar concentration to its mean value. Decreasing of the unmixedness on a plane transverse to the jet located downstream of the jet bend by a significant factor is the goal of DCE project at UTRC.

Figure 3.15 shows results of passive scalar measurements in UTRC experiments. The analysis of passive scalar pictures shows the effect of the counter-rotating vortex pair on the passive scalar distribution.

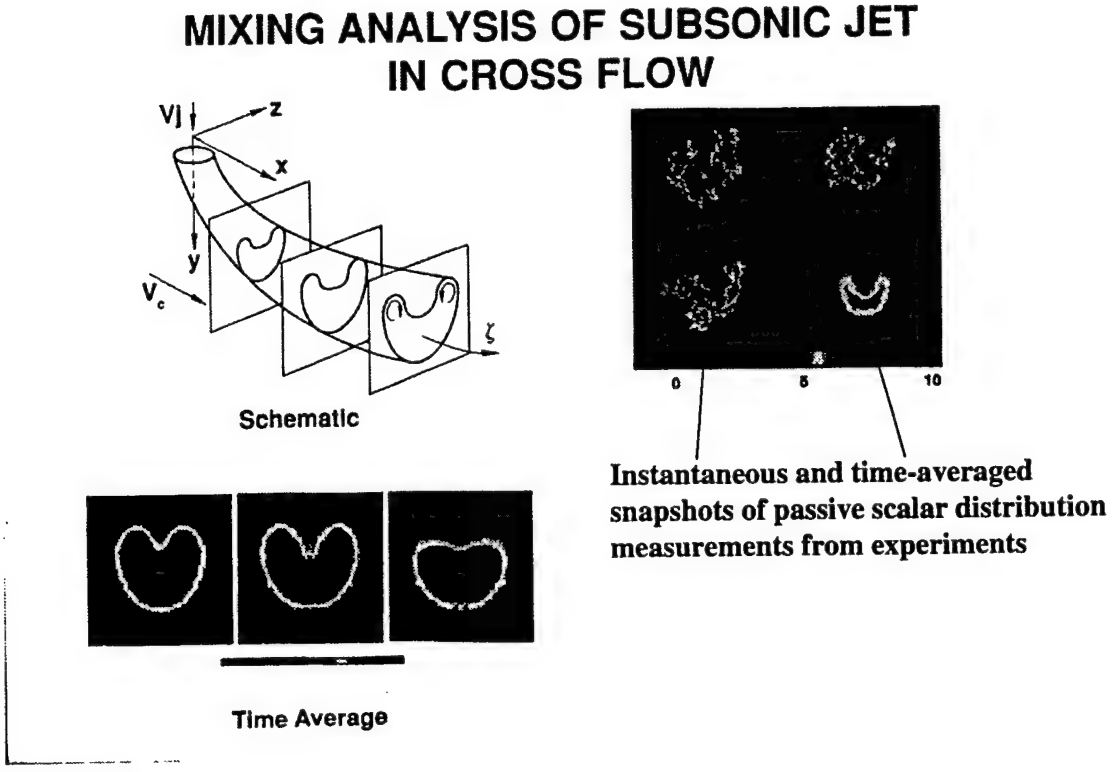

Figure 3.15: Experimentally measured passive scalar concentration in jet in cross flow experiments at UTRC

3.5.4 Mathematical description of the flow

We are interested in modeling a strong jet entering from a pipe into a crossflow. A schematic representation of such a jet is shown in Figure 3.13. The quantities U_∞ and U_{jet} are the velocities of the undisturbed crossflow and of the jet, and the radius of the jet is R_{jet}. We start with the assumption that for a strong jet in crossflow, the vorticity is concentrated on the surface of the jet [11]. Then the jet can be modeled by a cylindrical vortex sheet governed by the three-dimensional inviscid vorticity equation, i.e.

$$\frac{\partial \omega}{\partial t} + \mathbf{v}^T \nabla \omega - \omega^T \nabla \mathbf{v} = 0 \tag{3.11}$$

where $\mathbf{v}$ and ω are the velocity and vorticity vectors, and $\omega = \nabla \times \mathbf{v}$. In addition, the velocity vector $\mathbf{v}$ satisfies the incompressible continuity equation [6]

$$\nabla^T \mathbf{v} = 0 \tag{3.12}$$

Using Eq. (3.12), Eq. (3.11) can be further written in conservation form

$$\frac{\partial \omega}{\partial t} + (\nabla^T \mathbf{F}^T)^T = 0 \tag{3.13}$$

where $\mathbf{F}$ is the 3×3 flux matrix, i.e.

$$\mathbf{F} = \omega \mathbf{v}^T - \mathbf{v}\omega^T \tag{3.14}$$

The closure relation between the vorticity and velocity is given by the vorticity-induction equation (Biot-Savart law) [86]. The velocity $\mathbf{v}$ can be expressed as the sum of an irrotational component, the incoming crossflow velocity u_∞, and a solenoidal component, the vorticity-induction component $\mathbf{v}_\omega$

$$\mathbf{v} = \mathbf{u}_\infty + \mathbf{v}_\omega \ , \quad \mathbf{v}_\omega = \frac{1}{4\pi} \int_\nu \omega \times \frac{\mathbf{r}}{r^3} d\mathcal{V} \tag{3.15}$$

Passive scalar transport is described by the advection-diffusion equation

$$\frac{\partial c(x,t)}{\partial t} + \mathbf{v}(\mathbf{x},\mathbf{t})^T \nabla c(x,t) - \mu \Delta c(x,t) = 0. \tag{3.16}$$

For the flows of interest the advection term $\mathbf{v}(\mathbf{x},\mathbf{t})^T \nabla c(x,t)$ dominates the diffusion term $\mu \Delta c(x,t)$.

The passive scalar distribution from any model can be compared with experimental data obtained using the setup shown on Figure 3.14.

The control of the jet can be achieved by manipulation of boundary conditions. For instance, the profile of the flow entering the cross-flow from the pipe can be assumed to be a given function of time. The mixing performance can be measured by various functionals depending on the passive scalar concentration $c(x,t)$. For instance, the instantaneous unmixedness (the ratio of the standard deviation to the mean value) on the performance measurement plane $\mathcal{P}$ downstream of the jet bend.

The vorticity formulation of Navier-Stokes equation is an infinite-dimensional evolution equation with the right-hand side containing a nonlinear integral operator. The full infinite-dimensional model of jet in cross-flow is clearly intractable for analysis and control design. Reduced order modeling is a necessity. The current effort in control-orientted reduced-order modeling of jets in cross flow is described in the following sections.

3.5.5 Requirements for the control-oriented models

Since the goal of the project is to make an impact on Dynamic Combustion Enhancement future using methods of dynamical systems and control theory, we require the models to be *physically relevant*, *suitable for control design*, and *refinable*. Here is a more precise description of the metrics for the models.

1. **Physically relevant**. The models should adequately capture evolution and interactions of the most dominant coherent structures observed in the flow. In particular, this excludes input-output black-box models that do not use explicit physical parameters.

2. **Suitable for control design**. Models need to be suitable for *control design* using existing methods of control theory, not just *control simulations*. In particular, this implies strong preference for the following requirements.

(a) Explicit apperance of control input as a function of time, not just availability of few tunable parameters.
(b) Ability to explicitly calculate an instantaneous measure of mixing performance.
(c) Continuous finite dimensional description.

3. **Refinable.** The models should have a structure that allows one to obtain a more accurate spatial and temporal description of the flow when more computational elements are used. In the limit, the models should approach CFD accuracy of description.

The Lagrangian vortex models have many advantages over Eulerian CFD for simulations of shear flows at high Reynolds numbers [33, 33, 35]. The low order vortex models used effectively for dynamical systems studies of mixing. However, purely Lagrangian models are not best suited for traditional *control design* for the flows dominated by convection. The main problem is that the computational vortex elements have to be created and removed during *discrete events* determined by the computational algorithm. This makes Lagrangian models *hybrid.* Another disadvantage of Lagrangian vortex models is that the control input and surfaces on which the performance measure is evaluated are usually fixed in the Eulerian frame. Thus, in most cases of interest the Lagrangian models do not satisfy requirement of suitability for control design. Therefore, we decided to pursue an *alternative* modeling path. The concept of mixed Eulerian-Lagrangian models was introduced by Bernd Noack and Andrzej Banaszuk. A generalization of the concept for the three-dimensional vortex sheet was proposed Razvan Florea and is currently under development.

The model validation metrics has been defined as well. It has been determined that the models should agree with experimental data with respect to the following four metrics:
1. Jet centerline trajectory.
2. Counter-rotating vortex pair peak vorticity trajectories.
3. Circulation assigned to peak vorticity trajectory.
4. Passive scalar distribution.
All of these physical quantities can be obtained from experiments. The easiest ones to obtain are the jet centerline trajectory and concentration of passive scalar. The other two quantities require lengthy measurements of velocity fields by transversing a hotwire probe or a costly Particle Image Velocimetry (PIV) measurement.

3.5.6 Hierarchy of control-oriented models for jets in cross-flow

Hierarchy of models for jets in cross-flow created at UTRC includes the following models:
1. High complexity model: 3D spectral Direct Numerical Simulation (DNS) for jets in cross-flow including passive scalar transport equation to trace concentration of jet particles was developed and transitioned to UTRC by Thomas Bewley and Peter Blossey from UCSD. Code allows overnight simulations for both uncotrolled and controlled cases on UNIX workstations and fast PCs. DNS is considered physically relevant and refinable, but not directly suitable for control design (millions of states). The code was used for extraction of parameters of grey-box type models and for validation of low complexity models and control concepts derived using these models. After a suitable performance measure (penalizing nonuniform distribution of passive scalar) has been identified from studies of low complexity models we will attempt optimization of control laws and actuator locations.
2. Medium complexity models: 3D Eulerian/Lagrangian vortex sheet model has been introduced by Razvan Florea, Bernd Noack, and Andrzej Banaszuk and is currently being developed. The jet flow is modeled by a cylindrical vortex sheet. Starting with the incompressible vorticity equation, an integral formulation for the strength of the vortex sheet in a moving coordinate system is derived. The velocity field induced by the vortex sheet is given by the Biot-Savart law. The computational

mesh parametrizing the jet surface can move along planes locally transverse to the jet axis. This characterizes a "Lagrangian" part of the model. The transverse planes are either fixed, or can rotate with the jet surface but cannot move along the jet axis. This characterizes an "Eulerian" part of the model. The model is still under development. Boundary condition need to be fixed and the simulations results need to be validated. If the model is passes a validation test, it offers a great potential for control design. It is physically relevant, and refinable. The model uses a fixed number of states (of order of thousands). With the run time in minutes it is more suitable for control design than DNS. Unfortunately, control techniques applicable for models with thousands of states are still limited.
3. Low complexity model: parabolized two-dimensional two-vortex model has been developed by Thomas John, Satish Narayanan, Andrzej Banaszuk, and Shubhro Ghosh.

3.5.7 Control of jet in cross flow using DNS model

We have performed direct simulations of the jet in crossflow to evaluate the effect of forcing on mixing by the jet. Both forced and unforced cases were simulated at a Reynolds number $Re_j = U_j d_j/\nu = 3000$ and a jet velocity ratio $R = U_j/U_\infty = 6$. A number of forced cases were explored in shorter simulations, and two forced cases were chosen for long simulations to provide well-converged statistics for comparison with the unforced case. Both the time-averaged properties of the jets and the level of unsteadiness in mixing are evaluated using a number of metrics, including jet trajectory, spreading rate, entrainment and mixedness. The forced jets perform well in the time-averaged sense, although sometimes at the expense of an increase in unsteadiness. Results are described in papers [c12,j6].

The jet in crossflow has wide application in industrial and environmental flows. Dilution jets in combustors and cooling jets in turbines are examples of jets in crossflow in industrial flows. In the atmosphere, flows from smokestacks and chimneys as well as accidental ground level releases can be modeled as jets in crossflow. In some of these flows, buoyancy, heat release and compressibility may play important roles. However, the large-scale features of those flows may have much in common with a jet in crossflow in an incompressible flow. This study focuses on the study of mixing in such a fundamental setting through the tool of direct simulations. By modulating the jet inflow into the domain at a variety of frequencies, the effect of forcing on mixing is explored through a variety of steady and time-varying measures.

Study of the jet in crossflow has grown in recent years with new work by experimental and computational groups around the world. Detailed flow visualization studies have been performed by [19], [20] and [32]. The structure of the near field of the jet in crossflow was studied by [19], while [20] focused on the origin of vorticity in the wake of the jet in crossflow and found that separation events in the boundary layer surrounding the jet led to the formation of wake vortices. [32] further studied the formation of vorticity in the wake and the patterns of separation around the jet as well as in the pipe through which the jet flows into the domain.

Numerical Method

The governing equations used in these simulations of the jet in crossflow are the incompressible Navier–Stokes equations

$$\frac{\partial u_i}{\partial t} + \frac{\partial u_i u_j}{\partial x_j} = \frac{1}{Re}\frac{\partial^2 u_i}{\partial x_j \partial x_j} - \frac{\partial p}{\partial x_i} \tag{3.17}$$

$$\frac{\partial u_i}{\partial x_i} = 0 \tag{3.18}$$

An convection–diffusion equation is used to model the evolution of the scalar field:

$$\frac{\partial s}{\partial t} + \frac{\partial u_j s}{\partial x_j} = \frac{1}{Pr\,Re}\frac{\partial^2 s}{\partial x_j \partial x_j} \tag{3.19}$$

Both the Reynolds number of the channel flow Re_h, based on the free stream velocity U_∞ and the channel half-height, and the Reynolds number Re_d based on the jet diameter d and the centerline jet exit velocity U_j are 3000, while the velocity ratio $r = U_j/U_\infty$ is six in these simulations. The Prandtl number is taken to be that of air, i.e. $Pr = 0.7$.

Periodic boundary conditions are imposed in the streamwise and spanwise directions, and these directions are treated using the pseudospectral Fourier method. The wall-normal direction is discretized using a staggered, second-order finite difference technique developed by [8] . In the wall-parallel directions, the computation of the nonlinear terms is performed on a grid which contains 3/2 as many collocation points as the computational grid to eliminate the possibility of aliasing error. The Navier–Stokes equations are solved using a fractional step technique developed by [5]. The equations are advanced in time by a hybrid implicit–explicit scheme where the wall-normal convective and diffusive terms are treated implicitly. The implicit terms are handled by a Crank-Nicolson scheme while an explicit, low-storage, five-stage, fourth-order Runge–Kutta scheme [10] is used for explicit terms — the wall-parallel convective and diffusive terms. The implicit treatment of the wall-normal convection eases the restriction on the time step that would be imposed by the flow of the jet across the grid, which is refined in the wall-normal direction to resolve the large velocity gradients close to the wall. A linearization of the wall-normal convective term in the wall-normal momentum equation which preserves the second-order accuracy of the time integration [5] is employed to avoid the implicit solution of a nonlinear equation:

$$\frac{1}{2}\left(\frac{\partial u_2^{k+1}u_2^{k+1}}{\partial x_2} + \frac{\partial u_2^k u_2^k}{\partial x_2}\right) = \frac{\partial u_2^k u_2^{k+1}}{\partial x_2} + O(\Delta t^2) \tag{3.20}$$

The evolution equation for the scalar field is advanced in time using the same hybrid implicit–explicit scheme. However, the wall-normal direction is treated with an upwinding finite volume scheme for the scalar, and filtering of the high wavenumbers in the wall-parallel direction is also performed to avoid instabilities in the scalar computations.

Computational Setting

Although the use of a Fourier method for the wall-parallel directions provides a high degree of resolution, the grid is restricted to be uniform in these directions and cannot be refined in the neighborhood of the jet exit. As a result, the resolution in our simulations is marginal in the neighborhood of the jet exit. The computational grid is approximately 25 x 12 x 10 d in the streamwise, wall-normal and spanwise (x, y and z) directions, respectively. The grid spacing in the streamwise and spanwise directions is $\Delta x = \Delta z = 0.16 d_j$ on the computational grid, so that the jet orifice is represented by approximately twelve points. The grid in the wall-normal direction is defined using a hyperbolic tangent stretching function. The computational grid is 168 x 120 x 64, with 256 x 120 x 96 collocation points used in the computation of the nonlinear terms to eliminate aliasing error in the wall-parallel directions.

The domain of the simulations is channel flow, with periodic boundary conditions in the streamwise and spanwise directions and permeable, no-slip walls at the top and bottom of the boundary. The jet inflow is specified as part of the (possibly time-varying) boundary condition on the wall-normal velocity field. The boundary condition on the scalar is also specified at the top and bottom wall, allowing the scalar to be non-zero only at the jet exit. The inflow boundary condition upstream of the jet is enforced (weakly) through the use of a fringe region which removes disturbances 15 to 20 diameters downstream of the jet, creating a laminar inlet flow at the entrance to the box. The inlet flow is laminar, but the mean velocity profile is fuller than the parabolic steady state profile. The simulations used a profile of $U(y) = U_\infty (1 - y^8)$, which gives an initial boundary layer thickness of $\delta_{99\%} = 0.44h \approx 2d$. Thus, the boundary layer will grow as the flow moves through the domain but will not thicken substantially before reaching the jet orifice.

The jet is placed near the entrance to the domain in the streamwise direction and is centered in the box in the spanwise direction. The velocity profile at the jet exit is axisymmetric and is specified as a function of the radial distance from the centerline of the jet. A raised cosine filter is applied in Fourier space to the velocity profile at the jet exit to smooth the profile, preventing the excitation of high wavenumber oscillations in the velocity field by the jet. A region of distributed suction is placed near the exit of the domain to ensure that there is no net mass flux across each of wall.

The jet-in-crossflow has been simulated in a periodic channel-flow geometry, with the outflow velocity profile of the jet specified and the jet disturbances at the outflow of the domain removed by a fringe region to allow a nearly laminar inflow into the domain. The flow in the pipe leading to the jet outlet, which may separated before entering the domain at low jet velocity ratios [32], has been neglected in these simulations. The velocity profile where the pipe exhausts into the domain has been specified in the simulations as a Dirichlet boundary condition on the normal velocity, and the wall-parallel velocities on this plane have been set to zero. (The wall-parallel velocities could be non-zero, for example in the case of a swirling jet-in-crossflow.) Imposing the velocity profile does neglect the development of the pipe flow approaching the jet exhaust, but may be a reasonable approximation at higher jet velocity ratios. [32] noted that the flow in the pipe through which the jet flows into the domain did not separate for velocity ratios greater than six. The velocity ratio U_j/U_∞ is six. Although a top hat profile is desirable for the jet inflow, the non-dissipative Fourier spectral method used in the discretization of the wall-parallel directions requires smoothness in the velocity boundary conditions. As a result, the jet inflow is specified as an exponential function of the radial distance from the center of the jet and is then filtered using a raised cosine filter to remove high wavenumber content. The functional form of the jet inflow before filtering is:

$$U_j(r) \sim \exp(-\left(\frac{2r}{d_j}\right)^8) \tag{3.21}$$

where d_j is the specified diameter of the jet. Note that the velocity is not zero at the edge of the jet ($r = d_j/2$); it does, however, fall to zero quickly outside the edge of the jet. The mass flux into the domain from the jet is balanced by weak, distributed suction near the end of the computation domain. This suction overlaps with the fringe region and ensures that there is zero net mass flux across each of the wall-parallel planes in the channel in our incompressible flow.

Our computational domain is periodic in the streamwise and spanwise directions. If the fluctuations induced by the jet-in-crossflow are not removed before the end of the domain, they would substantially influence the flow dynamics around the emerging jet. A fringe region is added to the simulation domain to remove the fluctuations induced by the jet-in-crossflow and enforce the desired inflow conditions. The inflow is specified as $U_\infty(y) = (1 - (y/h)^8)$ with the wall-normal and spanwise velocities and the scalar set to zero at the entrance to the domain. Here, $y \in [-h, h]$ where h is the half-height of the channel. The displacement thickness of the boundary layer (computed over half of the channel) is somewhat smaller than the diameter of the jet exit ($\delta/d_j = 0.7$), while the momentum thickness is about a third of the jet diameter $\theta/d_j = 0.3$). The Reynolds number of these simulations based on jet diameter and free stream velocity $Re_\infty = U_\infty d_j/\nu$ is 500 with a velocity ratio U_j/U_∞ of six. One may also define the Reynolds number based on the jet exit velocity and jet diameter $Re_j = U_j d_j/\nu$ which is 3000 in these simulations.

Results

For a range of frequencies similar to but lower than those for round jets, forcing has a substantial impact on the structure and mixing of the jet. Forcing in the frequency range ($St_d = 0.1 - 0.25$) led to increased spreading of the scalar in the wall-normal direction and greater penetration into the crossflow. In these cases, the mean scalar profiles are qualitatively different from the unforced case, appearing

pinched in the center with legs of fluid stretched below. Fluctuations at the upper edge of the jet are enhanced by the forcing which excites the Kelvin-Helmholtz rollup. As expected (e.g. see [73]), forcing the jet at higher frequencies results in a jet which resembles closely the unforced jet. Examination of the frequency spectra at different locations in the jet shows that forcing at relatively high frequencies $St_d = 0.64$ persists only very close to the jet exit. Further from the jet, no peak in the spectra is visible at the forcing frequency: apparently, the jet in crossflow is not receptive to forcing at higher frequencies. Forcing at the lower frequencies $St_d = 0.1 - 0.25$ results in increased energy far away from the jet exit in this lower frequencies, providing an excitable band of frequencies which are beneficial for mixing. Figure 3.16 illustrates the effect of forcing on a downstream plane transverse to the jet. Forcing can have a substantial impact on the structure of and mixing by the jet in crossflow. We have

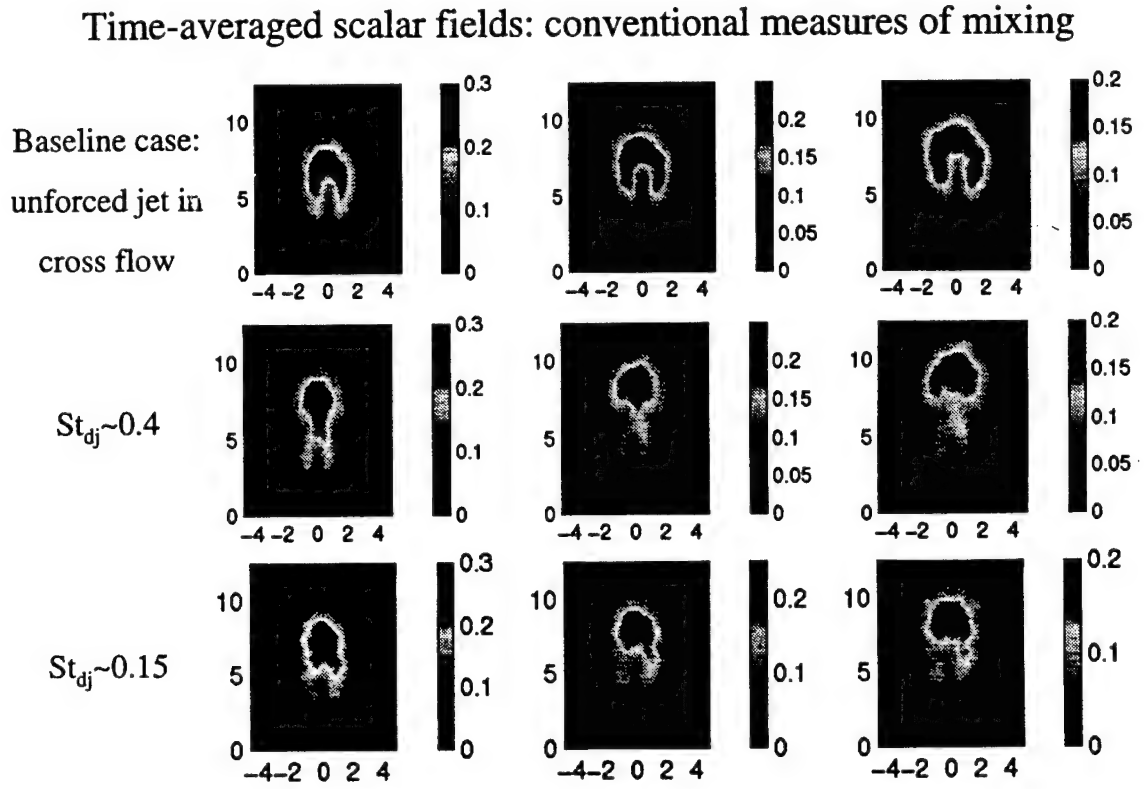

Figure 3.16:

simulated the jet in crossflow to examine the response of the jet to sinusoidal forcing at a variety of frequencies in the range $St_d = 0.1 - 0.64$. The effect of the forcing on the jet is most substantial in the range $St_d = 0.1 - 0.25$, with increased spreading, penetration and entrainment at those frequencies. The appropriate metric for mixing in the jets in crossflow is an open question. Increased spreading and entrainment often comes at the expense of increased unsteadiness and intermittency in the jet. The acceptability of this unsteadiness is primarily dependent on the timescale associated with the unsteadiness. In a cooling application for example, unsteadiness at timescales much faster than the characteristic heating/cooling timescale of a material may not result in substantial thermal cycling.

However, slower timescales could lead to substantial cycling and fatigue. Careful interpretation may lead to greater understanding of the importance of unsteadiness and the potential for increased mixing by forced jets in crossflow.

3.5.8 Three-dimensional Eulerian-Lagrangian vortex sheet model for the actuated jet in cross flow

A novel three-dimensional Eulerian/Lagrangian vortex sheet formulation was proposed to model the actuated jet in cross flow by Razvan Florea. An earlier version of a similar model was proposed by Bernd Noack and Andrzej Banaszuk.

The jet is modeled by a cylindrical vortex sheet. Starting with the incompressible vorticity equation, an integral formulation for the strength of the vortex sheet in a moving coordinate system is derived. The velocity field induced by the vortex sheet is given by the Biot-Savart law. The advantage of the present formulation is that a fixed number of states is required to describe the evolution of the jet in time. Such a formulation is very attractive for further developing of control strategies to enhance molecular mixing.

The motivation for the present approach is to derive a model that can both capture the mixing characteristics of a jet in cross flow and be further used in active control studies of the actuated jet. Some of the present models based on LES/DNS are very sophisticated and require an extremely large number of states and long time simulations with little physical insight. Other models, physical-based reduced order models, while are computational less expensive, are either derived in a Lagrangian frame with a variable (non-fixed) number of states [16], [17], or are too simplified and less relevant from the physical point of view [27]. For a review of the jet in crossflow research we refer to a paper by Margason [87]. All these models prove to be less appealing for active control studies. What we are looking for are reduced order models that can capture the main aspects of mixing and at the same time be used in active control studies. We want physically relevant reduced order models with a finite number of states.

The present investigation tries to incorporate in a rigorous manner the Eulerian/Lagrangian formulation into a novel three-dimensional integral formulation of the vorticity equation. Another attempt of the present formulation is to maintain the main characteristics of a CFD type discretization for a relatively smaller number of states system.

We are interested in modeling a strong jet issuing from a pipe into a crossflow using vortex type methods. For a review of such methods we refer to a paper by Leonard [85]. A schematic representation of such a jet is shown in Fig. 3.17. The quantities U_∞ and V_{jet} are the velocities of the undisturbed crossflow and of the jet, and the radius of the jet is R_{jet}. We start with the assumption that for a strong jet in crossflow, the vorticity is concentrated on the surface of the jet [11]. Then the jet can be modeled by a cylindrical vortex sheet governed by the three-dimensional vorticity equation (3.11), the incompressible continuity equation (3.12)

The closure relation between the vorticity and velocity is given by the vorticity-induction equation (Biot-Savart law) (3.15). The velocity $\mathbf{v}$, at a point defined by the position vector $\mathbf{x}$, is expressed as the sum of an irrotational component, the incoming crossflow velocity u_∞, and a solenoidal component, the vorticity-induction component $\mathbf{v}_\omega$

$$\mathbf{v} = \mathbf{u}_\infty + \mathbf{v}_\omega \ , \quad \mathbf{v}_\omega = \frac{1}{4\pi}\int_{\mathcal{V}} \omega \times \frac{\mathbf{x}-\mathbf{x}_0}{||\mathbf{x}-\mathbf{x}_0||^3} d\mathcal{V}(\mathbf{x}_0) \tag{3.22}$$

Here the quantity $\mathbf{x}_0$ is the position vector of any point of the sheet vorticity defining the jet.

To discretize Eq. (3.13) we consider an elemental volume $\mathcal{V}$ attached to the jet moving surface, and can move within the surface. Hence, the elemental volume $\mathcal{V}$ is not a material volume, it has a velocity $\mathbf{u}$ which can be different from the velocity $\mathbf{v}$ of the material volume that coincide with volume

$\mathcal{V}$ at time t. The velocity $\mathbf{u}$ is going to be the projection of $\mathbf{v}$ on some particular local surface that is going to be defined later. We integrate Eq. (3.13) over an elemental volume $\mathcal{V}$ and after applying the Reynolds transport theorem, we obtain

$$\frac{\partial}{\partial t}\int_{\mathcal{V}} \omega d\mathcal{V} + \int_{\mathcal{S}} \mathbf{F}_s d\mathcal{S} = 0 \tag{3.23}$$

The quantity $\mathcal{S}$ is the moving surface describing the boundary of the volume $\mathcal{V}$, and $\mathbf{F}_s$ is the flux matrix corresponding to the moving surface

$$\mathbf{F}_s = \omega(\mathbf{v}-\mathbf{u})^T - \mathbf{v}\omega^T = 0 \tag{3.24}$$

We assume that, at any moment t, the jet surface can be parameterized by a set of quasi-orthogonal system of coordinates (x_2, x_3), where x_2 is along the jet and x_3 is across the jet surface. Note, that this is a moving mesh which deforms in both space and time and has a fixed number of points. In addition, we introduce the coordinate x_1 normal to the jet surface, i.e. (x_1, x_2, x_3) form a three-dimensional system of coordinates, assumed to be orthogonal. Shown in Fig. 3.18 are the mesh parameterization of the jet surface, a view of of the elemental volume $\mathcal{V} = \Delta x_1 \times (EFHG) = \Delta x_1 \times \Delta x_2 \times \Delta x_3$, and the local system of coordinates.

For each point on the surface mesh we denote the corresponding versors associated with the local system by τ_1, τ_2 and τ_3, and the components of the velocity vector by v_1, v_2 and v_3 along these directions. Note that the vorticity ω, at any point on the mesh, is tangent to the surface mesh at that point. Hence, ω is defined locally only by the two components ω_2 and ω_3.

The position of each point on the mesh that describes the jet is given by the ordinary differential equation

$$\frac{d\mathbf{x}}{dt} = \mathbf{u} = v_1\tau_1 + v_3\tau_3 \tag{3.25}$$

Hence, its section is aloud to move to move with the jet surface but not along the jet. As a result, the number of sections and states needed to represent the jet is constant. This characteristics defines the "Eulerian" part of our Eulerian-Lagrangian model. In a three-dimensional Lagrangian vortex model [17], at each moment in time, as the jet penetrates the cross flow, new solutions and corresponding states are introduced. These states follow the flow and leave the domain as the flow crosses the downstream far-field boundary. This transport of states through the domain makes the Lagrangian vortex model to be less appealing for an efficient analysis of the jet actuation.

Next we describe shortly the numerical implementation of our model. For convenience we introduce two quantities γ_2 and γ_3 defined by

$$\int_{\mathcal{V}} \omega d\mathcal{V} \approx \omega \Delta x_1 \Delta x_2 \Delta x_3 = \underbrace{\omega_2 \Delta x_1 \Delta x_3}_{\gamma_2} \Delta x_2 \tau_2 + \underbrace{\omega_3 \Delta x_1 \Delta x_2}_{\gamma_3} \Delta x_3 \tau_3 \tag{3.26}$$

Then the differential form of the Eqs. (3.23) and (3.24) in the local system of coordinates (x_1, x_2, x_3) is given by

$$\frac{\partial}{\partial t}(\gamma_2 \Delta x_2) - (\Delta x_3)\frac{\partial}{\partial x_3}(v_2\gamma_3) = 0 \tag{3.27}$$

$$\frac{\partial}{\partial t}(\gamma_3 \Delta x_3) + (\gamma_2 \Delta x_2)\frac{\partial v_3}{\partial x_3} + (\Delta x_2)\frac{\partial}{\partial x_2}\left(v_2\gamma_3\frac{\Delta x_3}{\Delta x_2} - v_3\gamma_2\right) - (\Delta x_3)\frac{\partial}{\partial x_3}(v_3\gamma_3) = 0 \tag{3.28}$$

These equations are discretized in space using centered differences in the x_3 direction and upwinded differences in the x_2 direction. We integrate numerically Eq. (3.15) with the Gauss-Legendre quadrature rule. We use three-dimensional local cubic interpolation for the vector $\mathbf{x}$ that describes the jet surface and linear interpolation for the components γ_2 and γ_3 of ω. We use a simple corrected Euler (second order) for the time integration Equation (3.13) and the resulting space discretization of Eqs. (3.27) and (3.28).

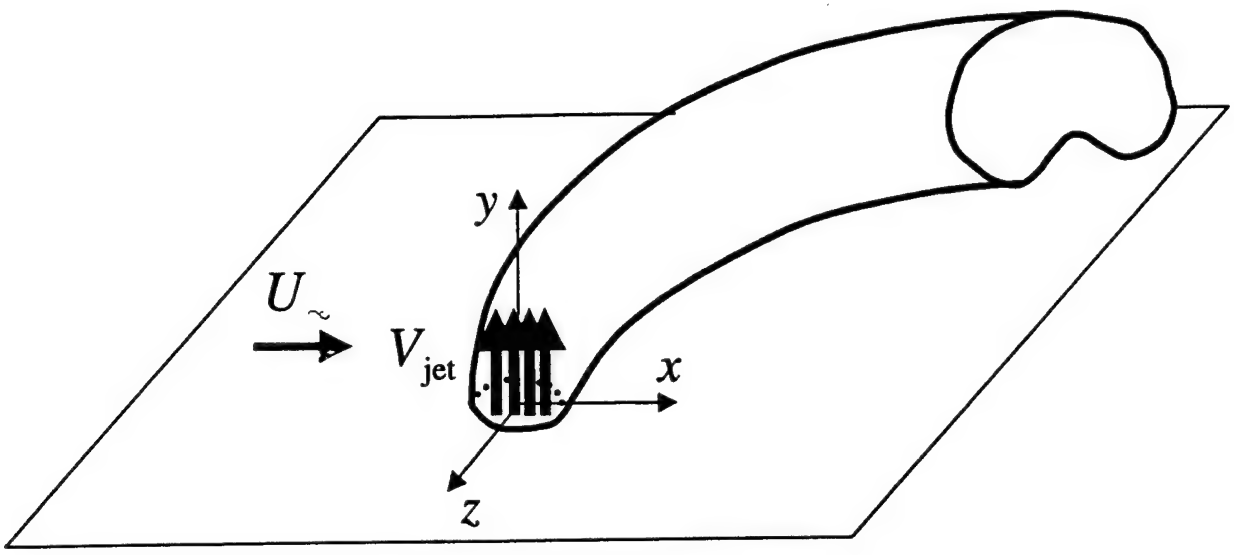

Figure 3.17: Jet in cross flow.

We impose that the flow around the wall is tangential to the wall. At the wall surface level, near the duct, outside the jet, the flow moves around the jet, tangential to the jet. We also impose the velocity of the jet flow, in a cross section of the duct, normal to the wall. We modeled these conditions using rings of distributed vorticity on the wall, around the duct, γ_{W3}, and on the duct wall, bellow the wall, γ_{D2} and γ_{D3}. Shown in Fig. 3.19 is the type of discretization we use for the initial jet, duct and wall. The above boundary conditions are solved implicitly at each moment in time. Using the velocity induced by different vortex sheets (wall, duct and jet), an algebraic system of equations is formed and the solution is found using an LU decomposition. Note that the matrix of this system does not change in time, the elements of this matrix are defined by the Biot-Savart law and as a result depend only the geometrical position of the wall and duct.

At $t = 0$, we impose the additional condition that the vorticity distributions below the wall, around the duct, and above the wall, on the jet are identical. This initial solution is further marched in time.

To show the effectiveness of the near-field boundary conditions, we show in Fig. 3.20 the initial velocity profiles in a vertical plane. The first case corresponds to a core size of 0.1 of the local mesh size, the second one corresponds to a core twice the local mesh size.

Computing the correct velocity of the jet surface in the Eulerian-Lagrangian formulation requires additional attention. At each moment in time, for a given geometry we compute the velocity induced (Biot-Savart) by the vortex sheet. Note that the surface is defined by rings that are allowed to deform with the jet surface but not allowed to move along the jet. Next, we allow the vortex surface to move in space and a new surface is defined. The new surface is interpolated at cross sections corresponding to the old rings and new rings are defined. The difference in space between the old and new rings determines the correct velocity of the jet surface. This approach requires further investigations to understand the effect of the additional errors introduced with the interpolation. These errors may become important when geometrical instabilities form on the surface of the jet.

The finite number of j sections which define the jet, and the finite length of the jet cause additional difficulties. For the moment, we used an increased core for the vorticity at the end of the jet. However the effect of these approximations require further investigations.

To assess the effectiveness of the near-field boundary conditions we model the evolution of a jet in cross flow defined by the following parameters: $U_\infty = 1.$, $V_{\text{jet}} = 6.$, , $R_{\text{jet}} = 1$. The jet is modeled by $j = 35$ rings with $k = 19$ points per ring.

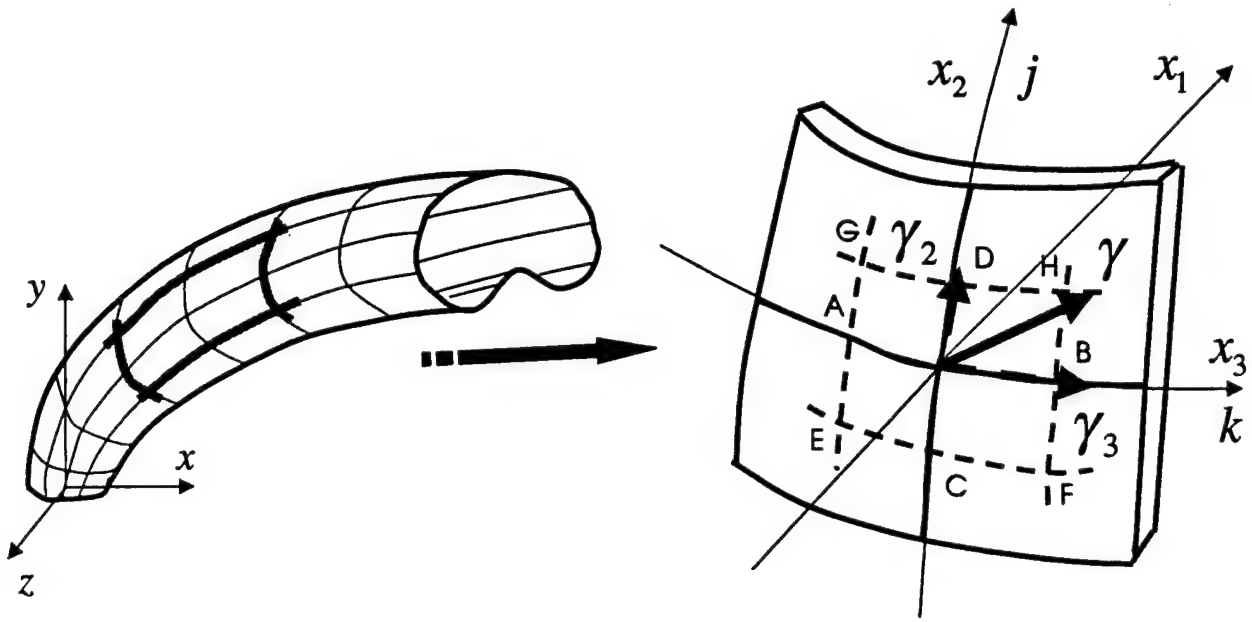

Figure 3.18: Jet in cross flow. Left: quasi-orthogonal mesh parameterization of the jet surface. Right: elemental volume $\mathcal{V} = \Delta x_1 \times (EFHG)$, and local system of coordinates.

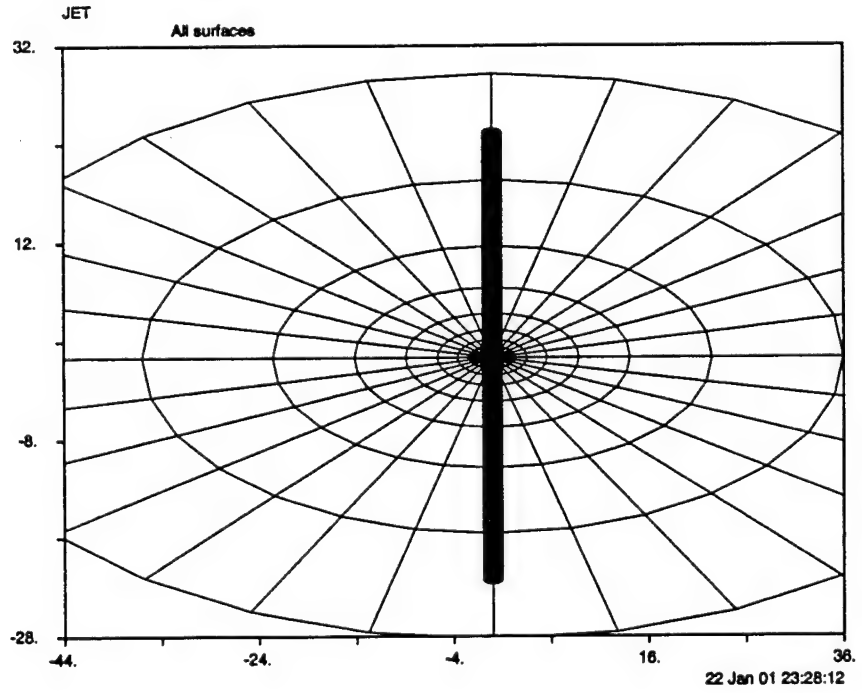

Figure 3.19: Initial jet, duct and wall discretization.

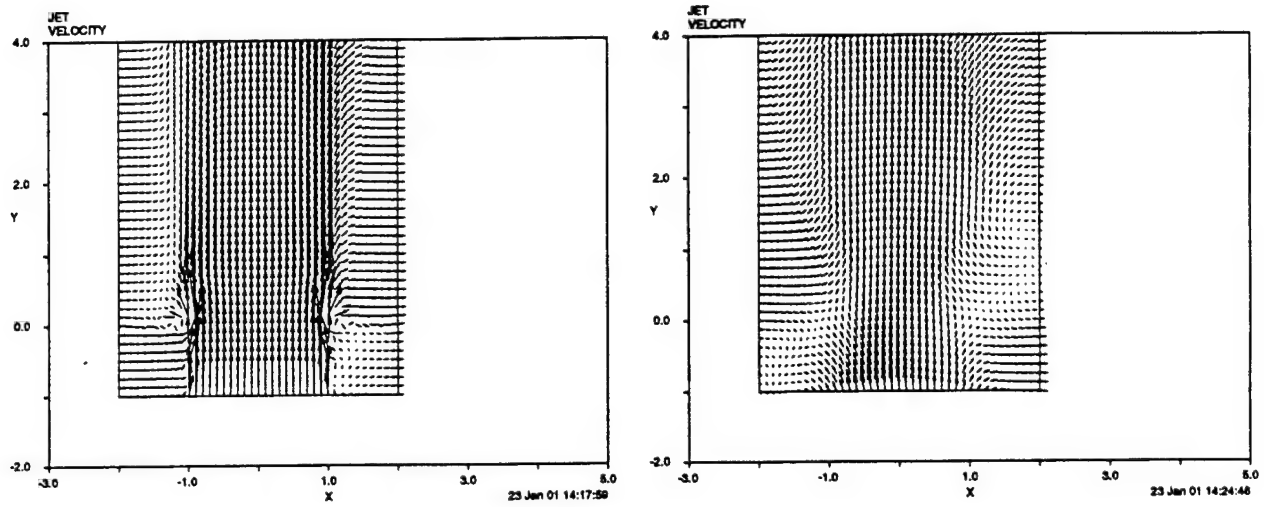

Figure 3.20: Initial velocity profiles in a vertical plane through the jet center. Left, core size of $0.1 \times \Delta s$. Right, core size of $2. \times \Delta s$. Δs - local mesh size parameter.

To accelerate the convergence of the jet to its final position, the jet is also constantly moved (rotated) in the direction of the U_∞ for the first 100 iterations. We show in Fig. 3.21 the jet evolution after 20, 60, 100, 200 and 1000 iterations. In addition, we also show in Fig. 3.22 shape sections of the jet (after 1000 iterations). We note that due to errors in interpolation (described in Section C.), the jet starts to loose its symmetry.

For the same kinematic conditions, we varied initial conditions (length of jet, imposed motion of the jet in the x direction) and the mesh density. We found that the most dynamic part of the jet is near the wall where the counter rotating vortex pairs are formed. The upper part of the jet behaves in a more static way. Based on its length and inclination, it induces a component of the jet velocity near the wall that has direct effect on the jet bending and the CVP formation. As a result, the combination of the initial conditions and the errors in the interpolation process has direct effect on the solution evolution, preventing the jet to evolve to the correct position.

3.5.9 Two-vortex model for the actuated jet in cross flow

A parabolized two-dimensional two-vortex model has been developed by Thomas John, Satish Narayanan, Andrzej Banaszuk, and Shubhro Ghosh.

The dynamically significant flow structures appear to be (see Figure 3.13) the shear layer structures generated by the Kelvin-Helmholtz (KH) instability, the counter-rotating vortex pair (CVP), a typically weak horseshoe vortex (appearing for low jet Reynolds numbers near the jet and cross-flow bottom juncture), and an upright/wake vortex system that develops very close behind the jet (resembling a wake of vortices). Of these, we only discuss and model the KH and CVP dynamics and mixing characteristics. In doing so, we use inviscid descriptions of the flow features and structures, ignoring fine-scale turbulence driven viscous effects. We do not attempt to model or explain the appearance of the KH or CVP structures, but, given their presence and from their observed behavior, we provide a modeling framework for studying the KH-CVP system dynamics to analyze/derive control solutions for mixing enhancement.

Kelso, Lim & Perry [32] based on their experimental study of jets in cross-flow, hypothesize the formation of vortex rings (as a result of the Kelvin-Helmholtz instability of the jet shear layer) from the jet which get distorted due to the crossflow such that: the upstream portion stays in a plane transverse to the jet and the downstream portion bends *along* the direction of the jet. while being positioned in a high speed region of the jet, resulting in its stretching (i.e. vorticity intensification).

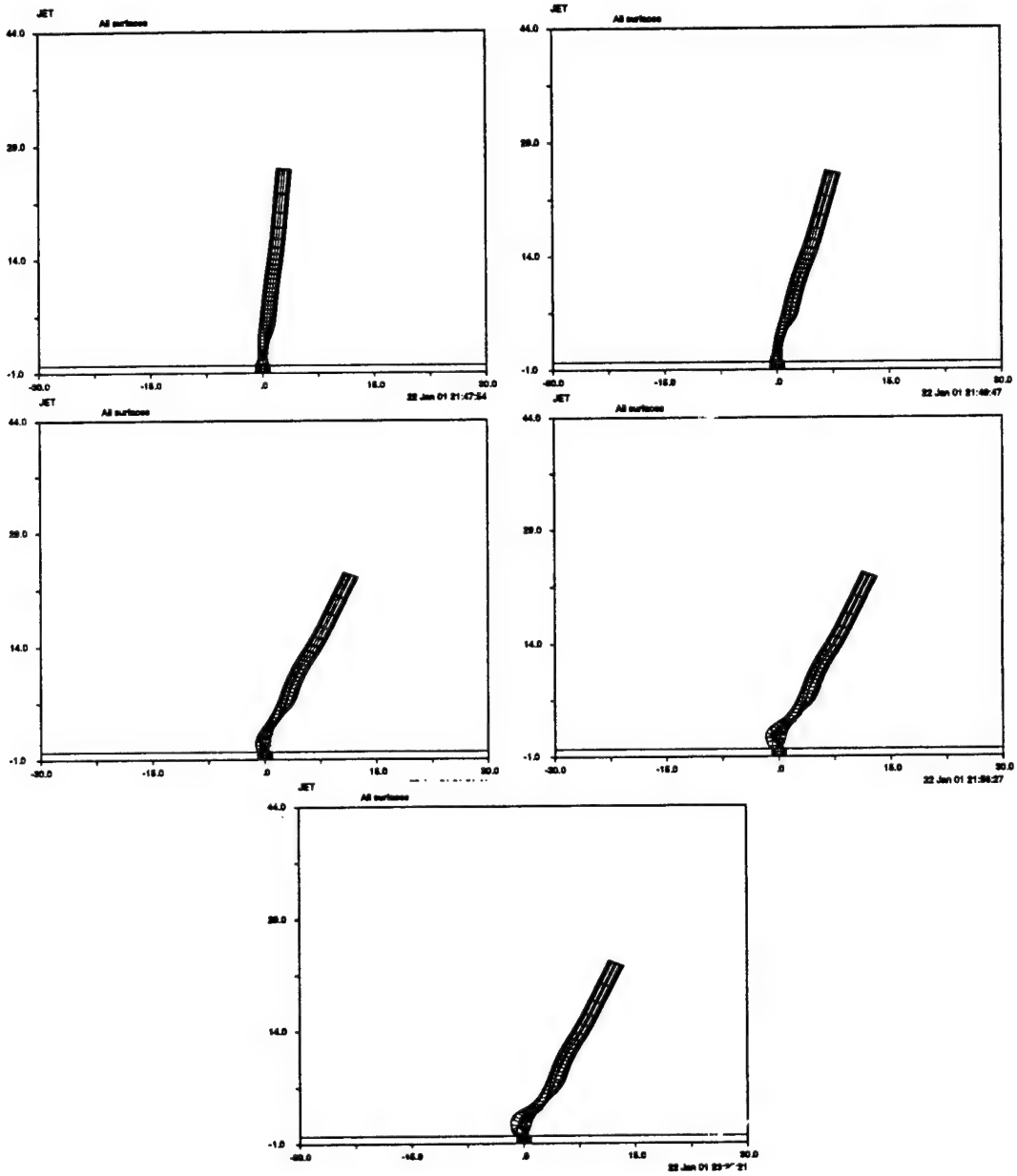

Figure 3.21: Jet evolution after 20, 60, 100, 200 and 1000 iterations.

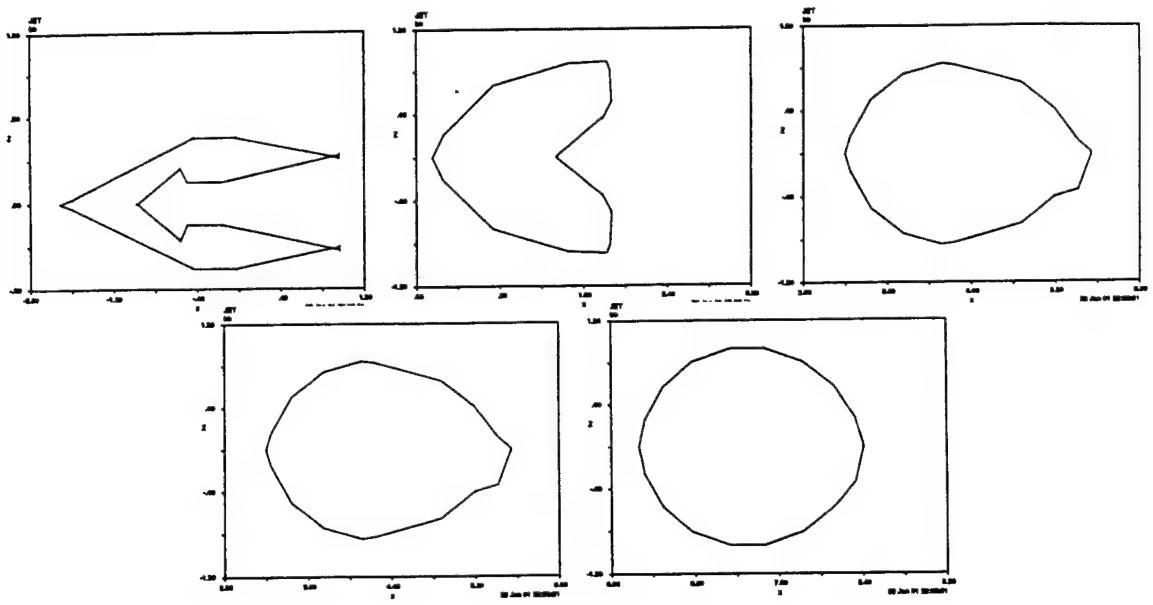

Figure 3.22: Shape sections of the jet at $J = 5, 10, 15, 20, 30$.

Cortelezzi & Karagozian note similar behavior of the vortex rings in their simulations of a jet in cross-flow using 3D vortex filament simulations.

Using a direct numerical simulation (DNS) of jet in cross-flow (P. Blossey & T.Bewley, UCSD), the circulation in a plane normal to the jet trajectory was computed to obtain the circulation in the CVP at several points along the trajectory. The circulation is seen to increase and then decrease along the trajectory (see Fig. 3.23).

We now focus on the evolution region from 2 to 6 jet diameters, where the KH formation has been initiated and the out-of-plane vorticity necessary to initiate the CVP motion has already been set up.

We simplify and represent the array of vortex rings by "horizontal" (transverse to the jet direction) rods of vorticity, representing the upstream KH ring and two growing (stretching)"legs" to represent the jet portion that has been bent along the jet direction(see fig. 3.24).

(More features may be added if they are felt to be important for mixing studies.) The transverse rod is moving at a speed of U/2 (typical convection velocity of structures in a shear layer) and the legs are growing with respect to the rod at a rate of U/2 (since they are in a portion of the jet which is moving at a higher velocity, say U)

As mentioned before, the legs grow away from the transverse rod at the same rate that the rod moves away from the jet exit. So, if the rod if s_1 away from the pipe, the tip of the leg is $2s_1$ from the mouth (see fig. 3.25).

The long bar on the side represents the initial circulation in the CVP (Γ_0). As seen from the figure, if we were to add up the circulation in a plane transverse to the jet, its value would increase as one moves downstream.

Now we consider as our model plane, a plane moving at a speed of U along the jet trajectory. This plane sees an array of vortex rings (in reality from KH structures formed) that are moving at a speed of U/2 into it(see fig. 3.5.9).

As each of these rods crosses the plane, it leaves its leg in the plane forever and thus the circulation of the CVP on the plane is always increasing ; note the similar circulation growth feature from the DNS studies summarized earlier. Furthermore, note that the frequency of KH rods is twice that of the pulsations of the CVP. Please see figures 3.5.9, 3.5.9 & 3.5.9.

The slope of the increase of the CVP is thus dependent on two quantities – the frequency of the

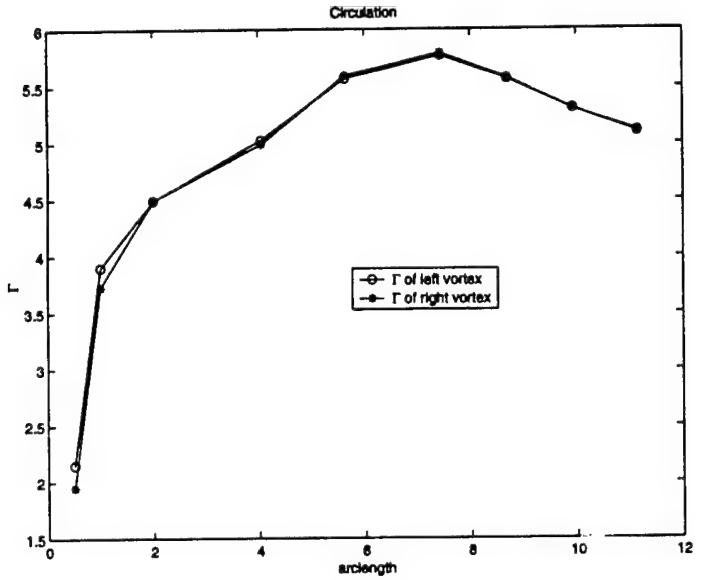

Figure 3.23:

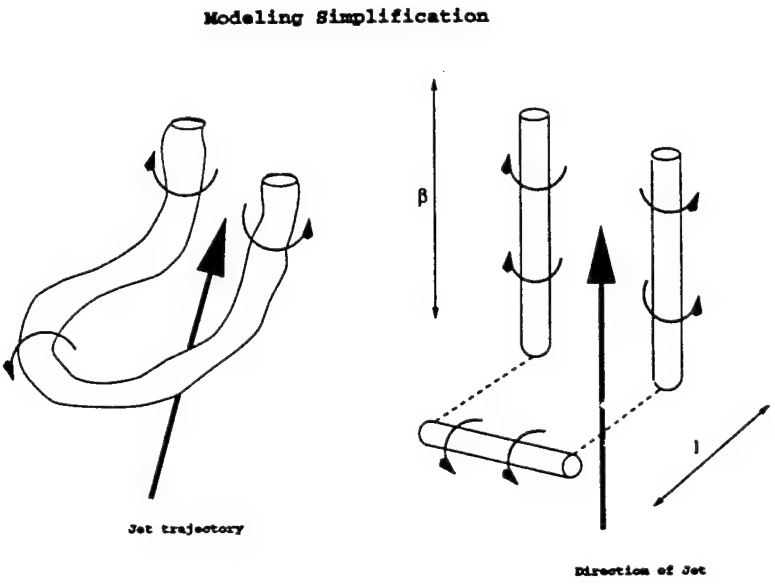

Figure 3.24:

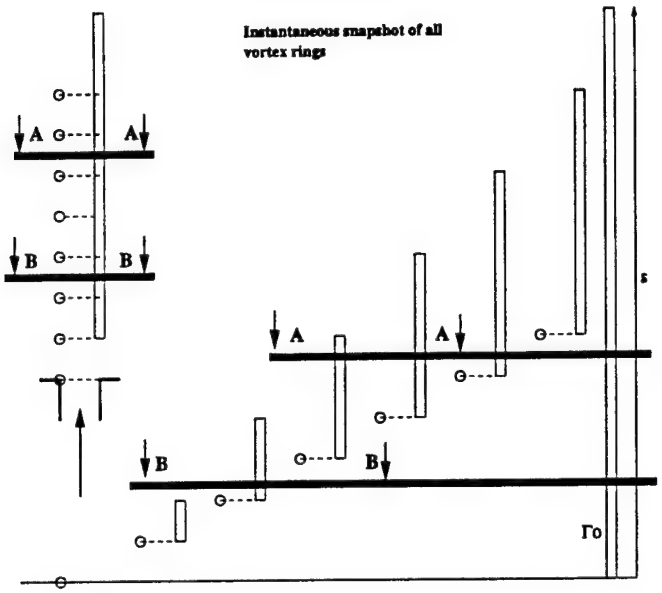

Figure 3.25:

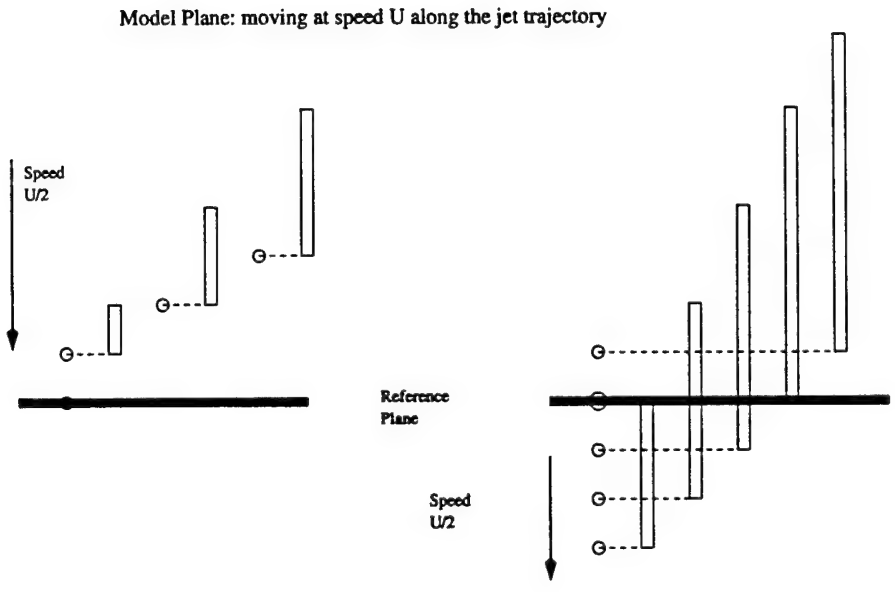

Figure 3.26:

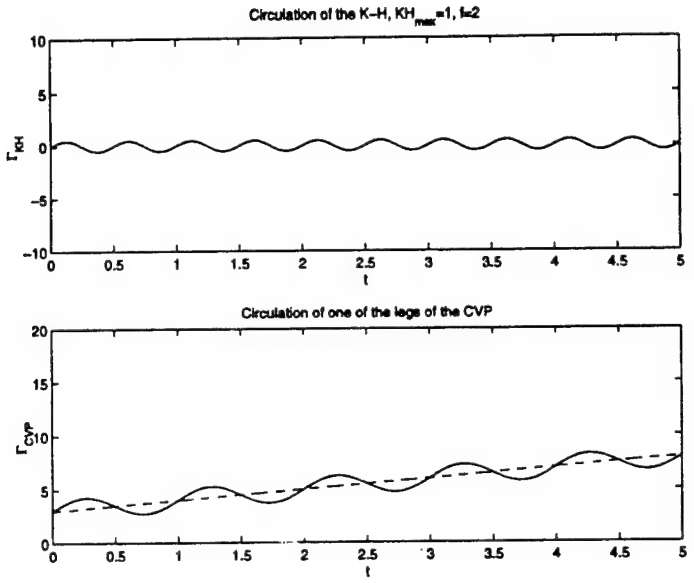

Figure 3.27:

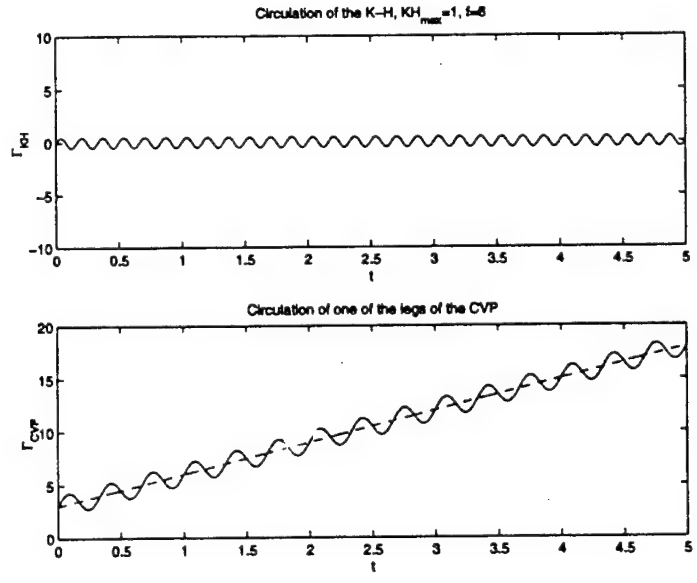

Figure 3.28:

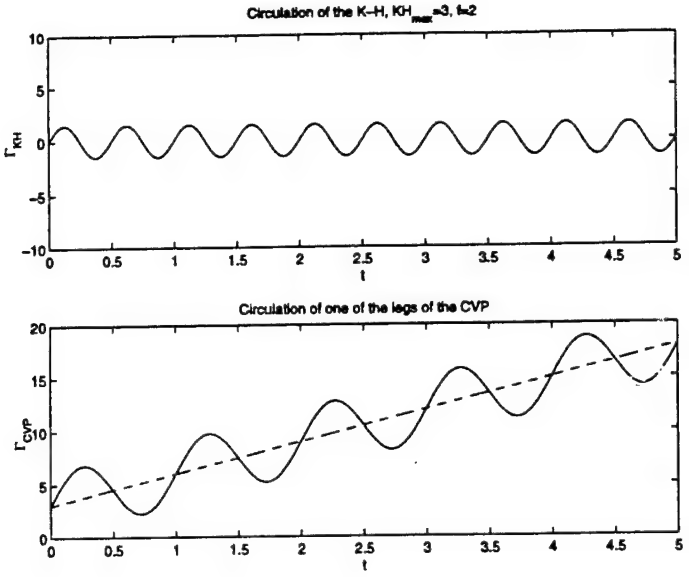

Figure 3.29:

KH roll-up and its strength. Below, we evaluate the effect of changing these parameters.

If we fix the momentum ratio (jet to cross-stream), the control parameters are λ which is the spacing of the KH vortices, ϕ which indicates the phase difference between the KH crossings and the pulsation of the CVP at a fixed (control) frequency, Γ_0 which denotes the initial CVP circulation and $\sigma_{0_{KH}}$ which is the initial core radius for the KH roll-up (a function of the initial boundary layer thickness). The expressions for the velocity fields can be written as

$$v_x(x,y,t) = \frac{-\Gamma_{CVP}}{2\pi}\frac{y}{r_{pos}^2}(1-e^{\frac{-r_{pos}^2}{\sigma_{CVP}^2}}) + \frac{\Gamma_{CVP}}{2\pi}\frac{y}{r_{neg}^2}(1-e^{\frac{-r_{neg}^2}{\sigma_{CVP}^2}}) \tag{3.29}$$

where

$$r_{pos}^2 = (x+d)^2 + y^2 \tag{3.30}$$

$$r_{neg}^2 = (x-d)^2 + y^2 \tag{3.31}$$

$$\sigma_{CVP}^2 = \sigma_0^2 + 4\nu t \tag{3.32}$$

$$\Gamma_{CVP} = \Gamma_0 + (\frac{\Gamma_{KH}U}{4\lambda_{KH}})t + \frac{\Gamma}{2}\sin(\frac{\pi U t}{2\lambda_{KH}} + 2\phi) \tag{3.33}$$

$$\phi \in [0, 2\pi) \tag{3.34}$$

$$v_y(x,y,t) = \frac{\Gamma_{CVP}}{2\pi}\frac{x+d}{r_{pos}^2}(1-e^{\frac{-r_{pos}^2}{\sigma_{CVP}^2}}) + \frac{-\Gamma_{CVP}}{2\pi}\frac{x-d}{r_{neg}^2}(1-e^{\frac{-r_{neg}^2}{\sigma_{CVP}^2}}) - \frac{U}{6}\sin\theta + \frac{\Gamma_{KH}}{2\pi}\sum_{i=1}^{Ntot}\frac{-z_i}{r_i^2}(1-e^{\frac{-r_i^2}{\sigma_i^2}}) \tag{3.35}$$

where

$$r_i^2 = (y-l)^2 + z_i^2 \tag{3.36}$$

$$z_i = (i-1)\lambda_{KH} - \frac{U}{2}t \tag{3.37}$$

$$\sigma_i^2 = \sigma_{KH_0}^2 + 4\nu t \tag{3.38}$$

$$\theta = 0.0025s^3 - 0.0453s^2 + 0.1114s + 1.4518; \quad s = Ut \tag{3.39}$$

Which may in turn be represented in terms of the control parameters as

$$\dot{x} = v_x(x,y,t) = \eta(p_1,p_2,p_3,p_4,t)F(x,y,t) \tag{3.40}$$

$$\dot{y} = v_y(x,y,t) = \eta(p_1,p_2,p_3,p_4,t)G(x,y,t) + \sum_i H_i(y,p_4,t) + A\sin(\theta(t)) \tag{3.41}$$

where

$$p_1 = \Gamma_0 \tag{3.42}$$

$$p_2 = \lambda_{KH} \tag{3.43}$$

$$p_3 = \phi \tag{3.44}$$

$$p_4 = \sigma_{0_{KH}} \tag{3.45}$$

F,G & H are time-dependent non-linear functions
η contains a time-independent term, a linear growth in time and an time-oscillating term

All vortex cores were assumed to be distributed as Gaussian functions, taking into account that their core is growing in time (thereby mimicking viscous diffusion and avoiding singularities). A series of these KH rods was first arranged parallel to each other in a plane perpendicular to the model plane and allowed to cross the plane with a velocity of U/2. The CVP in the plane is growing and pulsing as described above.

Passive scalar transport is described by the advection-diffusion equation (3.16). For the flows of interest the advection term $\mathbf{v}(\mathbf{x},\mathbf{y},\mathbf{t})^T\nabla c(x,y,t)$ dominates the diffusion term $\mu\Delta c(x,y,t)$. The advection diffusion equation can be studied in an Eulerian frame. Various control problems (including optimal ones) will be studied with this description, as various mixing measures can be determined by penalizing nonuniformity of the passive scalar concentration $c(x,y,t)$ in space and time. In fact, in a parabolized model, mixing performance can be specified in terms of of $c(x,y,T_{final})$, where T_{final} is the time when the transverse plane reaches a fixed position downstream (representing position of a turbine inlet guide vane). Note that the result of the mixing performance evaluation will depend on the initial condition. In case of periodic bulk jet forcing, one should calculate a cumulative measure of mixing performance over one period of forcing from "instantaneous" measures of performance that depend on the initial conditions corresponding to a particular control phase.

Alternatively, neglecting the diffusion term, one can study the passive scalar mixing using Lagrangian simulation advecting tracer particles along the direction of the flow given by velocity filed $\mathbf{v}(\mathbf{x},\mathbf{y},\mathbf{t})$. The mixing can be studied using methods of dynamical system theory.

In a preliminary study, particles were introduced on the plane with a Gaussian probability distribution centered at the origin and the effect of KH frequency on the final particle distribution was examined. One can see from Figures 3.30 and that low frequency forcing was much more effective in spreading the jet particles than high frequency. Note that the parabolized two-vortex model does not explain the creation or interactions of the KH or CVP structures, hence, it does not satisfy Property 1 (physical relevance). However, one could imagine construction of a "grey box" model that would use parametrization of the vorticity field with temporal coefficients dynamics reconstructed from DNS simulations. The parabolized model is not arbitrarily refinable, but one could develop a refinable 3D version. However, even in its present version the model is still very useful, as it provides a framework for studying effects of KH-CVP structures on particle mixing. Note that the model is suitable for control design using methods of dynamical systems and control theory. In particular, one can study *desirable* dynamics of coherent structures using dynamical systems or control theory and limits of achievable mixing performance. Once the desired behavior has been identified, one can attempt to *enforce* this behavior in a flow model (Eulerian-Lagrangian or DNS) by solving numerically a tracking problem, which in turn can be approached as an optimization problem.

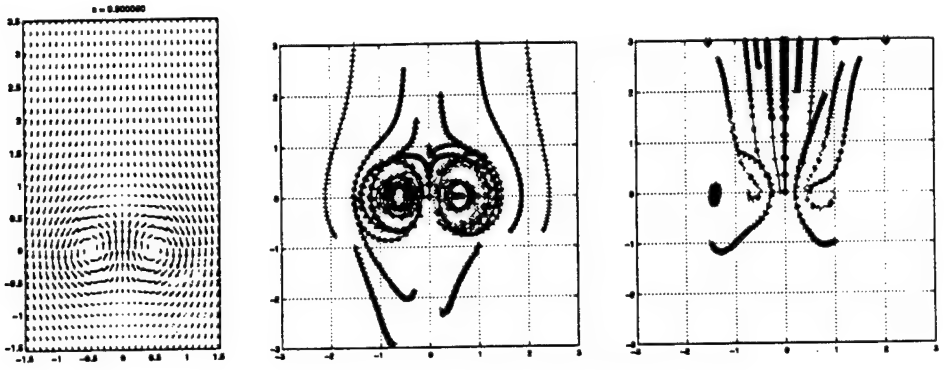

Figure 3.30: A snapshot of a typical velocity field, and particle trajectories for high (left) and low (right) control frequency

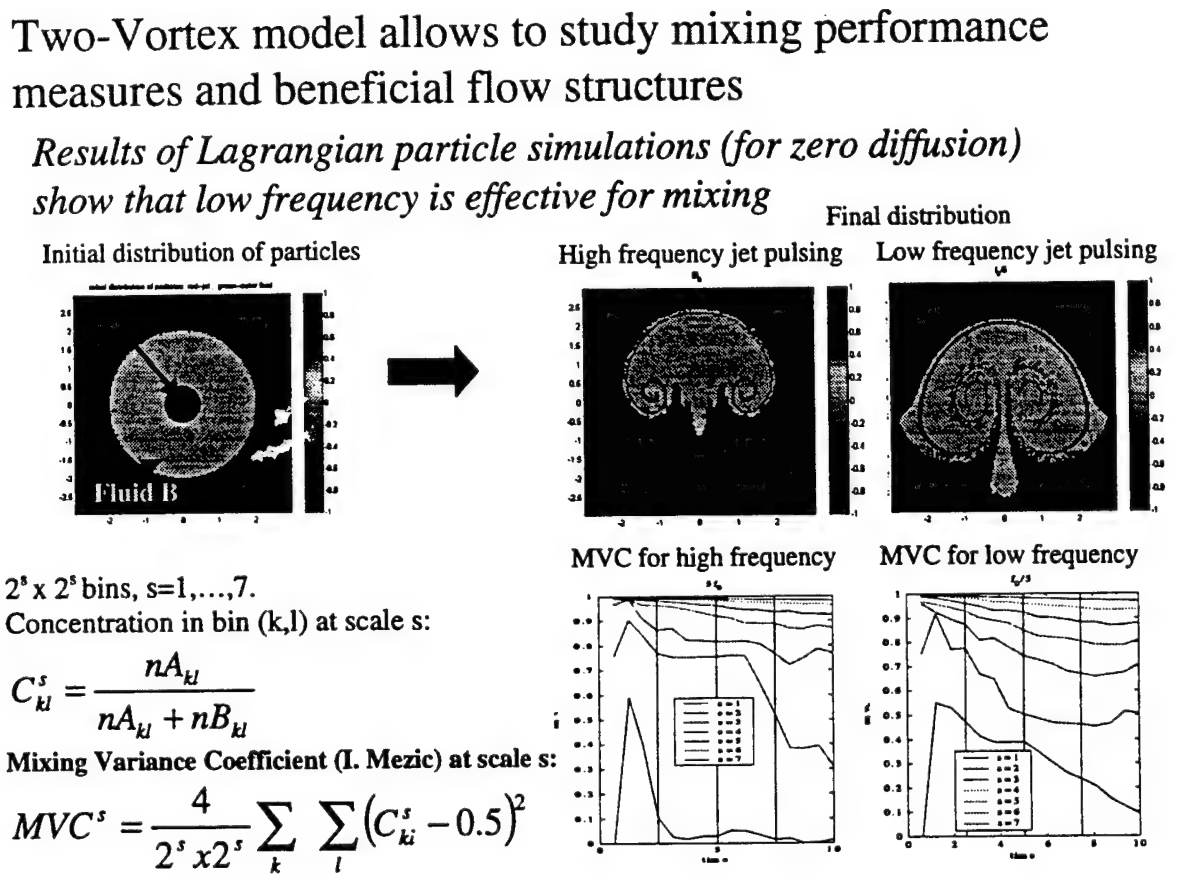

Figure 3.31: Effect of high and low control frequency on the Mixing Variance Coefficient

3.5.10 Control of jet in cross flow: experimental results

Experiments with control of jet in cross flow were performed in a UTRC facility shown in Figure 3.32 by Satish Narayanan and Prabir Barooah. This work was funded from UTRC internal DCE funds, but it was closely tied to AFOSR effort. Some experiment were guided by prediction of AFOSR-funded project described in this report. The data collected from the experiment will be used to validate models developed in AFOSR project.

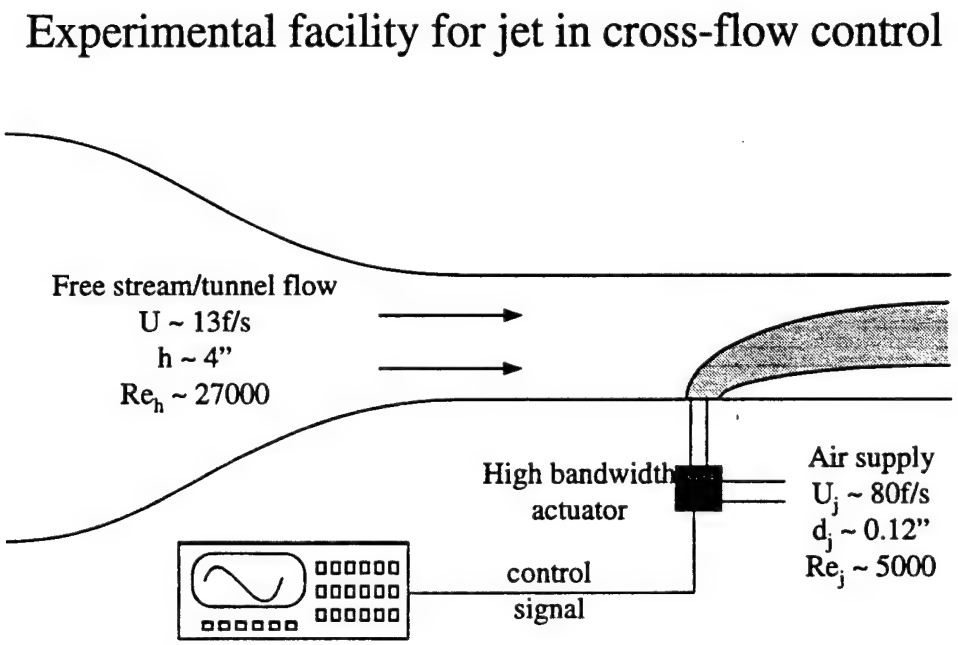

Figure 3.32: Experimentally measured mean velocity profiles in jet in cross flow experiments at UTRC

Objectives of the experiments with control of jet in cross flow was to determine physical mechanisms to be affected by actuation to achieve mixing enhancement and demonstrate mixing enhancement. The experimental rig had a non-reacting, single jet in cross-flow. Diagnostics involved hot-film anemometry, and Mie scattering. High bandwidth actuator was used to excite the whole jet flow.

Cold, non-reacting sub-scale experiments were conducted of the forced and unforced jet in crossflow with a velocity ratio of 6 (as in the DNS simulations). Slightly higher Reynolds numbers based on channel height were used but similar jet Reynolds numbers were used.

A mechanical actuator (namely, a spinning valve) was used to modulate the jet at several frequencies around the forcing frequency predicted by the simulations as being the effective one (namely, $St_d = 0.1 - 0.25$). Similar mixing and entrainment/mixing enhancements were noted with flow visualization and quantitative measurements of the velocity field, confirming and supporting the effectiveness

of "low frequency" actuation.

Preliminary results shown in Figure 3.33 indicate mixing enhancement at low forcing frequencies, in good agreement with predictions of analysis using DNS and Two-Vortex model presented in the previous sections.

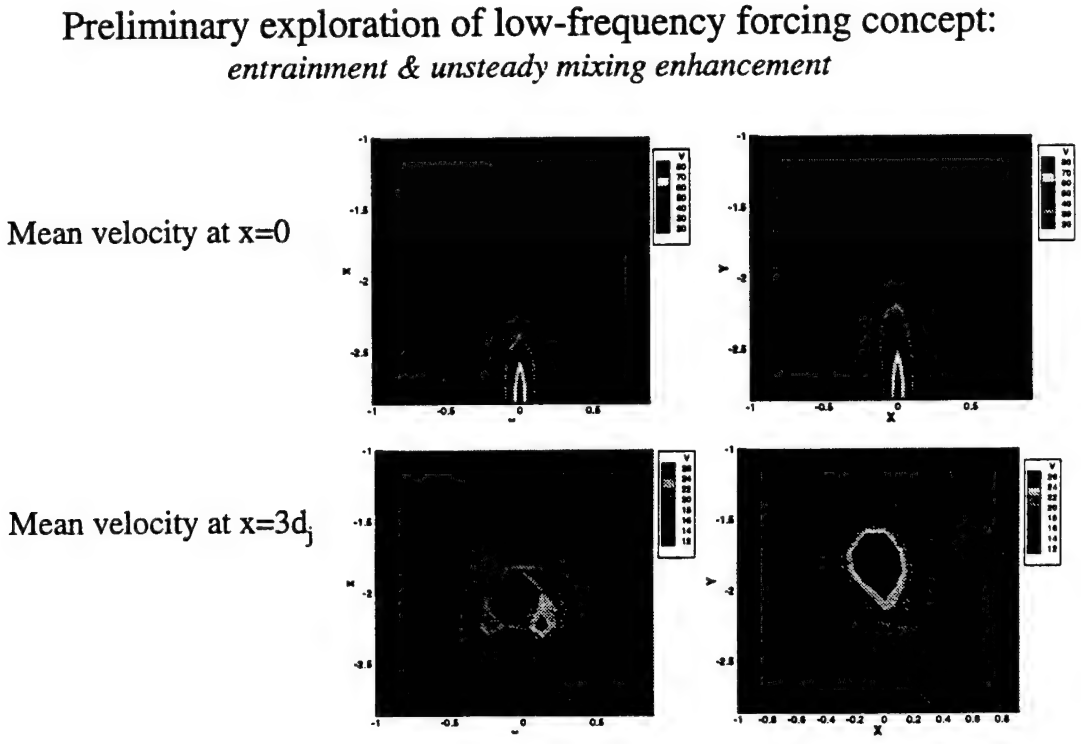

Figure 3.33: Experimentally measured mean velocity profiles in jet in cross flow experiments at UTRC

Chapter 4

Personnel Supported

UTRC personnel: Andrzej Banaszuk, Bernd Noack, Razvan Florea, Satish Narayanan, Alex Khibnik, Shubhro Ghosh, Scott Copeland, Clas Jacobson. Academic personnel: Thomas Bewley (UCSD), Peter Blossey (UCSD), Ahmed Ghoniem (MIT), John Hauser (UC Boulder), Thomas John (intern, Cornell), Igor Mezic (Harvard), Gilead Tadmor (Northeastern), Kurt Lust (University of Minnesota).

Chapter 5

Publications

5.1 Journal papers

[j1] A.I. Khibnik, S. Narayanan, C.A. Jacobson, and K. Lust. Analysis of low dimensional dynamics of flow separation. Submitted to Notes in Computational Fluid Dynamics (Proceedings of Ercoftac and Euromech Colloqium 383 "Continuation Methods in Fluid Dynamics", Aussois, France, 6-9 September 1998).
[j2] I. Mezic and A. Banaszuk, "Comparison of systems with complex behavior", submitted under review in *Physica D.*
[j3] B.R. Noack, I. Mezic, A. Banaszuk, and G. Tadmor, "Controlling vortex motion and chaotic advection", submitted to *Physics of Fluids.*
[j4] A. Banaszuk, K.B. Ariyur, M. Krstic, and C.A. Jacobson, "An Adaptive Algorithm for Control of Combustion Instability", submitted to *Automatica.*
[j5] G. Tadmor, A. Banaszuk, "Observer-based control of vortex motion in a recirculation zone", submitted to IEEE Transaction on Controls Systems Technology.
[j6] P. Blossey, S. Narayanan, T.R. Bewley, "Dynamics & control of a jet in cross-flow: direct numerical simulations & experiments", in preparation.
[j7] P. Mehta, A. Banaszuk, "On the identification of heat release nonlinearity in the thermoacoustic feedback loop", in preparation.

5.2 Conference papers

[c1] G.S. Copeland, I.G. Kevrekidis, R. Rico-Martinez, Adaptive detection of instabilities and nonlinear analysis of a reduced-order model for flutter and rotating stall in turbomachinery, 1999 CCA, Hawaii.
[c2] S. Narayanan, A.I. Khibnik, C.A. Jacobson, I.G. Kevrekidis, R. Rico-Martinez, and K. Lust. Low dimensional models for active control of flow separation. 1999 CCA, Hawaii.
[c3] A. Banaszuk and J. Hauser, On control of planar periodic orbits, 1999 CDC, December 1999, Phoenix.
[c4] R. Smith, A. Banaszuk, and G. Dullerud, Model validation approaches for nonlinear feedback systems using frequency response measurements, 1999 CDC, December 1999, Phoenix.
[c5] A. Banaszuk, Y. Zhang, and C.A. Jacobson. Active Control of Combustion Instabilities in Gas Turbine Engines for Low Emissions. Part II: Adaptive Control Algorithm Development, Demonstration and Performance Limitations, AVT Symposium on Active Control Technology for Enhanced Performance Operation Capabilities of Military Aircraft, Land Vehicles, and Sea Vehicles, May 2000, Braunschweig.

[c6] B. Coller, B. Noack, S. Narayanan, A. Banaszuk, and A. Khibnik, "Reduced-Basis Model for Active Separation Control in a Planar Diffuser Flow", *paper AIAA-2000-2562, Fluids 2000*, June 2000, Denver.
[c7] A. Banaszuk, Y. Zhang, and C.A. Jacobson. Adaptive Control of Combustion Instability Using Extremum-Seeking, 2000 ACC, June 2000, Chicago.
[c8] I. Mezic and A. Banaszuk, "Comparison of Systems with Complex Behavior: Spectral Methods", 2000 CDC, Sydney, December 2000.
[c9] B.R. Noack, I. Mezic, and A. Banaszuk, "Controlling vortex motion and chaotic advection", 2000 CDC, Sydney, December 2000.
[c10] K.B. Ariyur, A. Banaszuk, M. Krstic, "Identification of averaged dynamics of a controlled combustion instability", 2000 CDC, Sydney, December 2000.
[c11] G. Tadmor, A. Banaszuk, "Observer-based control of vortex motion in a recirculation zone", submitted to 2001 NOLCOS, St. Petersburg, July 2001.
[c12] P. Blossey, S. Narayanan, T.R. Bewley, "Dynamics & control of a jet in cross-flow: direct numerical simulations & experiments", submitted to 2001 (IUTAM) Symposium on Turbulent Mixing and Combustion, June 3-6, 2001, Kingston.
[c13] P. Mehta, A. Banaszuk, "On the identification of heat release nonlinearity in the thermoacoustic feedback loop", submitted to 2001 CDC, Orlando. December 2001.

5.3 Invited Sessions

The following invited sessions were organized with AFOSR support and contain AFOSR-funded papers:
Control applications in flows and turbomachines (organized by Scott Copeland and Satish Narayanan). CCA 99, Hawaii.
Theory and Applications of Extremum-Seeking Control (organized by Andrzej Banaszuk and Mario Rotea). ACC 2000, Chicago.
Control of Mixing in Shear Flows (organized by Andrzej Banaszuk and Luca Cortelezzi). CDC 2000, Sydney.
Nonlinear Model Validation (organized by Roy Smith and Andrzej Banaszuk). CDC 2000, Sydney.

5.4 Talks at meetings

The talks at meetings that do not have proceedings include:
Talk at Flow Control Worskshop, Boston University, October 1999

Andrzej Banaszuk, Bernd R. Noack, Igor Mezic
A hierarchy of vortex-based models for coherent-structure control
The shear flow phenomena strongly affect operations of industrial products like jet engines, helicopters, and HVAC devices. For instance, in the case of airfoils at high angle of attack the flow separates close to the leading edge causing decrease in lift and increase in drag. Full attachment of the flow is desirable, but not yet technologically feasible goal in most industrial cases, because of limited actuator authority. However, experiments show that one can significantly increase the lift and reduce drag by exciting beneficial coherent structures in the separated shear layer using relatively small actuation effort. Abundance of shear flow phenomena in industrial products, high potential benefits from shear flow control, technical feasibility of shear flow control demonstrated in experiments indicate need to focus research in the area of shear flow control. In our talk we present a general framework for modeling, analysis, and control of shear flows using tools from dynamical systems and control theory. We show an

example of application of the framework to control of mixing in combustors. We also identify areas of basic research in control of shear flows that can support technology transition in reasonably short time.

Talks at APS (Americam Physical Society) meeting, November 2000, Washington DC
Peter Blossey, Thomas Bewley (University of California, San Diego, CA), Satish Narayanan (United Technologies Research Center, East Hartford, CT)
Direct numerical simulations of a jet in crossflow
The mixing characteristics of a jet in cross-flow can be substantially enhanced using unsteady modulation of the jet flow, as noted in prior experimental investigations. We explore the dynamics of a jet in crossflow with direct numerical simulations to assess the impact of unsteady forcing on its spatiotemporal mixing properties. The Reynolds number ($\mathrm{Re} = U_j d/\nu$) for the jet is 3000 with a velocity ratio (U_j/U_∞) of 6. The simulations are performed in a periodic channel flow geometry and include a fringe region to remove disturbances from the flow at the domain entrance. In addition to exploring the vorticity dynamics in the flow field, we study the statistical properties of this highly 3D, unsteady flow, particularly of its cross-stream mixing. A conserved scalar has been added to the simulations to enable quantification of the jet mixing, and a variety of mixing metrics are assessed to evaluate the effect of unsteady jet forcing. Conventional, time-averaged measures of mixing can be misleading in this flow. Higher order statistics of mixing, however, are shown to be insightful in discriminating the extent of mixing among various unsteady flow patterns.

Thomas John (Cornell University, Ithaca, NY), Satish Narayanan, Andrzej Banaszuk, Shubhro Ghosh (United Technologies Research Center, East Hartford, CT)
Reduced-order model for mixing in a jet in cross-flow
We present a reduced-order model describing the unsteady mixing associated with the three-dimensional coherent structure dynamics of a jet in cross-flow. The dynamically significant flow features are the shear layer structures emanating in the jet near field, and a pair of counter-rotating vortices emerging in the intermediate and far fields of the jet (where the jet begins to bend and align with the oncoming cross flow). We postulate a "parabolized" vortex model consistent with the observed dominant vortex dynamics. The velocity and vorticity fields obtained from the model compare well qualitatively with prior experimental and direct numerical simulation results. Lagrangian particle simulations are used to quantify the extent of mixing, relative to a mixing dynamical system, at several spatial scales. The model appears to be suitable for use in the development of novel control laws for mixing enhancement.

Andrzej Banaszuk (United Technologies Research Center), Igor Mezic (Division of Engineering and Applied Sciences, Harvard University)
Control of point vortex systems
We present results on controllability and observability of point vortex motion actuated by external potential fields. Sufficient conditions for transformation of a point vortex system into the so-called flat coordinates which allow for simple description of controllability and observability of the system will be presented. Control of statistical, large-scale properties of point vortex systems is also considered. We present a number of examples of specific vortex configurations such as counterrotating vortex pairs.

Chapter 6

References

Bibliography

[1] H. Aref. Stirring by chaotic advection. *Journal of Fluid Mechanics*, 143:1–21, 1984.

[2] H. Aref and S. Balachandar. Chaotic advection in a Stokes flow. *Physics of Fluids*, 29:3515–3521, 1986.

[3] H. Aref and S.W. Jones. Enhanced separation of diffusing particles by chaotic advection. *Phys. Fluids A*, 1:470, 1989.

[4] N. Aubry, P. Holmes, J.L. Lumley, and E. Stone. The dynamics of coherent structures in the wall region of a turbulent boundary layer. *J. Fluid Mech.*, 192:115–173, 1988.

[5] K. Akselvoll and P. Moin. Large eddy simulation of turbulent confined coannular jets and turbulent flow over a backward facing step. Technical Report TF–63, Stanford University, 1995.

[6] G. K. Batchelor. *An Introduction to Fluid Dynamics.* Cambridge University Press, Cambridge, 1967.

[7] T. Bewley, P. Moin, and R. Temam. DNS-based predictive control of turbulence: an optimal benchmark for feedback algorithms. *J. Fluid Mech.*, 1999.

[8] T. R. Bewley and P. Moin, Optimal and robust control and estimation of transition, convection, and turbulence, Stanford University, Department of Mechanical Engineering, report TF–76, 1999.

[9] J. Burns , B.B. King, and D. Rubio Feedback control of thermal fluid using state estimation. *International Journal of Computational Fluid Dynamics*, 1999.

[10] M. H. Carpenter and C. A. Kennedy, Fourth-order, 2N-storage Runge–Kutta schemes. NASA report TM 109112, 1994.

[11] Sergio L. Coelho and J.C.R. Hunt. The dynamics of the near field of strong jets in crossflows. 200:95–120, 1989.

[12] B. Coller, B.R. Noack, S. Narayanan, A. Banaszuk, and A.F. Khibnik. Reduced-basis model for active separation control in a planar diffuser flow. In *paper AIAA-2000-2562, Fluids 2000, Denver*, 2000.

[13] L. Cortelezzi, A. Leonard, and J.C. Doyle. An example of active circulation control of the unsteady separated flow past a semi-infinite plate. *J. Fluid Mech.*, 260:127–154, 1994.

[14] L. Cortelezzi. Nonlinear feedback control of the wake past a plate with a suction point on the downstream wall. *J. Fluid Mech.*, 327:303–324, 1996.

[15] L. Cortelezzi, Y.-C. Chen, and H.-L. Chang. Nonlinear feedback control of the wake past a plate: from a low-order model to a high-order model. *Phys. Fluids*, 9:2009–2022, 1997.

[16] L. Cortelezzi and A. R. Karagozian. On the Formation of Counter-Rotating Vortex Pair in Transverse Jets. 43(9), 1998.

[17] L. Cortelezzi and A. R. Karagozian. On the Evolution of Vorticity in Pulsating Jets in Cross Flow. 44(8), 1999.

[18] M. Flies, J. Levine, P. Martin P, and P. Rouchon. On differentially flat nonlinear-systems. 315:619–624, 1992.

[19] T. F. Fric and A. Roshko, Vortical structure in the wake of a transverse jet, Turbulent Shear Flows 7, 1991, Springer

[20] T. F. Fric and A. Roshko, Vortical structure in the wake of a transverse jet, *J. Fluid Mech.*, 279, 1994, pp 1-47.

[21] M. Gad-El-Hak and D. Bushnell. Status and outlook of flow separation control. In *29th Aerospace Sciences Meeting*, AIAA–91–0037, Reno, Nevada, 1991.

[22] S. Ghosh, A. Leonard, S. Wiggins. Diffusion of a Passive Scalar From a No-Slip Boundary Into a Chaotic Advection Field. *J. Fluid Mech.*, 1998.

[23] J. Guckenheimer and P. Holmes. *Nonlinear Oscillations, Dynamical Systems, and Bifurcation of Vector Fields.* Springer, New York, 1986.

[24] G. Haller and A.C. Poje. Finite time transport in aperiodic flows. *Phys. D*, 119:352–380, 1998.

[25] J. Hauser and D. G. Meyer. The trajectory manifold of a nonlinear control system. *Proceedings of the IEEE Conference on Control and Applications*, Tampa, Florida, December 1998.

[26] J. Hauser and D. G. Meyer. Trajectory morphing for nonlinear systems. *Proceedings of the Automatic Control Conference*, Philadelphia, June 1998.

[27] S. D. Heister and A. R. Karagozian. Vortex Modelling of Gaseous Jets in a Compressible Crossflow. *Journal of Propulsion*, 6(1):85–92, 1990.

[28] A. R. Karagozian and V. S. Manda. Flame structure and fuel consumption in the field of a vortex pair. *Combustion Science and Technology*, 49:185–200, 1986.

[29] A. R. Karagozian and F. E. Marble. Study of a diffusion flame in a stretched vortex. *Combustion Science and Technology*, 45:65–84, 1986.

[30] A. R. Karagozian, Y. Suganuma, and B. D. Strom. Experimental studies in vortex pair motion coincident with a liquid reaction. *Physics of Fluids*, 31:1862–1871, 1988.

[31] A.R. Karagozian and B.V.S. Manda. Flame structure and fuel consumption in the field of a vortex pair. *Combust. Sci. and Tech.*, 49:185–200, 1986.

[32] R. M. Kelso, T. T. Lim, and A. E. Perry. An expermental study of round jets in a cross-flow. *J. Fluid Mech.*, 306:111–144, 1996.

[33] A. Leonard. Vortex methods for flow simulations. *Journal of Computational Physics*, 37:289-335, 1980.

[34] A. Leonard. Computing three-dimensional incompressible flows with vortex elements. *Ann. Rev. Fluid Mech*, 17:523-559, 1985.

[35] S. Green (editor). Fluid Vortices. *Fluid Mechanics and its Applications*, Vol. 30, Kluwer Academic Publishers, 1995

[36] T.C. Lieuwen and B.T. Zinn, "Investigation of limit cycle oscillations in an unstable gas turbine combustor," in *AIAA paper 2000-0707, 38th AIAA Aerospace Sciences Meeting, Reno, January 2000.* 2000, AIAA.

[37] C. A. Mansoux, D. L. Gysling, J. D. Setiawan, and J. D. Paduano. Distributed nonlinear modeling and stability analysis of axial compressor stall and surge. In *Proc. American Control Conference*, pages 2305–2316, 1994.

[38] D.C. McCormick. Boundary layer separation control with directed synthetic jets. In *39th AIAA Aerospace Sciences Meeting and Exhibit*, 1999. submitted.

[39] K.R. McManus, U. Vandsburger, and C.T. Bowman. Combustor performance enhancement through direct shear layer excitation. *Combustion and Flame*, 82:75–92, 1990.

[40] I. Mezić and A. Banaszuk. Comparison of complex systems. Submitted to Physica D, 2000.

[41] L.M. Milne-Thomson. *Theoretical Hydrodynamics.* Dover Publications, New York, 1968.

[42] S. Narayanan, B.R. Noack, A. Banaszuk, and A.I. Khibnik. Dynamic separation control in 2D diffuser. Technical report, United Technologies Research Center, 1999.

[43] H. Nijmeijer and A.J. van der Schaft. *Nonlinear Dynamical Control Systems.* Springer–Verlag, New York, 1990.

[44] B. R. Noack, A. Banaszuk, and I. Mezić. Controlling vortex motion and chaotic advection. submitted to Physics of Fluids, 2000.

[45] J. M. Ottino. Unity and diversity in mixing - stretching, diffusion, breakup, and aggregation in chaotic flows. *Physics of Fluids A*, 3:1417–1430, 1991.

[46] J.M. Ottino. *The Kinematics of Mixing: Stretching, Chaos and Transport.* Cambridge University Press, Cambridge, 1989.

[47] V. Rom-Kedar, A. Leonard, and S. Wiggins. An analytical study of transport, mixing and chaos in unsteady vortical flow. *J. Fluid Mech.*, 214:347–394, 1990.

[48] S. Wiggins. *Chaotic Transport in Dynamical Systems.* Springer-Verlag, New York, 1992.

[49] I. Wygnanski and A. Seifert. The control of separation by periodic oscillations. In *18th AIAA Aerospace Ground Testing Conference*, June 20–23, 1994 / Colorado Springs, CO, 1994. also as AIAA–94–2608 paper.

[50] B.D.O. Anderson and J.B. Moore, *Optimal Filtering*, Prentice-Hall, Englewood Cliffs, New Jersey, 1979.

[51] K. J. Astrom and B. Wittenmark, *Adaptive Control*, 2nd edition, Reading, MA: Addison-Wesley, 1995.

[52] A. Banaszuk, "A note on combustion instabilities," *UTRC Technical Report*, September 1997.

[53] A. Banaszuk, C. A. Jacobson, A. I. Khibnik, P. G. Mehta,"Linear and nonlinear analysis of controlled combustion processes. Part I: Linear analysis," *Proc. of the IEEE Conf. on Control Applications*, Kohala-Coast, Hawai, pp. 199–205, Aug. 1999.

[54] A. Banaszuk, C. A. Jacobson, A. I. Khibnik, P. G. Mehta,"Linear and nonlinear analysis of controlled combustion processes. Part II: Nonlinear analysis," *Proc. of the IEEE Conf. on Control Applications*, Kohala-Coast, Hawai, pp. 206–212, Aug. 1999.

[55] A. Banaszuk, J. Hauser, "On control of planar periodic orbits," *Proc. of the IEEE Conf. on Decision and Control*, Phoenix, Arizona, Dec. 1999.

[56] A. Banaszuk, Y. Zhang, C. A. Jacobson," Adaptive Control of Combustion Instability Using Extremum-Seeking ," *Proc. of the American Control Conference*, Chicago, June 2000.

[57] C. A. Jacobson, A. I. Khibnik, A. Banaszuk, J. M. Cohen, W. P. Proscia, " Active Control of Combustion Instabilities in Gas Turbine Engines for Low Emissions. Part I: Physics-Based and Experimentally Identified Models of Combustion Instability ," *Proc. of the NATO AVT/RTO Symposium*, 2000.

[58] A. Banaszuk, W. Sluis,"On nonlinear observers with approximately linear error dynamics ," *Proc. of 1997 ACC* , June 1997, Albuquerque.

[59] A. Banaszuk, Y. Zhang, C. A. Jacobson," Active Control of Combustion Instabilities in Gas Turbine Engines for Low Emissions. Part II: Adaptive Control Algorithm Development, Demonstration and Performance Limitations ," *Proc. of the NATO AVT/RTO Symposium*, 2000.

[60] A. Banaszuk, K. Aryiur, M. Krstic, C. A. Jacobson,"An Adaptive Algorithm for Control of Combustion Instability," *to be submitted to Automatica*, 2000.

[61] P. F. Blackman, "Extremum-seeking regulators," in J. H. Westcott, Ed., *An Exposition of Adaptive Control*, New York, NY: The Macmillan Company, 1962.

[62] T. B. Co and S. Ungarala, "Batch scheme recursive parameter estimation of continuous-time systems using the modulating functions method," *Automatica*, vol. 33, pp. 1185–1191, 1997.

[63] J. M. Cohen, N. M. Rey, C. A. Jacobson, T. J. Anderson, "Active control of combustion instability in a liquid-fueled low-NO_x combustor," *ASME/IGTI Gas turbine Expo and Congress*, Stockholm, Sweden, June 1998.

[64] L. Cortelezzi, J. King, R. Lobbia, R. T. M'Closkey & A. R. Karagozian 2000. Actively controlled transverse jet injection, *Bulletin of the American Physical Society* **45**(9): 85.

[65] F. E. C. Culick, "Technical evaluation report, Combustion Instabilities in Liquid-fuelled Propulsion Systems," 72^{nd} *Propulsion and Energetics Panel Specialists' Meeting*, Bath, UK, 1988.

[66] C. S. Drapper and Y. T. Li, "Principles of optimalizing control systems and an application to the internal combustion engine," *ASME*, vol. 160, pp. 1–16, 1951, also in R. Oldenburger, Ed., *Optimal and Self-Optimizing Control,* Boston, MA: The M.I.T. Press, 1966.

[67] A. L. Frey, W. B. Deem, and R. J. Altpeter, "Stability and optimal gain in extremum-seeking adaptive control of a gas furnace," *Proceedings of the Third IFAC World Congress,* London, 48A, 1966.

[68] Y. T. Fung and V. Yang, "Active control of nonlinear pressure oscillations in combustion chambers," *Journal of Propulsion and Power*, vol. 8, pp. 1282–1289, 1992.

[69] J. P. Hathout, A. M. Annaswamy, M. Fleifil, A. F. Ghoniem,"A model-based active control design for thermoacoustic instability", *Combustion Sci. and Tech.*, vol. 132, pp. 99–105, 1998.

[70] J. R. Hibshman, J. M. Cohen, A. Banaszuk, T. J. Anderson, and H. A. Alholm, "Active control of combustion instability in a liquid-fueled combustor," *Proceedings of 1999 ASME Turbo Expo,* Indianapolis, 1999.

[71] O. L. R. Jacobs and G. C. Shering, "Design of a single-input sinusoidal-perturbation extremum-control system," *Proceedings IEE,* vol. 115, pp. 212-217, 1968.

[72] H. Johari, M. Pacheco-Tougas & J. C. Hermanson 1999. Penetration and mixing of fully modulated turbulent jets in crossflow. *AIAA J.* **37**(7): 842–850.

[73] T. Schuller, J. King, A. Majamaki & A. R. Karagozian 1999. An experimental study of acoustically controlled gas jets in crossflow, *Bulletin of the American Physical Society* **44**(8): 111.

[74] V. V. Kazakevich, "Extremum control of objects with inertia and of unstable objects," *Soviet Physics,* Dokl. 5, pp. 658-661, 1960.

[75] H. K. Khalil, *Nonlinear Systems*, 2nd edition, Englewood Cliffs, NJ: Prentice Hall, 1996.

[76] A. Krener and W. Respondek. Nonlinear observers with linearizable error dynamics. *SIAM Journal on Control and Optimization*, 23:197–216, 1985.

[77] M. Krstic and H. Deng, *Stabilization of Nonlinear Uncertain Systems*, Springer, London, 1998.

[78] M. Krstić and H. H. Wang, "Stability of extremum seeking feedback for general nonlinear dynamic systems," accepted for *Automatica*, 1998.

[79] M. Krstic, "Performance improvement and limitations in extremum seeking control," *System and Control Letters*, to appear.

[80] A. Krupadanam, M. Krstic, C. Jacobson,"Self-tuning control of a nonlinear model of combustion instabilities", *IEEE Trans. on Control Systems Technology*, vol. 7, pp. 424–436, July 1999.

[81] W. Lang, T. Poinsot, S. Candel,"Active control of combustion instability", *Combustion and Flame*, vol. 70, pp. 281–289, 1987.

[82] P. J. Langhorne, A. P. Dowling, N, Hooper, "Practical active control system for combustion oscillations," *Journal of Propulsion*, vol. 6, pp. 324–333, 1990.

[83] B. La Scala, "Approaches to Frequency Tracking and Vibration Control," *Ph.D. Thesis*, Dept. of Systems Engineering, The Australian National University, December 1994.

[84] M. Leblanc, "Sur l'electrification des chemins de fer au moyen de courants alternatifs de frequence elevee," *Revue Generale de l'Electricite,* 1922.

[85] A. Leonard. Vortex Methods for Flow Simulation. *Journal of Computational Physics.*, 37:289–335, 1980.

[86] Hans J. Lugt. *Introduction to Vortex Theory.* Vortex Flow Press, Potomac, 1996.

[87] Richard J. Margason. Fifty Years of Jet in Cross Flow Research. Presented at the AGARD Meeting on 'Computational and Experimental Assessment of Jets in Cross Flow,' April, 1993.

[88] K. R. McManus, J. C. Magill, M. F. Miller,"Control of unstable combustion oscillations in liquid-fueled gas turbines", *Proc. of the IEEE Conf. on Control Applications*, Trieste, Italy, pp. 1170–1174, Sept. 1998.

[89] S. M. Meerkov, "Asymptotic Methods for investigating quasistationary states in continuous systems of automatic optimization," *Automation and Remote Control,* no. 11, pp. 1726-1743, 1967.

[90] S. M. Meerkov, "Asymptotic methods for investigating a class of forced states in extremal systems," *Automation and Remote Control,* no. 12, pp. 1916-1920, 1967.

[91] S. M. Meerkov, "Asymptotic methods for investigating stability of continuous systems of automatic optimization subjected to disturbance action," (in Russian) *Avtomatika i Telemekhanika,* no. 12, pp. 14-24, 1968.

[92] I. S. Morosanov, "Method of extremum control," *Automation & Remote Control,* vol. 18, pp. 1077-1092, 1957.

[93] R.M. Murray, C.A. Jacobson, R. Casas, A.I. Khibnik, C.R. Johnson Jr., R. Bitmead, A.A. Peracchio, and W.M. Proscia, "System Identification for Limit Cycling Systems: A Case Study for Combustion Instabilities," *Proceedings of 1998 American Control Conference*, Philadelphia, June 1997.

[94] Y. Neumeier, B. T. Zinn,"Active control of combustion instabilities using real-time identification of combustor modes", *Proc. of the IEEE Conf. on Control Applications*, Albany, NY, pp. 691–698, Sept. 1995.

[95] I. I. Ostrovskii, "Extremum regulation," *Automation & Remote Control,* vol. 18, pp. 900-907, 1957.

[96] C. O. Paschereit, E. Gutmark, W. Weisenstein,"Acoustic control of combustion instabilities and emissions in a gas-turbine combustor", *Proc. of the IEEE Conf. on Control Applications*, Trieste, Italy, pp. 1175–1179, Sept. 1998.

[97] A. A. Peracchio and W. M. Proscia, "Nonlinear heat-release/acoustic model for thermoacoustic instability in lean premixed combustors," *ASME/IGTI Turbo Expo '98*, Stockholm, Sweden, June 1998.

[98] A. A. Pervozvanskii, "Continuous extremum control system in the presence of random noise," *Automation & Remote Control,* vol. 21, pp. 673-677, 1960.

[99] J. Sternby, "Extremum control systems: An area for adaptive control?" Preprints of the *Joint American Control Conference,* San Francisco, CA, 1980, WA2-A.

[100] J. W. S. Rayleigh, *Theory of Sound*, Vol. 2, Dover, New York, 1945.

[101] G. A. Richards and M. C. Janus, "Characterization of oscillations during premix gas turbine combustion," *Trans. of the ASME, Journal of Eng. for Gas Turbines and Power*, vol. 120, pp. 294–310, 1998.

[102] J. W. Rumsey, M. Fleifil, A. M. Annaswamy, A. F. Ghoniem,"Low-order nonlinear models of thermoacoustic instabilities and model-based control ", *Proc. of the IEEE Conf. on Control Applications*, Trieste, Italy, pp. 1419–1423, Sept. 1998.

[103] J.R. Seume, N. Vortmeyer, W. Krause, J. Hermann, C.-C. Hantschk, P. Zangl, S. Gleis, D. Vortmeyer, and A. Orthmann,"Application of Active Combustion Instability Control to a Heavy Duty Gas Turbine, ", *Proc. of ASME Asia '97 Congress and Exhibition*, Singapore, October 1997, ASME Paper 97-AA-119.

[104] R. Smith, G. Dullerud, A. Banaszuk,"Model Validation Approaches for Nonlinear Feedback Systems using Frequency Response Measurements," *Proc. of the IEEE Conf. on Decision and Control*, Phoenix, Arizona, Dec. 1999.

[105] G. Tadmor, A. Banaszuk, "Observer-based control of vortex motion in a recirculation zone", *submitted to 2001 NOLCOS.*

[106] P.J. Vermeulen, C. F. Chin & W. K. Yu 1990. Mixing of an acoustically pulsed air jet with a confined cross-flow. *J. Prop. Power* **6**(6): 777–783.

[107] I. Wygnanski and A. Seifert. The control of separation by periodic oscillations. In *18th AIAA Aerospace Ground Testing Conference*, AIAA–94–2608, Colorado Springs, CO, 1994.

[108] K. Yu, K. J. Wilson, K. C. Schadow, "Liquid fueled active instability suppression," *27th International Symposium on Combustion*, The Combustion Institute, Pittsburgh, PA, pp. 2039–2046, 1998.

[109] Y. Zhang,"Stability and Performance Tradeoff with Discrete Time Triangular Search Minimum Seeking", *Proc. of American Control Conference*, Chicago, June 2000.